



Contribution to the monitoring of hydraulic axial piston pumps for helicopters, with special focus on lumped parameter modelling

Geneviève Mkadara

► To cite this version:

Geneviève Mkadara. Contribution to the monitoring of hydraulic axial piston pumps for helicopters, with special focus on lumped parameter modelling. Mechanics of materials [physics.class-ph]. INSA de Toulouse, 2020. English. NNT : 2020ISAT0020 . tel-03186032

HAL Id: tel-03186032

<https://theses.hal.science/tel-03186032>

Submitted on 30 Mar 2021

HAL is a multi-disciplinary open access archive for the deposit and dissemination of scientific research documents, whether they are published or not. The documents may come from teaching and research institutions in France or abroad, or from public or private research centers.

L'archive ouverte pluridisciplinaire **HAL**, est destinée au dépôt et à la diffusion de documents scientifiques de niveau recherche, publiés ou non, émanant des établissements d'enseignement et de recherche français ou étrangers, des laboratoires publics ou privés.



THÈSE

**En vue de l'obtention du
DOCTORAT DE L'UNIVERSITÉ DE TOULOUSE
Délivré par l'Institut National des Sciences Appliquées de
Toulouse**

**Présentée et soutenue par
Geneviève MKADARA**

Le 8 octobre 2020

**Contribution à la surveillance des pompes hydrauliques à pistons
axiaux pour les hélicoptères, avec un accent particulier sur la
modélisation à paramètres localisés**

Ecole doctorale : **MEGEP - Mécanique, Energétique, Génie civil, Procédés**

Spécialité : **Génie mécanique, mécanique des matériaux**

Unité de recherche :
ICA - Institut Clément Ader

Thèse dirigée par
Jean-Charles MARE

Jury

M. Giovanni JACAZIO, Rapporteur
M. Esteban CODINA MACIà, Rapporteur
Mme Christine PRELLE, Présidente du Jury
M. Marc BUDINGER, Examinateur
M. Jean-Charles MARE, Directeur de thèse
M. Gregor PAULMANN, Co-directeur de thèse

Preface

If someone had told me five years ago that I would write a preface for my doctoral thesis manuscript, I wouldn't have believed it. Well, it seems that, despite everything, I really have done a Ph.-D... And there has to be a preface to the manuscript! Many people have supported me during these years of research, and have allowed me to complete this work. I can't name them all and I hope no one will take offence.

First of all, I would like to thank Prof. Jean-Charles Maré and Gregor Paulmann, who have always pushed me to do better, who have both taught me a lot and given me so much good advice both professionally and privately. Thank you for always being attentive to my ideas. I think I have become a better person, certainly more pragmatic, in your contact.

Next, I would like to thank Bruno C., Thomas B. and Olivier N., as well as all my team at Airbus Helicopters, for all the help they gave me during my research. I am happy to have been part of this very nice team.

I would also like to thank the industrial partner we cooperated with during the thesis, for his reactivity and for all his precious advice.

Thanks to Odile, Marion, and my family for the welcome and the desserts. Many thanks to my roommates and all of my friends (from ICA, INSA, Airbus Helicopters as well as the Swing dance team) for the moral support, dancing and laughter. I don't think I could have reached this far without you.

And then, to all the musicians out there, thank you for the music you bring to the world. You certainly don't know it, but you have contributed greatly to the writing of this manuscript.

Préface

Si quelqu'un m'avait dit il y a cinq ans que j'écrirais une préface pour mon manuscrit de thèse de doctorat, je ne l'aurais pas cru. Et bien il semble que, malgré tout, j'ai réellement fait un doctorat... Et il faut bien une préface au manuscrit ! Beaucoup de personnes m'ont soutenue pendant ces années de recherche, et m'ont permis d'aller au bout de ce travail. Je ne peux pas les citer tous et j'espère que personne n'en prendra ombrage.

Je souhaite remercier tout d'abord Pr. Jean-Charles Maré et Gregor Paulmann, qui m'ont toujours poussé à faire mieux, qui m'ont tous deux beaucoup appris et donné tant de bons conseils tant professionnels que privés. Merci de vous être toujours montré attentif à mes idées et ressentis. Je pense être devenue une meilleure personne, certainement plus pragmatique, à votre contact.

Je tiens ensuite à remercier Bruno C., Thomas B. et Olivier N., ainsi que toute mon équipe à Airbus Helicopters, pour toute l'aide qu'ils m'ont fourni pendant ma recherche. Je suis heureuse d'avoir pu faire partie de cette très sympathique équipe.

Je souhaite aussi remercier le partenaire industriel avec qui nous avons coopéré pendant la thèse, pour sa réactivité et pour tous ses précieux conseils.

Merci à Odile, Marion et ma famille pour l'accueil et les desserts. Merci beaucoup à mes colocataires ainsi qu'à tous mes amis (de l'ICA, de l'INSA, d'Airbus Helicopters et du Swing) pour le soutien moral, la danse et les rires. Je ne pense pas que j'aurais pu venir à bout de ce travail sans vous.

Et puis, à tous les musiciens qui vivent et ont un jour vécu, merci pour la musique que vous apportez au monde. Vous ne le savez certainement pas, mais vous avez grandement contribué à l'écriture de ce manuscrit.

Abstract

This dissertation presents a contribution to helicopter axial piston pump monitoring through modelling and simulation. A lumped-parameter model of such pump is developed to serve as a virtual test bench for monitoring studies. As lumped-parameter models of axial piston pumps are less detailed than distributed-parameter models, the author proposes improvements of lumped-parameter modelling state-of-the-art, focusing on the monitoring industrial need. The proposal concentrates on the pressure compensator simulation in degraded conditions, and on the slipper/swashplate leakage computation through a variable gap height. The developed pump model is compared to experimental data. Then, a graphical tool is proposed, which allows for the isolation of pump degradation within the hydraulic system. The study is concluded by recommendations for increasing the maturity level of the proposed monitoring approach.

Résumé

Cette thèse présente une contribution à la surveillance des pompes à pistons axiaux des hélicoptères par modélisation et simulation. Un modèle de pompe à paramètres localisés est développé pour servir de banc d'essai pour les études de surveillance. L'auteure propose des améliorations de l'état de l'art de la modélisation à paramètres localisés des pompes à pistons axiaux, en se concentrant sur le besoin industriel de surveillance. La proposition se concentre sur la simulation du régulateur de pression dans des conditions dégradées, et sur le calcul des fuites de patin/plateau à travers un jeu de hauteur variable. Le modèle de pompe développé est comparé à des données expérimentales. Un outil graphique est ensuite proposé. Cet outil permet d'isoler la dégradation de la pompe dans le système hydraulique. L'étude se termine par des recommandations pour augmenter le niveau de maturité technologique de l'approche proposée.

Content

Preface	1
Préface	2
Abstract.....	3
Résumé.....	3
Content	4
1. General introduction	7
1.1. About maintenance: benefits of monitoring	7
1.2. H/C hydraulics: a help to fly.....	9
1.3. H/C hydraulic pumps and maintenance.....	11
1.4. Manuscript organization.....	14
2. Improvement of lumped parameter modelling of axial piston pumps	15
2.1. Introduction.....	15
2.2. Model architecting	20
2.2.1. Architecting process.....	20
2.2.2. Definition of architecture structure and causality	22
2.3. About Bond-Graphs	25
2.4. Generic L_0^d axial-piston pump model	27
2.4.1. Fluid compressibility.....	28
2.4.2. Flow through orifices.....	28
2.4.3. Generic pump main clearance models	30
2.4.4. Contact management models.....	33
2.5. Improvement of pressure compensator modelling.....	35
2.5.1. Literature review	36
2.5.2. Compensator model for condition monitoring- implementation proposal.....	44
2.5.3. Verification of compensator model and discussion	49
2.6. Proposition of a variable slipper/swashplate gap height model.....	55
2.6.1. Literature review	56

2.6.2.	Variable gap model of the slipper/swashplate interface	59
2.6.3.	Model verification and discussion	67
2.7.	Conclusion	73
3.	Model assessment	77
3.1.	Introduction	77
3.2.	Experiments	78
3.2.1.	Test procedure	79
3.2.2.	Test bench set up	80
3.2.3.	Analysis of the measurements	83
3.3.	Model assessment	94
3.3.1.	Test bench model	94
3.3.2.	Pump model evaluation process	102
3.4.	Conclusion	111
4.	Helicopter axial piston pump monitoring	115
4.1.	General considerations	115
4.2.	Case pressure as a monitoring means	116
4.2.1.	Theoretical considerations	116
4.2.2.	Pump model simulations	117
4.2.3.	Pump vs. hydraulic system degradation	118
4.3.	Feasibility study of the proposed approach	122
4.4.	About implementation on helicopter	132
4.4.1.	Measurement conditions on H/C	132
4.4.2.	Other considerations	133
4.5.	Conclusion	134
5.	General conclusion	137
	References	141
	Abbreviations	148
	Definitions	149
	Nomenclature	150
	List of figures	154
	List of tables	156
	Résumé de la thèse en français	157

Annexes	161
A-1 Test procedure for data gathering	
A-2 Test bench photos	
A-3 Test bench data (hoses and sensor locations)	
A-4 Test pump ATP results	
A-5 Additional graphs from experiments	
A-6 Published papers	

1. General introduction

Prior to anything, it is brought to the readers' attention that the present work is the fruit of the cooperation of the Institut Clément Ader (ICA) public laboratory and Airbus Helicopters (AH), via an Industrial Convention of Training through Research (in French, CIFRE¹). The research, started in May 2017, focuses on monitoring of helicopter hydraulic pumps, with the aid of modelling and simulation. The rationale behind the present research is introduced hereafter. For information, the published scientific documents are provided in Annex A-6.

1.1. About maintenance: benefits of monitoring

Maintenance is defined as “the work needed to keep a road, building, machine, etc. in good condition”². In practice, two main paradigms can be highlighted: unplanned and/or planned maintenance. In the first paradigm, the health of the product is ignored and the product is replaced when it fails. The second one acknowledges that some products (which can be systems, subsystems, equipment, components, etc.) require maintenance. As maintenance is deemed necessary, verifications and modifications are made on the product throughout its *life*³ and usage.

Planned maintenance involves three types of tasks: unscheduled, scheduled and condition-based. Unscheduled tasks are planned but without explicit consideration to product amount of *service* or life. Scheduled tasks are realised according to a schedule that is defined from product use or ageing. Condition-based maintenance tasks are triggered by the evaluation of the product degradation, whether through visual inspection or measurement of variables of interest (i.e. condition monitoring). In that manner, condition-based maintenance tasks are engaged only when necessary, opposite to scheduled tasks. It is to be noted that unscheduled maintenance tasks are equivalent to condition-based ones when the monitored product has failed. It is considered within this dissertation

¹ Conventions Industrielles de Formation par la Recherche.

² Definition supplied by the Cambridge Dictionary.

³ Words written with an italic format are explained in Annex – Definitions.

(although it is not the common definition at AH) that condition-based maintenance tasks are done prior to product failure.

Then, another pair of paradigms can be added to the first one: preventive against predictive maintenance. On the one hand, preventive maintenance aims at avoiding unexpected *failures* by realizing maintenance tasks at fixed interval (service or life). On the other hand, predictive maintenance reduces downtime through optimized maintenance schedule. In this case, maintenance is anticipated by: 1) Monitoring the product condition (taking measurements and deducing health status), 2) Computing the remaining life or service (simulating an evolution model against statistical use rate of the product), and 3) Scheduling the next required maintenance task.

Figure 1-1 is proposed to summarize the described categorisation with two pairs of paradigms and three types of maintenance tasks.

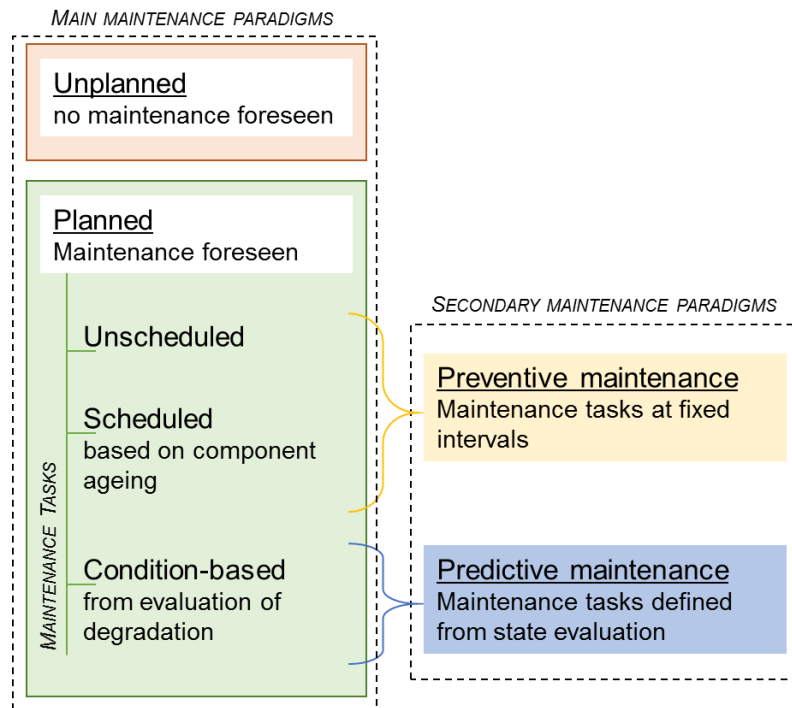


Figure 1-1: Maintenance types as schematics

Preventive maintenance is the most common approach deployed in the aerospace industry to ensure flight safety, including at Airbus Helicopters. The amount of life or service is quantified using calendar time, start/stop cycles, number of landings or flight hours (FH), respectively. In practice, maintenance schedules are defined in terms of inspection intervals, time between overhaul (TBO), etc.

However, unexpected failures may occur. The related maintenance effort can ground a helicopter (H/C) for a long time, even more when the supply chain of

spare parts or work force is disturbed and/or the H/C is operated in a remote place. In this context, introducing predictive maintenance will generate several benefits. By allowing anticipated order of spares and working schedules for crews, it improves aircraft availability and therefore clients' satisfaction. For Airbus Helicopters itself, it increases the current knowledge on the effective service and the condition evolution of the product. Last but not least, it supports the continuous improvement of the design as well as early identification of the most frequent *faults* and *failure mechanisms*.

Several studies have been launched to study and propose condition-based maintenance solutions on H/C, see e.g. (Nesci, et al., 2020). AH has launched several projects to move towards condition-based maintenance. One of them, the present research, focuses on condition monitoring (CM) of H/C hydraulic pumps. The needs for hydraulics on helicopters as well as maintenance of hydraulic pumps are addressed in the next section.

1.2. H/C hydraulics: a help to fly

H/C attitude and trajectory are piloted by actions on the pitch of the main and tail rotor blades. To this end, pilots position three interfaces: the cyclic stick, the collective lever, and the pedals. On smaller helicopters without automatic flight control systems, these actions can be transmitted to the rotors by pure mechanical linkage (i.e. mechanical flight controls) as can be seen on Figure 1-2. However, this is not only signalling because force is required to hold the position of the inceptors and balance aerodynamic loads. For larger weight helicopters equipped with automatic flight control systems for stabilization and guidance, it is no more possible for the pilot/automatic systems to apply and to maintain these forces. Assistance is therefore provided through mechanically-signalled, hydraulically supplied, position servo-actuators. Additionally, hydraulic power is sometimes used to supply some electro-hydraulic actuators that are connected to the mechanical linkage from the pilot to perform stability and control augmentation (e.g. on AS332, Tiger). In H/C with fly-by-wire flight control systems (e.g. NH90), pilot actions are exclusively transmitted through electrical links to servo actuators which remain hydraulically supplied (i.e. electro-hydraulic servo-actuators).

The loss of blade pitch control is mainly classified as a “catastrophic” event. To meet the corresponding reliability requirement ($<10^{-9}$ event/FH), the hydraulic system is made redundant with segregated channels. As such, any failure of a given hydraulic system channel is classified as “major” (reliability target $<$

10^{-5} event/FH) and leads to mission interruption or cancelling which means either un-planned landing if in flight or H/C not available for the mission.

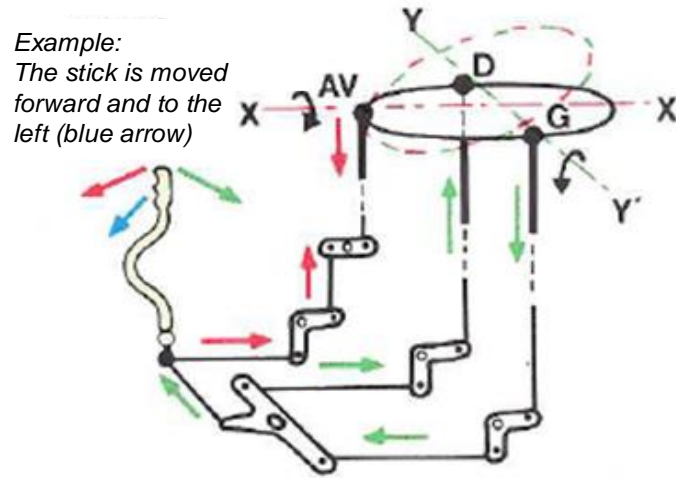


Figure 1-2: Illustration of mechanical linkage from pilot stick to rotor swashplate, adapted from (Raletz, 2009, p. 49)

As displayed by the example given on Figure 1-3, the H/C hydraulic system is composed of generic elements (including main rotor-driven pumps or auxiliary/emergency electro pumps, by-pass valves, filters, check valves, pressure switches, accumulators, etc.) that are combined to meet the functional and the safety requirements. It is worth noting that, on Figure 1-3, left and right hydraulic system are hydraulically independent: a failure in one hydraulic system cannot propagate to the other system.

Hydraulic pumps are the power source of the hydraulic system. As such, any loss of a main pump is classified as “major”, and leads in practice to cancel/abort the mission. Therefore deploying a predictive maintenance approach for hydraulic systems and their pumps in particular is an efficient mean to improve helicopter availability and safe operation. The next section focuses on hydraulic pumps in H/C, giving a glimpse of the importance of their maintenance.

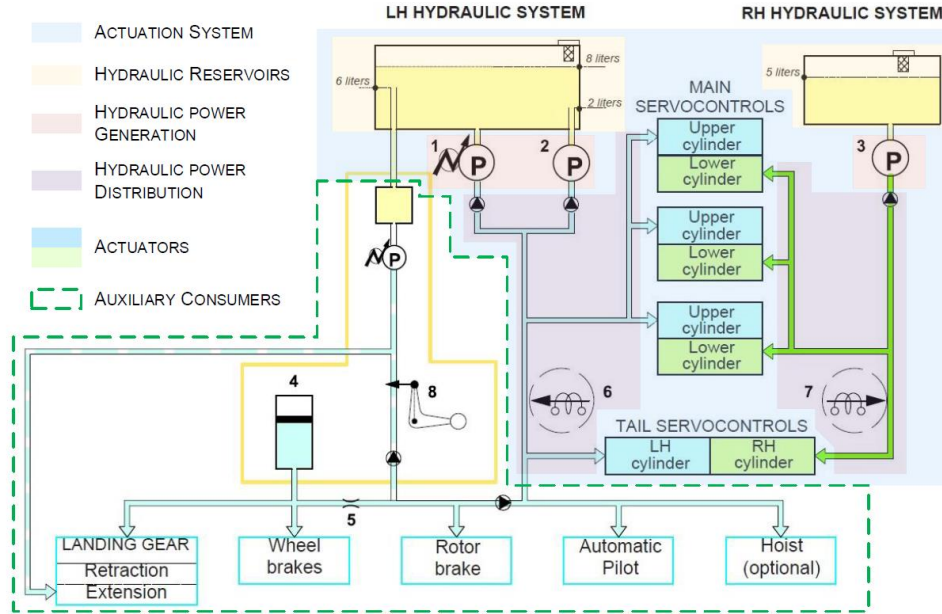


Figure 1-3: Example of a typical H/C hydraulic system (Coïc, 2017)

1.3. H/C hydraulic pumps and maintenance

The main hydraulic pumps used on AH H/C are driven by the engine. In nominal operating conditions, the pump rotating speed is consequently almost constant.

Two pump technologies are used on H/C: gear pumps and pressure regulated axial piston pumps. Compared with axial piston pumps, gear pumps are cheaper and have better reliability due to fewer internal parts. However, in order to provide a constant pressure source, they must be combined with additional components (e.g. pressure relief valve). Due to lower power efficiency and associated additional thermal control demands compared to pressure regulated axial piston pumps, this design is only selected for low power applications.

Pressure regulated axial piston pumps are chosen for high power applications and are the focus of this work. The regulation of these pumps is accomplished by a pure hydro-mechanical mechanism without any electrical element in the control loop. Such type of pump has three main hydraulic ports: suction, discharge, and case drain. The pump sucks in fluid from the tank at suction port and, after pressurization, delivers it into the hydraulic system at discharge port. Dynamic sealing between internal moving parts is performed with resort to calibrated clearances, which also enable lubrication. Consequent leakage flows are collected in the pump case and exit at the case drain port. In that manner, case drain port avoids the case pressure to rise and enables the heat produced by the pump energy losses to be evacuated. Dynamic external sealing is performed between the

rotating drive shaft and the housing. The leakage here is mostly collected and dissipated by the additional seal drain port.

The function of the axial piston pump is to provide the users with fluid at a constant pressure, whatever the demanded flow. As a consequence, pump failure is defined here as the “inability of the pump to keep pressure at rated value in the hydraulic system” in the planned operational range. Pump degradation, prior to failure, can be detected during the overhauls that occur at fixed FH or year intervals. In between overhauls, two events are currently used at AH to try and detect pump failure:

- External droplet leakage at seal drain port observed during a visual inspection. This inspection mainly highlights seal wear, and not the internal state of the pump.
- Spontaneous light up of the “hydraulic pressure” indicator in the cockpit. This event happens when the system pressure goes out of a reference pressure zone for a certain time. However, pump failure is not the only reason for the system pressure rise or to drop (e.g. hose leak). In this light, this indicator only gives the information that something, which might be the pump, has already failed in the hydraulic system.

On latest H/C with increased avionic capabilities, the trend of the hydraulic system pressure evolution is also monitored, giving information of creeping degradation of the hydraulic system. None of these approaches allows to detect pump failure with certainty. As such, there is a need to develop new monitoring approaches for condition-based maintenance of hydraulic pumps on helicopters.

However, the wide range of possible operation environmental conditions (altitude as high as 7000m and temperature from -45 to +50°C) constrains monitoring approaches to solutions that are independent from ambient pressure and temperature. Another point to be considered is the diversity of types, operating conditions, and displacement of pumps. As an example, Table 1-1 illustrates the range of axial piston pumps used in Airbus Helicopter fleet. The aim of the project is to develop a monitoring approach applicable to every axial piston pump of the fleet. As a consequence, any considered monitoring approach must use non pump-intrusive sensors: using intrusive sensors would mean designing the approach for one pump in particular.

Table 1-1: Key figures of axial piston pumps on AH fleet (Paulmann & Mkadara, 2018)

	Flow rate [L/min]	Pressure [bar]	Weight [kg]	Max power consumption [W]
Range	8 to 60	103 to 210	1.1 to 5.6	1700 to 22000

Condition monitoring approaches for hydraulic pumps are already implemented on static applications (e.g. for industrial plant pumps: DMT PlantSafe®,

Prüftechnik Vibnode®). A continuous extensive research work is undertaken to develop fault *detection* and *diagnosis* concepts for hydraulic pumps, e.g. (Succi & Chin, 1996) and (Torikka, 2011). However, in the Airbus Helicopters industrial context, the only necessity is to detect pump degradation on H/C level: there is no need to diagnose which part of the pump is the root cause of its failure.

Pump degradation generally leads to increased internal leakage, loss of pressure, increase of drive torque, abnormal vibration and/or rise of temperature. All five variables impacted by pump degradation (flow, pressure, torque, acceleration, and temperature, respectively) can be used to monitor the pump state.

Temperature measurement is very informative and could be used, but due to complex environmental constraints defined earlier, it was decided to leave it out the current study. This decision also comes from the fact that not all Airbus Helicopter H/C are equipped with temperature sensors in hydraulic systems, which makes the usage of this variable more difficult.

The highly vibratory helicopter environment is hardly reproducible on a ground test bench. As such, accelerations measurement, however commonly used for the study of rotating machinery, was also excluded of the current study.

Finally, drive torque measurement is highly intrusive and cannot be implemented without deep modification of the pump integration, which is why it was also left aside.

In this context and due to the current project constraints, priority has been given in this work to pump leakage monitoring. However, off-the-shelf flow sensors qualified for aerospace applications are rare and non-qualified ones are not accepted on H/C for safety reasons: most flow sensors use turbines put in the stream, that could get blocked by particles and generate unacceptable hydraulic resistance in the hydraulic circuit. Possible fracture of flow turbine, generating additional polluting particles, also has to be considered. The calibration of flow sensors over the larger temperature range of the H/C hydraulic fluid can also be seen as an obstacle. Given these considerations, pressure sensors are seen as the most attractive and feasible monitoring option.

As the overall pump leakage flows at case drain port, this research work aims at investigating pump monitoring through pressure measurement at case port. Thus, the industrial questions that this dissertation has to answer to are the following:

Q1. On H/C, can external case pressure sensors be used to detect pump degradation prior to failure?

Q2. Can pump degradation be *isolated* from hydraulic system degradation when using one additional case pressure sensor only?

The merits of condition monitoring approaches can be assessed using degraded pumps. Unfortunately, the current maintenance process at AH does not make such pumps available for test (without contractual changes between AH, the customers and suppliers). To go around this issue, pumps could be purposely degraded as discussed in Chapter 3. There are several examples of this approach in literature, e.g. (Chen, et al., 2016), however, it is very difficult to artificially create real in-service damage, and/or to cope with the multiple possible permutations of damages. In addition, this option is very destructive and costly. In the end, developing and simulating a realistic pump model has been found the most attractive alternative. Following this choice, scientific questions were identified:

Q3. What is the current state of the art for axial piston pump modelling?

Q4. What improvements can be made from state of the art 1-D pump modelling in the view of condition monitoring and what do those improvements bring?

Q5. Is the pump model, running a simulated test in given operating conditions, able to reproduce the same result data and patterns as real tests made in the same operating conditions?

The research work performed to answer all scientific and industrial questions is reported in the following dissertation, using the structure introduced in the section 1.4.

1.4. Manuscript organization

In order to answer the five highlighted questions, the manuscript is organized as follows.

The discussion is opened on scientific questions in the **second chapter**, where improvements of the current axial piston pump lumped-parameter models state of the art are implemented and discussed.

The **third chapter** focusses on model validation to answer the question Q5.

Then the **fourth chapter** answers the industrial questions on the basis of the developed and validated models.

2. Improvement of lumped parameter modelling of axial piston pumps

2.1. Introduction

Most of the hydraulic axial piston pumps used on H/C are engine gearbox-driven, variable-displacement, and hydro-mechanically pressure-compensated (see pump cut displayed on Figure 2-1). The shaft **1** is driven by an external source of mechanical power (the main gear box), leading the barrel **2** into rotation with respect to the pump housing. The pistons **3**, being placed inside the barrel cylinders, are forced into a combined rotating-translating motion due to their link to the inclined swashplate **4** through the slippers **5**. The pistons translation inside the barrel allows for the suction and discharge of the fluid through the barrel and valve-plate ports (not explicit on Figure 2-1 but marked **6**). The swashplate tilt, setting the pump displacement, is controlled through the pressure compensating device, composed of a compensating valve **7** supplying flow to the stroking piston **8** that reduce swashplate tilt when in extension. The last part of the compensating mechanism is the rate piston **9** that tends to push back the swashplate to full displacement position in the pump housing (or case) **10**. This pressure compensation mechanism makes the pump a source of near constant pressure.

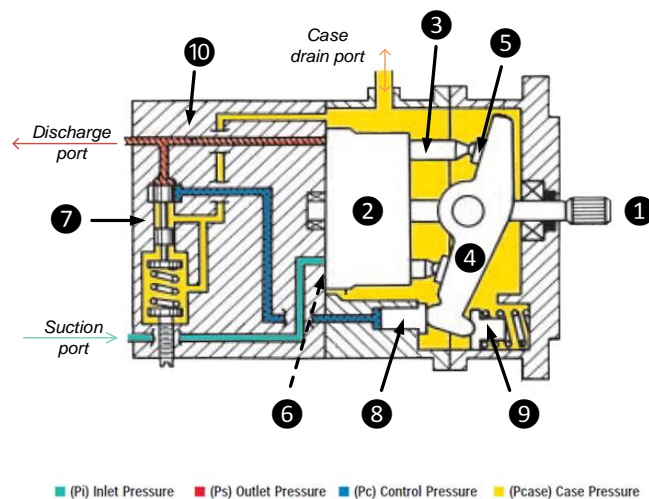


Figure 2-1: Cut scheme of an axial piston pump, based on (Eaton Corporation, 2000)

The pump parts are completely immersed in hydraulic fluid inside the pump case. Designed-in leakages flow to the pump case and exit the housing at case drain port (as explained in section 1.3). There are many contact pairs between moving bodies: piston/barrel, barrel/valve-plate, piston/slipper, slipper/swashplate, stroking piston/case, rate piston/case, and compensating valve spool/case. They are lubricated through calibrated gaps. An increase of these built-in gaps and clearances intensifies the pump leakage, and provides an image of the pump wear.

A pump simulation model is developed to serve as a virtual test bench for the study of pump leakage through pressure measurement. This pump model is based on one of the H225 pumps, which characteristics are given on Table 1-1 hereafter. These characteristics originate from Acceptance Test Procedure (ATP) specifications, which define the proper behaviour of the pump upon reception by AH. During the acceptance tests, performed on each produced pump, key functions of the pump are obtained to demonstrate conformity of a production pump to characteristics of the pumps used for qualification.

Table 2-1: H225 axial piston pump steady state characteristics during ATP

Operating conditions	Zero flow	Full flow
Discharge pressure [bar]	175 ± 2	Min 160
Discharge flow [L/min]	0	27.0–28.0
Case drain pressure [bar]	0.8-1	0-1
Case drain flow [L/min]	0.3-1.5	Max 1.5
Fluid temperature [°C]	60 ± 5	

Several approaches exist when considering modelling. Two main paradigms can be highlighted: data driven models or physics-based models.

Data-driven (or knowledge-based) models are constructed from history data measured on the monitored system, and do not need any information about the system inner workings. On the contrary, physics-based models require a deep understanding of the system physics. In between both paradigm lay mixed approaches. Due to lack of history data, data-driven approaches are not implementable. Consequently, a physics-based approach is chosen.

In the physics-based paradigm, lumped-parameter approaches are distinguished from distributed-parameter approaches. Several model classifications exist: static or dynamic models, lumped or distributed, against geometrical dimensions, etc.

A generic way to classify them all could be to change the usual short identification of the model type (0-D, 1-D or 3-D with D understood as geometrical Direction) which is often source of discussion and lack of mutual understanding, to a new approach. Here we propose the notation X_z^y where X is either L(umped) or D(istributed), y is either s(tatic) or d(ynamic) and z

corresponds to the number of spatial dimensions considered for the variation of a physical variable. For example, a static lumped parameter model is classified as L_0^s while a distributed-parameter model of the flow in a pipe simplified in 2-D with temporal variation of the upstream pressure will be classified as D_2^d .

An extensive work has been done using lumped and distributed approaches for axial piston pumps. Table 2-2 shows that model purposes drive the choice of the modelling approach in literature.

Table 2-2: Examples of lumped and distributed parameters modelling approaches in literature

	Lumped parameters	Distributed parameters	Mixed
Study of design		(Wieczorek & Ivantysynova, 2002) (Pelosi & Ivantysynova, 2009) (Ivantysynova & Baker, 2009)	
Study of lubrication phenomena		(Chao, et al., 2018)	
Development of analytical models	(Bergada, et al., 2012)		
Comparison of approaches	(Corvaglia & Rundo, 2018)	(Corvaglia & Rundo, 2018)	
Study of interactions with hydraulic system	(Aaltonen, 2016)		
Use of model for definition of Health Monitoring approaches	(Bayer & Engen-Rosenblatt, 2011)		
Software applications			(Deléchéle, 2019)

In the light of physics-based approaches, AH does not need a highly detailed D_V^d model, which would generate high computational loads, but a system-level one that can be interfaced with already existing hydraulic system models. This point had driven the choice of a lumped-parameter approach for the present project.

However, when considering leakage modelling, L_0^d models are very light compared to D_V^d (Computational Fluid Dynamics or CFD models in fluid mechanics) models, as can be seen on Table 2-3. A void cell means that no explicit mention of the physical effect is made in the cited paper.

Table 2-3: Comparison of 3-D and 0-D models considering the pump main leakage paths

Interface	Physical effect considered	(Wieczorek & Ivantysynova, 2002)	(Pelosi & Ivantysynova, 2009)	(Ivantysynova & Baker, 2009)	(Chao, et al., 2018)	(Bergada, et al., 2012)	(Aaltonen, 2016)
(1) : Piston/barrel type	Tilt	O	O				
	Axial relative velocity	O	O			⊥	Δ
	Eccentricity	O	O				Δ
	Spin		O				
	Hydrodynamic forces	O	O				
	Varying gap length	O	O				
	Variable gap height	O	O				
	Solid to solid contact	O	O				
	Local thermal effects	O	O				
	Elastic deformations		O				
(2) : Slipper/swashplate	Tilt	O			O	⊥	
	Relative velocity	O			O	⊥	
	Spin				O		
	Hydrodynamic forces	O					
	Variable gap	O			O		
	Solid to solid contact	O					
	Local thermal effects	O					
	Elastic deformations						
(3) : Barrel / valve-plate	Tilt	O		O		⊥	Δ
	Relative velocity	O		O		⊥	Δ
	Timing grooves					⊥	
	Hydrodynamic forces	O		O			
	Variable gap	O		O			
	Solid to solid contact	O					
	Local thermal effects	O		O			
	Elastic deformations			O			

Legend:

Δ	Lumped parameters	O	Distributed parameters
Δ	Compared to experiments	<i>O</i>	Compared to CFD models

The observation of Table 2-3 gives rise to the scientific questions drawn in section 1.3 and reminded hereafter:

Q3. What is the current state of the art for axial piston pump modelling?

Q4. What improvements can be made from state of the art 1-D pump modelling in the view of condition monitoring and what do those improvements bring?

Q5. Is the pump model, running a simulated test in given operating conditions, able to reproduce the same result data and patterns as real tests made in the same operating conditions?

In this chapter, scientific questions Q3 and Q4 are answered focusing on two pump mechanisms (pressure compensator and slipper), and improvements of the current state of the art of lumped-parameter modelling for axial piston pumps are discussed.

Scientific questions must be answered to. However, it is to be reminded that the model is initially developed to answer industrial questions. Thus, the model must meet industrial requirements with priority. The said requirements are defined in Table 2-4, where two types are highlighted: requirements from project purpose and requirements for *durability*. Durability is a very important consideration in the industry, where cooperation is needed in the everyday-work. It is very frequent for models to be shared with other company departments. Models can also be improved by several persons throughout their life, and it frequently happens that the final user of the model is not the model creator. However, the usual model development process (through step-by-step improvement) leads to prototype-like models. This type of model is hardly readable for any person other than the model creator.

Table 2-4: List of requirements for the pump model

Project Purpose	
Rq1	Shall simulate accurate behaviour for internal leakage, as well as suction and discharge pressure and flow
Rq2	Shall be ready for simulation of pump degradation leading to increased internal leakage
Rq3	Shall enable to assess the monitoring approach
Durability	
Rq4	Shall be as generic as possible for further modifications, easy to assemble and modify (e.g. changing the number of pistons)
Rq5	Shall allow for parameters and mathematical expression modifications
Rq6	Shall grant easy access to the basic components of the model
Rq7	Shall be usable as a digital twin, also as “plug and simulate” (only applicable to the whole pump model)

While Table 2-4 requirements defined under “project purpose” must be met through relevant modelling, “durability” requirements can be met through a proper model architecture. In the following section 2.2, the definition of the model architecture is presented. Section 2.3 gives basic information about Bond-Graphs, which formalism is used throughout this chapter to generated and explain the proposed models, and section 2.4 about generic lumped-parameter axial piston pump models. Then, sections 2.5 and 2.6 are focused on improvements to be made on the pressure compensator mechanism and on the slipper/swashplate interface

using the lumped-parameter approach and in the frame of condition monitoring. Finally, the chapter conclusion is given in section 2.7.

2.2. Model architecting

Model architecting is seldom discussed in literature as it a product of pragmatism. When architecture is needed, it is generally managed implicitly through the modellers' experience. Distributed parameters models have explicit architecture as they tend to be the perfect image of the real product. This is not the case of lumped-parameters models. In the case of the latter, a few published papers show architected models without discussing architecting or structuration methodology, e.g. (Poole, et al., 2011) or (Mancò, et al., 2002). In (Maré & Akitani, 2018), the authors define an electro mechanical actuator model architecture derived from the product topology. The author of (Maré, 2019), after defining “Workshare” and “Capitalization” requirements, emphasizes that a topology-based architecture allows to partially meet those requirements as it helps model understanding and reuse. Then (Mkadara & Maré, 2020) stated that architecture should be fixed during the first phases of a project, however anticipating future modifications.

2.2.1. Architecting process

Model architecting is the process of suggesting/offering a structure to something that is initially abstract. Doing so, one must think about the elements that compose the structure and the links between them. In this dissertation, it is chosen to define the structure elements as “blocks”, and the links as “interconnections”. Blocks are box-like objects, meant be filled with models. Nevertheless, architecture must be defined in the early phases of a project. Thus, blocks must be ready for any evolution or upgrade: every possible interconnection to another block, through “ports”, must be prepared. A port is a lumped interface of a block to another, through which the interconnection passes.

Figure 2-2 illustrates a block that would contain a complete pump model. This pump block shows every pump ports and interfaces, including dynamics of the housing:

- For hydraulics: Suction (*s*), Discharge (*d*), and Case ports (*c*) with pressure (P_x) and volume flow rate (Q_x) at each port;
- For mechanics: Drive shaft (*m*) and Base (*b*) ports, with Torque (Γ_x) and angular velocity (ω_x) at each port;
- The thermal port with temperature (T_x) and heat flux (Φ_x) power variables.

The orientation of the arrows on Figure 2-2 shows the power positive sign convention.

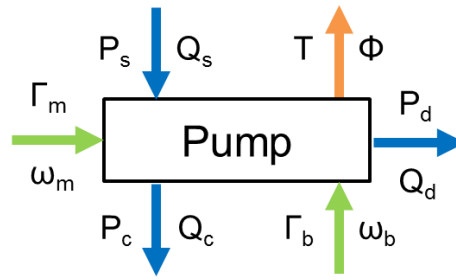


Figure 2-2: Pump block illustration

Blocks are prepared for any model. However, it is possible to fill the blocks with very simple models, leading to completely or partially unused ports. For example, one could develop a purely hydraulic model. In this case, the thermal port and the base mechanical port of Figure 2-2 would be completely unused. The drive shaft mechanical port would be partly used as only rotating speed is needed to model the pumping motion, and the torque is of no interest.

With the formalism of Figure 2-2, a completely used port means that the interconnection is of power type. Partially used ports are most likely to be used with signal type interconnections. If possible, explicit distinction between both types should be made. In addition, it is better to represent the architecture so as to visually distinguish technical domains as illustrated on Figure 2-2. In this dissertation, the colour code used for this differentiation is the following:

- shades of green highlight the mechanical domain;
- dark blue is used for hydraulics;
- orange is for heat transfer;
- red shows signal/control domain (not used on Figure 2-2);

Figure 2-3 summarizes the architecting process with regards to the complete model development process. The first step of this process is to define the structure outline. This step is discussed in the following section.

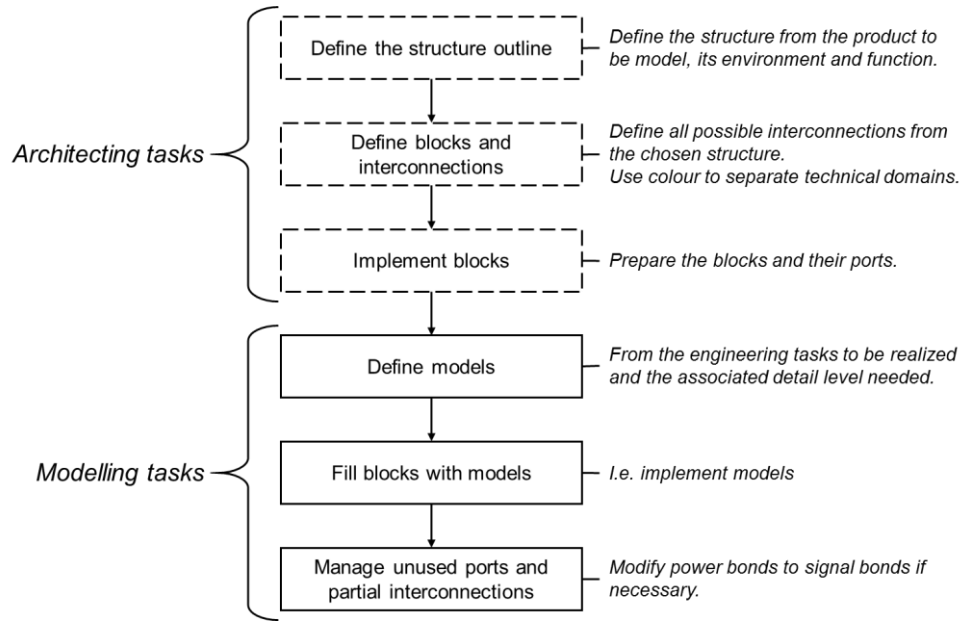


Figure 2-3: Architecting process proposal

2.2.2. Definition of architecture structure and causality

The structure of the model architecture answers the question: how can one make a coherent ensemble of the to-be-modelled product subparts? Two options are presented hereafter: a structure based on subpart function or on product topology.

The pump topology is shown on Figure 2-4-a. Figure 2-4-b and Figure 2-4-c illustrate both options for model structure (by function or topology, respectively) applied to it. For the sake of clarity, only mechanical and hydraulic interconnections are shown on these figures. The “pump block” is represented by a dotted box to highlight the pump and the complete model interfaces.

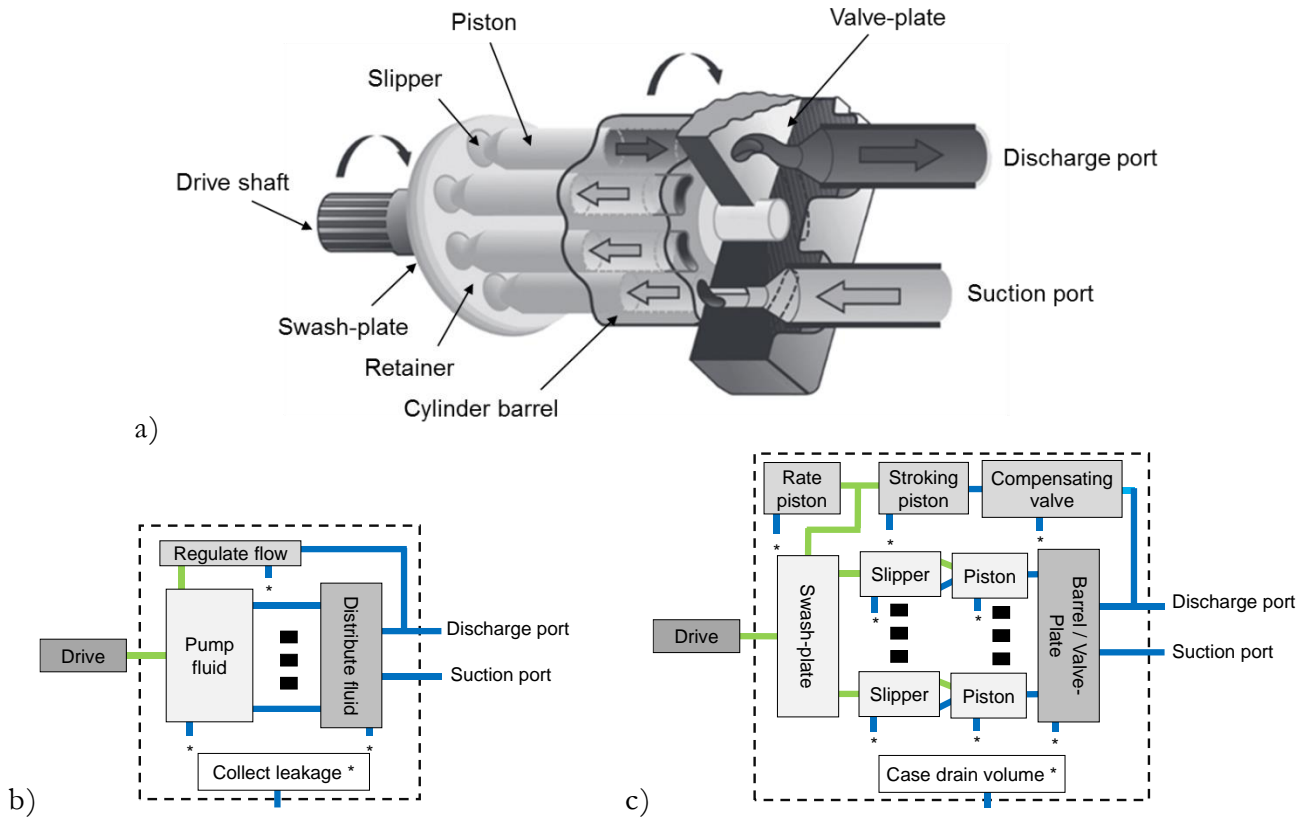


Figure 2-4: Proposition of architecture structures

a) Pump transparent view. b) Structure by function. c) Structure by pump part.

It was previously discussed that durability requirements can be answered by a well-defined architecture. These requirements drive the final choice of an architecture. The structure by function (Figure 2-4-b) is simpler in appearance than the topological one (Figure 2-4-c), which increases its attractiveness.

Requirement Rq4 of Table 2-4 (p. 19) asks for easiness of model (and structure) modification. To this end, at least one block per pump part should be defined, the interconnections with other blocks must be straightforward and the architecture prepared for future modifications. The model structure is constructed as a matryoshka doll: with blocks inside other blocks. Consequently, pump part blocks could be included in the function blocks.

In order to grant easy access to the models (as required by Rq6), the architecture should be less than two-blocks deep. It means that the models must be available opening two blocks at most, including the pump block, as illustrated by Figure 2-5. In the light of these two requirements, the structure by function is ruled out and a topology-based architecture is implemented.

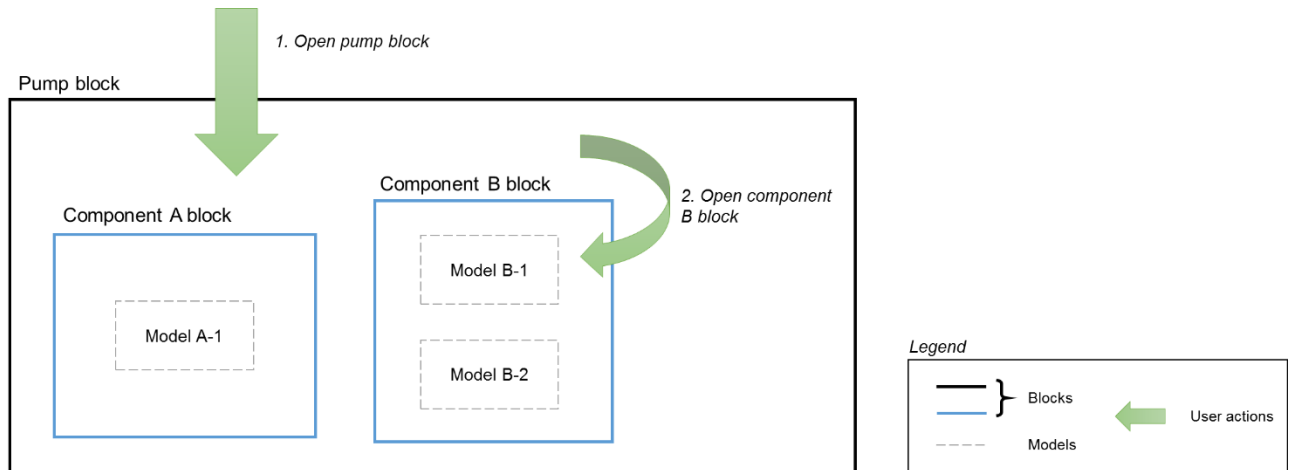


Figure 2-5 : Illustration of a “matryoshka” block

The model is implemented in a causal commercial simulation environment, which can generate causality constraints. Causality comes from the concept of cause and consequence. In modelling and simulation, causality is about defining the sequence of computation. Taking the example of Newton’s second law, it is possible to compute a body velocity when all forces applied on the said body are known. On the other hand, knowing velocity, and all forces on a body except one, it is possible to compute the missing force. In a causal simulation environment, the sequence of computation is pre-defined. In a non-causal simulation environment, the solver deals with the model equations resolution by itself during computation, given known variables. A-causality can be seen as the best option for a simulation environment, as the user does not need to manage sequences of computation. However, letting the software manage them on its own may cause increased computation times (e.g. due to the presence of algebraic loops). As such, causal simulation environments are unavoidable for real-time simulation applications, in which sometimes complex models are expected to run synchronously to other systems, for example in flight simulators.

In the present project, the model implementation environment, Simcenter AMESim, is causal. It means that once the model is implemented in the defined blocks of the architecture, the blocks causalities are frozen.

The example of the swashplate is taken to illustrate this statement. In a variable displacement axial piston pump, the swashplate is actuated by the stroking and rate pistons, in order to tilt it and modify the pump displacement. The swashplate block proposed in the present study (for a variable displacement pump) is interconnected mechanically to stroking and compensating pistons blocks. Causality-wise, force must be supplied to the swashplate block at both mechanical interfaces. In the case of a fixed displacement axial piston pump, the swashplate angular stroke is limited by end-stops, which counterbalance any force aiming to tilt the swashplate. To model such a pump, the most straightforward approach

would be to supply a fixed tilt value to the rest of the pump model through a signal link. In this case, the swashplate block could be reduced to a signal duplicator, which transforms one incoming tilt information into n outgoing information, one per piston. The causality of a block is frozen as soon as it is filled with a model. Deleting the model does not remove the causality of the block. As such, if one would want to reuse the proposed swashplate block for a fixed displacement axial piston pump simulation model, one would need to use the mechanical interfaces of the presented block towards stroking and compensating pistons, and to follow the defined causality (force supplied to the block).

As a conclusion, it is to be remembered that the choice of the architecture (definition of blocks with ports and interconnections), and its alliance with the models, result in fixed blocks that can only be reused as are.

2.3. About Bond-Graphs

Bond-Graphs (BG) are oriented graphs showing the energy and information transfers from one system or object to another. It was first introduced by: (Paynter, 1961). BG are mainly meant to model the dynamics of power systems with a lumped parameters approach.

The BG formalism is widely spread due to its following benefits: it is usable (and the formalism is the same) for any physical domain, it helps understanding power paths, and enables simulating multi-domain systems without necessarily writing all equations, while effectively allowing for identification of the said mathematical equations. BG are used mainly in modelling, control, monitoring and diagnostic (e.g. (Khemliche, et al., 2004) and (Coïc, 2017)). In this dissertation BG are used to define the proposed models and to help the identification of the necessary model modifications to be made when considering condition monitoring.

The process of BG creation is not detailed in the body of this dissertation, the reader should refer to literature like (Thoma, 1975) or (Dauphin-Tanguy, 2000) if he/she ever needs more information about Bond-Graphs. However, the main components of BG modelling used in this dissertation are highlighted in Table 2-5 based on (Maré, 2015), with examples from several physical domains.

Table 2-5: Basics of Bond-Graph elements

BG component	Domain Description	Electricity	Hydraulics	Translational Mechanics
Flow F	Power variable	Current	Volume flow rate	Velocity
Effort E	Power variable	Voltage	Pressure drop	Force
Dissipative element R	Dissipates energy, with algebraic relation between effort and flow	Resistance	Short orifice	Friction
Capacitive element C	Stores and restores energy. The energy is stored as a function of displacement (integral of flow)	Capacitance	Domain of compressible fluid	Spring
Inertial element I	Stores and restores energy. The energy is stored as a function of momentum (integral of effort)	Inductance	Hydraulic inertia	Inertia
Transformer TF	Two port element used for ideal power transmission or conversion of k coefficient.	Examples: Hydraulics/mechanics: pistons Mechanics/mechanics: gear box, lever arm		
Gyrator GY	Two port element used for ideal power transmission or conversion of k coefficient.	Examples: Electricity/mechanics: electric motor Hydraulics/mechanics: hydraulic motor or pump Mechanics/mechanics: gyroscope		
0 Junction	Multiport balance of flux, all effort variables are equal	Kirchhoff's law	Mass conservation	Ex: spring damper system in series
1 Junction	Multiport balance of effort, all flux variables are equal	Kirchhoff's voltage law	Ex: actuator with double hydraulic chambers and same symmetrical piston area	Newton's second law

“Flow” and “effort” power variables are sometimes respectively classified as “through” and “across” variables, which use is anterior to the development of bond-graphs. The Bond-Graph formalism allows for describing dynamic systems of several physical domains with the same elements. However, it is said that two systems of analogous schematics diagrams have analogous Bond-Graphs only if the flow variable is “that variable which is divided between parallel elements in the system” (Fairlie-Clarke, 1999). In that case and contrary to Table 2-5, the mechanical force should be considered as the flow variable. It was proposed by (Fairlie-Clarke, 1999) to use the term “potential” variable instead of “effort”, in order to make the analogy between force and the flow (through) variables clearer.

Despite this discussion, the use of mechanical force as an effort variable is currently widely spread in literature. In this dissertation, force is considered an “effort/across” variable, while velocity is a “flow/through” variable.

In some cases, the Bond-Graphs elements R, TF and GY can be “modulated”. When it is the case, the letter “M” is put before the element (e.g. MTF). This modulation is used when the component behaviour depends on variable external

parameters, and allows to go from signal to power domain. Literature strongly advises against modulating energy storing elements (I, C), as it could fail in complying with the law of energy conservation (Dauphin-Tanguy, 2000).

In BG, power flows are highlighted by half arrows that indicate their sign convention. The convention used in this document is to write the flow on the same side as the half arrow. To distinguish them from power-bonds, signal (or information) bonds bear a full arrow. When necessary, bond causality is marked on the power half arrow using a perpendicular straight line. The line is put on the side of the arrow which receives the effort (i.e. which supplies the flow) for computation of the model. Figure 2-6 shows the different bonds that will be used in this dissertation. Figure 2-6.c) shows a causal power bond. In this example, the model on the right hand-side of the bond receives the flow (v) and returns the effort (F) to the model on the left hand-side of the bond. I and C have preferred causality to avoid numerical derivation. Non-linear R elements may have preferred causality to allow computation. Going against them require derivation in simulation instead of integration, which generally reduce accuracy and/or introduces phase lag.

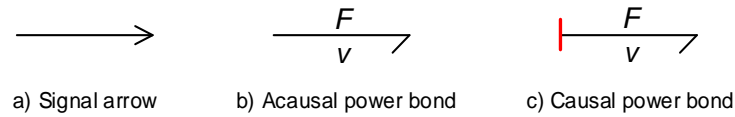


Figure 2-6: Examples of bonds used throughout the dissertation

BG can be simulated in directly graph form using BG-oriented software like 20-sim, see (20-sim) reference, or after extraction of equations, e.g. in Matlab/Simulink. The BG formalism focusing of power flows is also the base of some well-established software in the industry, for example Simcenter AMESim or Dymola.

2.4. Generic L_0^d axial-piston pump model

In the lumped-parameter modelling paradigm, the real distributed behaviour of a system is approximated by discrete elements. In the case of hydraulic equipment or systems, flow passages (including leakage paths) are modelled as local orifices and an equivalent domain pressure is computed considering fluid compressibility. Mechanical bodies are considered rigid and are taken into account through their inertia, while contacts between them can be approximated as spring-dampers. In this section, generic models of the local elements are discussed.

2.4.1. Fluid compressibility

The compressibility coefficient β of a fluid highlights its tendency to change volume (V) due to pressure (P). The isothermal compressibility coefficient of a fluid is written as follows:

$$\beta = -\frac{1}{V} \left(\frac{dV}{dP} \right)_T \quad (2-1)$$

The fluid bulk modulus B is the inverse of the compressibility coefficient. For hydraulic fluids used in aerospace, fluid bulk modulus is theoretically large. E.g. for fluid MIL-PRF-83282, the isothermal bulk modulus ranges from 8000 to 18000 bar for fluid temperatures between 40 and 150 °C and pressures from 0 to 550 bar (rel) (SAE International, 2000). However, fluid compressibility depends on the free air or gas content. In practice, it is possible to simulate air pollution and its effect on a hydraulic system performance through reduction of the fluid bulk modulus parameter.

The pressure of a given fluid domain is linked to the flow and volume balance in this domain, considering fluid compressibility. It is modelled following the equation hereafter. By convention, flow or volume entering the domain are positive, otherwise negative.

$$\frac{dP}{dt} = \frac{B \sum_i Q_i}{Vol} \quad (2-2)$$

where:

- Q_i volumetric flow rate in/ing/outing the fluid domain [m^3]
- t time [s]
- Vol current fluid volume in the domain [m^3]

2.4.2. Flow through orifices

(Meritt, 1967) models the steady state flow Q of an incompressible fluid through an orifice with the following equation:

$$Q = C_d A \sqrt{\frac{2}{\rho} (P_0 - P_1)} \quad (2-3)$$

with:

- ρ fluid density [kg/m^3]
- A orifice passage area [m^2]
- C_d orifice discharge coefficient [-]
- P_0 orifice upstream pressure [Pa]
- P_1 orifice downstream pressure [Pa]

In the absence of more accurate data, the discharge coefficient can be defined through an asymptotic model as a function of the Reynolds number Re (Viersma, 1961) as per equation (2-4).

$$C_d = \begin{cases} \delta_{Re} \sqrt{Re} & \text{if } Re < Re_t \\ C_{d\infty} & \text{if } Re \geq Re_t \end{cases} \quad (2-4)$$

With:

- δ_{Re} laminar flow coefficient of the orifice [-], dependent on geometry
- $C_{d\infty}$ limit discharge coefficient [-]
- Re_t transition Reynolds number [-], defined as per equation (2-5) (Viersma, 1961).

$$Re_t = \left(\frac{C_{d\infty}}{\delta_{Re}} \right)^2 \quad (2-5)$$

In practice, the discharge coefficient C_d , which is difficult to measure, is replaced by the flow coefficient C_q which value is very close to that of C_d and follows the same asymptotic model (Mc Cloy, 1968).

The model (2-3) of the flow through an orifice as several shortcomings: a) it does not account for the possible flow inversion generated by a downstream P_1 greater than the upstream pressure P_0 , b) the computation assumes an incompressible fluid, when it is in reality compressible. The first shortcoming can be tackled through the use of the pressure difference absolute value and applying the pressure difference sign to the computed flow. The second drawback of the model can be overcome via the correction of the flow by the fluid density. Coupling both solutions leads to equation (2-6), used in Simcenter AMESim (LMS AMESim, 2015). In AMESim, flow is computed at a mean fluid density, then brought back at the correct value at each orifice port with the corresponding density. Doing so, flow conservation is ensured.

$$Q = C_q A \frac{\rho}{\rho(0)} \sqrt{\frac{2}{\rho} |P_0 - P_1|} \operatorname{sgn}(P_0 - P_1) \quad (2-6)$$

With:

- ρ fluid density at pressure $(P_0 + P_1)/2$ [kg/m³]
- $\rho(0)$ fluid density at the reference pressure [kg/m³]

One computational problem arises when using equation (2-3) or (2-6), which is due to the definition of the flow coefficient C_q . This coefficient is a function of the Reynolds number, which itself depends on the flow rate. This interdependence generates in practice an algebraic loop during simulation. To cut the algebraic loop, C_q can be computed as a function of the maximum flow coefficient $C_{q\infty}$. For

example in Simcenter AMESim, transition from zero to this maximum coefficient is made through an hyperbolic tangent of the flow number λ .

$$C_q = \begin{cases} C_{q\infty} \tanh\left(\frac{2\lambda}{\lambda_{crit}}\right) & \text{if } \lambda \leq \lambda_{crit} \\ C_{q\infty} & \text{if } \lambda > \lambda_{crit} \end{cases} \quad (2-7)$$

Where:

λ_{crit} critical flow number at which flow changes from laminar to turbulent
[-]
 $C_{q\infty}$ limit flow coefficient [-]

The flow number is computed as a function of the pressure difference following the next equation (MacLellan, et al., 1960):

$$\lambda = \frac{h_d}{\nu} \sqrt{\frac{2}{\rho} |(P_0 - P_1)|} \quad (2-8)$$

With:

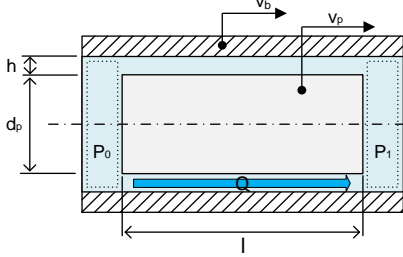
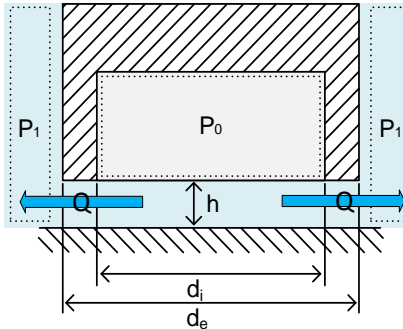
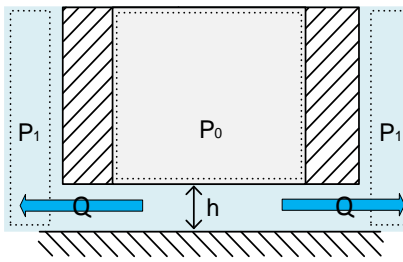
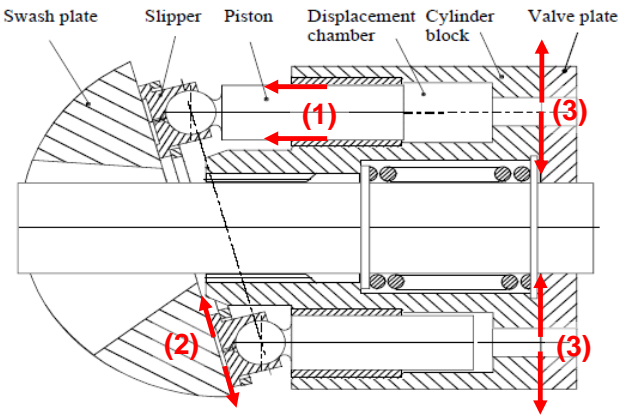
h_d hydraulic diameter [m]
 ν fluid kinematic viscosity [m²/s]

2.4.3. Generic pump main clearance models

Every clearance can be modelled as an equivalent orifice. However, each clearance has its own distinctive geometry, leading to the declination of several models in literature. In (Mkadara & Maré, 2020), the authors summarize the well-known lumped-parameter models relative to the generic leakage sources that appear in pressure-compensated axial-piston pumps. Although several leakage paths exist at barrel/valve plate interface, only the leakage from a valve plate port to the case is considered in Table 2-6.

As leakage type (1) of Table 2-6 on the next page can be used for several parts of the pump (e.g. the pistons, stroking and compensating pistons), it is discussed in details hereafter with inclusion of eccentricity.

Table 2-6: Generic main pump leakage lumped-parameter models

Leakage	Generic form of the leakage	Analytical formulation (Ivantysyn & Ivantysynova, 2003)
(1) Annular leakage with variable length: Pistons / housing		For a centred piston with speed and no spin: $Q = \frac{\pi}{6\mu} \frac{P_0 - P_1}{l} r \left(\frac{d_p}{2} \right)^3 + \pi \frac{d_p}{2} (v_b + v_p) h$ <p>Where d_p is the piston diameter, h the gap height, v_p the piston velocity, and v_h the housing velocity, P_0 and P_1 the chamber and case pressures respectively.</p>
(2) Hydrostatic bearing: Slippers		Laminar flow and logarithmic variation of the pressure along the radius, without spin or tangential velocity: $Q = (P_0 - P_1) \frac{\pi h^3}{6\mu \ln \left(\frac{d_e}{d_i} \right)}$ <p>Where h is the gap height, d_e and d_i the bearing external and internal diameter respectively, P_0 and P_1 the internal and external bearing pressures respectively.</p>
(3) Valve-plate / barrel		Laminar flow, barrel not tilted and relative speed not considered: $Q = (P_0 - P_1) \frac{\pi h^3}{12\mu} \int \frac{1}{l} d\gamma$ <p>Where P_0 is the port pressure, P_1 the case pressure, h the gap height and l and γ geometrical features depending on barrel angular position.</p>
		

In order to avoid any non-linear friction, sealing at pistons is achieved with resort to low clearances, only. This is paid by leakage that reduces the volumetric efficiency. The common model considers that the piston and housing axes are parallel, making an annular gap, as illustrated by Figure 2-7. It also assumes the leakage flow to be laminar in steady-state conditions.

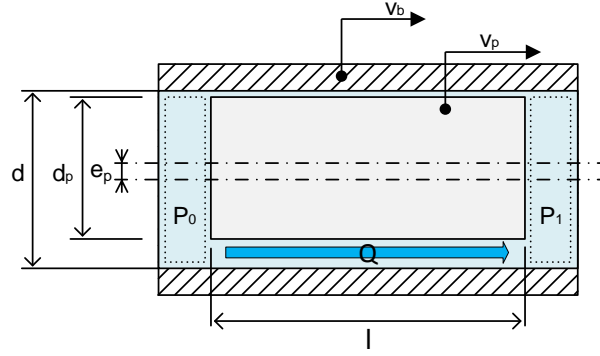


Figure 2-7: Schematics of an eccentric piston in a bushing with annular leakage

These assumptions enable getting a formal model from the Navier-Stokes equations giving, based on (Blackburn, et al., 1960), for a pressure and velocity induced flow in an annular passage:

$$Q = -\frac{(P_0 - P_1)}{12\mu l} b^3 \pi d_b \left(1 + \frac{3}{2} \left(\frac{e_p}{b}\right)^2\right) + \frac{(v_b + v_p)}{2} b \pi d_b \quad (2-9)$$

where:

- μ absolute viscosity of the fluid [Pa.s]
- b radial clearance between piston and bushing [m]
- d_b bushing diameter [m]
- e_p eccentricity of the piston in the bushing [m]
- l length of the piston in the housing [m]
- P_0 upstream pressure [Pa]
- P_1 downstream pressure [Pa]
- v_b housing absolute velocity [m/s]
- v_p piston absolute velocity [m/s]

The clearance b between piston and housing is defined as $\frac{d_b - d_p}{2}$, where d_p is the diameter of the piston. This model is implemented in Simcenter AMESim within the HCD (hydraulic component design) library.

Frictional losses on the moving body (here the piston) due to pressure difference and relative velocity is adapted from the force model from the fluid flow between a moving plates, see e.g. (Blackburn, et al., 1960), and written as:

$$F_{/p} = -\pi b \frac{d_p}{2} (P_0 - P_1) + \mu l \frac{\pi d_p}{b} (v_p - v_b) \quad (2-10)$$

One drawback of equation (2-10) is that shaft eccentricity in the cylinder is not considered. A model which includes the effect of eccentricity is proposed in (Linköping University, 2008):

$$F_{/p} = -\pi b \frac{d_p}{2} (P_0 - P_1) + \mu l \frac{\pi d_p}{b \sqrt{1 - \left(\frac{2ep}{d_p}\right)^2}} (v_p - v_b) \quad (2-11)$$

Equations (2-9) and (2-11) show that in this case, mechanical and hydraulics domains are intertwined. Relative velocity is necessary to compute the flow rate while the pressure drop within the annular gap is needed to compute the friction force. This is traduced in Bong-Graph theory as an “R field” and is illustrated on Figure 2-8 with causality.

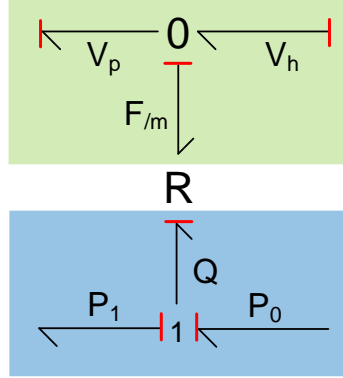


Figure 2-8: Annular gap model as an "R field" in Bond-Graph theory

It was mentioned that this model, with parallel piston and housing axes, is the common lumped-parameter one. It does not take into account the effects of the possible piston tilt and rotation in the bushing on flow and force. Both effects are the result of all pressure, friction and mechanical forces applied to the piston. Correctly introducing the piston tilt and rotation effects on the gap flow and friction force asks for much more detailed models as shown by the literature (see abstract in Table 2-3 p18).

2.4.4. Contact management models

In this section the focus is put on models for the modelling of contacts between bodies in lumped-parameter literature.

Mechanical linkage between two bodies can be modelled following two ways: permanent contact or possible play. In the first case, and in the lumped-parameter paradigm, it is generally assumed that the bodies permanently in contact are both non-deformable and that the displacement of one is equal to that of the other.

In the second case, both bodies can be sporadically separated. Then, two states can be defined: two objects in contact / two objects free from each other. A transition model between both states must be integrated, to deal with discontinuities in force and displacement vs. actual state. In this dissertation, this type of models is referred as “contact management” models.

Contacts forces have two components: the normal force, perpendicular to the contact area, and the frictional force, tangent to it. In the project currently discussed, the pump mechanical efficiency is of little (to none) interest, and it is considered that the contact friction force has little impact on the pump displacement regulation. As such, the frictional components of the contact force are left out of this dissertation.

Generally, lumped-parameter models of contacts involve a spring-damper systems as per the Kelvin-Voigt model (see e.g. (Sidoroff, 2010) for formulation). Those models compute the contact force as the combination of an elastic and a dissipative force. When modelled in a linear manner, the elastic force F_e is a pure function of the contact deformation δ . The dissipative force F_d is computed as a function of the bodies relative velocity. It often uses a constant damping coefficient d_{eff} . In some simulation environments (e.g. MatLab® Simscape), it is possible to choose between damped or undamped rebound. The contact force F_c computed for damped rebound is then the following:

$$\begin{cases} F_e = k\delta \\ F_d = d_{eff}\dot{\delta} \\ F_c = F_e + F_d \end{cases} \quad (2-12)$$

with:

δ	contact deformation [m]
d_{eff}	damping coefficient [N/(m/s)]
k	elastic coefficient [N/m]

However, this model is not acceptable as a) it makes the contact force discontinuous when the contact is reached or left, b) it can make the contact force attractive when the speed to leave the contact makes the dissipative force greater than the elastic force. The first issue is fixed (as done e.g. in Simcenter AMESim (LMS AMESim, 2015)) by making the effective damping coefficient d_{eff} computed as is a first-order type to the contact deformation, as per equation (2-13). In this equation, δ_0 is the reference contact deformation (of one body into another) at which the damping coefficient reaches 95% of its maximal value d_{effm} .

$$d_{eff} = d_{effm} \left(1 - e^{-\frac{\delta}{\delta_0}} \right) \quad (2-13)$$

with:

δ_0	reference contact deformation at which d_{eff} reaches 95% of d_{effm} [m]
d_{effm}	maximal value of d_{eff} [N/(m/s)]

Both issues (discontinuous and attractive forces) can be solved by bounding the damping force to the elastic force (in magnitude), e.g. in Modelica (Modelica Association). The implemented equations in (Maré & Akitani, 2018) are the following:

$$\begin{cases} F_e = k\delta^n \\ F_d = \text{sgn}(\dot{\delta}) \cdot \min(F_e, d\dot{\delta}) \\ F_c = F_e + F_d \end{cases} \quad (2-14)$$

The dimensionless coefficient n is defined from the Hertz theory. It equals unity for ideal plane to plane facing surfaces and 2/3 for sphere to plane contacts.

2.5. Improvement of pressure compensator modelling

The displacement of axial piston pumps can be varied through several means, e.g. through an electrical command or mechanically. On AH fleet, the internal compensating mechanism of axial piston pumps, shown on Figure 2-9, is purely hydro-mechanical. In the current application, it is composed of four parts: a compensating valve, a stroking piston (also named yoke piston), a compensating piston (with spring, also known as rate piston), and the pump swashplate.

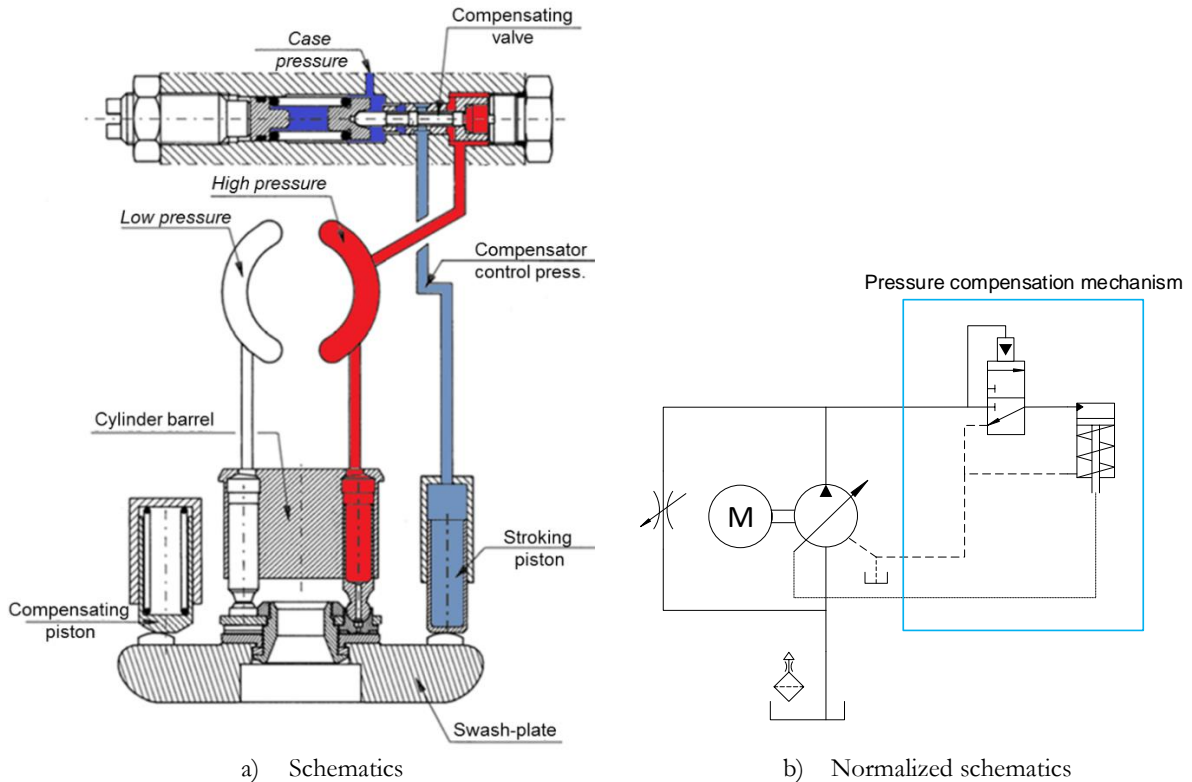


Figure 2-9: Schematics of a hydro-mechanical pump displacement compensation mechanism

The compensating valve paces the hydraulic power used to actuate the stroking piston between case and discharge (high) pressure. The swashplate tilt on its

bearing axis (i.e. the pump displacement) is the result of the force balance between stroking piston acting force and compensating spring compression force, as well as the resultant torque from the slippers, and the bearings resistive torque. The compensation chain is illustrated on Figure 2-10 through a block diagram.

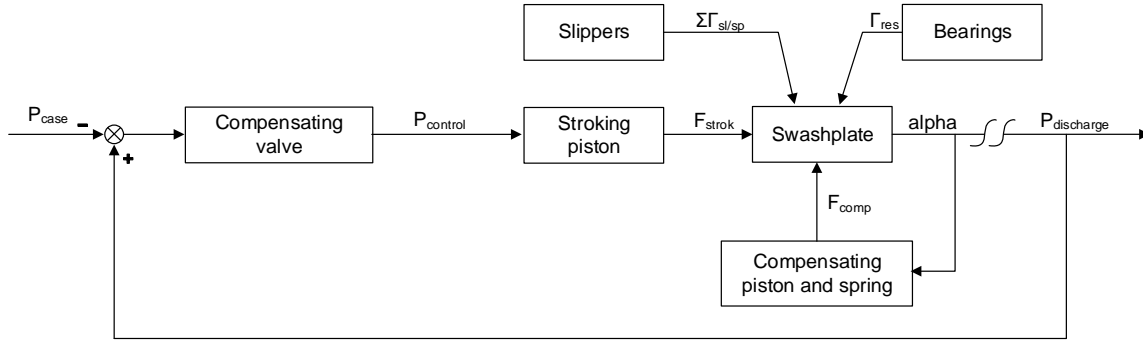


Figure 2-10: Swashplate type axial piston pump compensation process schematics

Modelling the pressure compensation of axial piston pump is already well addressed in literature. A review of valve and complete pressure compensation in lumped-parameter modelling literature is made in the next section. Then, a way to implement pressure compensator models for condition monitoring purpose is proposed and the models are verified.

2.5.1. Literature review

The pressure compensator can be described using the generic models discussed in section 2.4. However, valve models have yet to be discussed in this dissertation. As such, the literature review is decomposed into two sections, the first one focussing on valve models and the second one on the complete compensating device.

2.5.1.1. Valve models

The pressure compensator of the studied pump involves a power metering device that controls the power exchange between the pump high pressure and case domains, and the stroking piston. For this purpose, the regulation function is achieved by the valve opening that is proportional to the difference between the pressure setpoint and the pump output pressure. This function is embodied as a two-land, three-way, direct-acting, closed-centre, sliding valve as shown on Figure 2-11. The pressure setpoint is adjusted at factory by setting the preload of the valve spring.

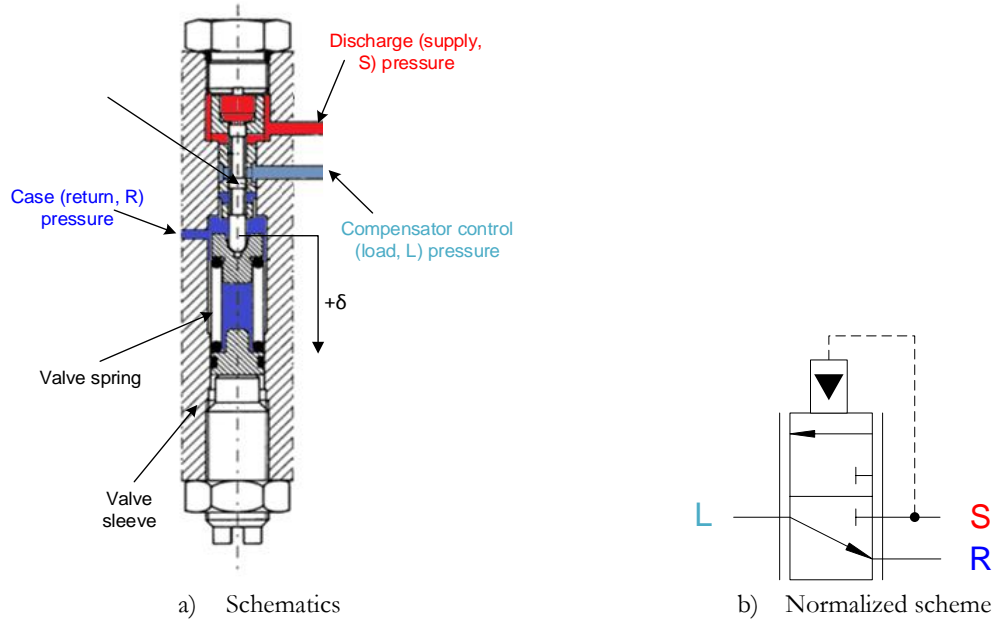


Figure 2-11: Example of a two-land three-way valve

2.5.1.1.1. Flow through the valve

The flow through the valve is dependent on spool displacement and orifice opening. Both overlapped and underlapped states of the orifice by the spool are illustrated on Figure 2-12. The underlap of one valve orifice is defined as (Maré, 1993):

$$X_i = X_{i0} + \epsilon_i X_t \quad (2-15)$$

with

- ϵ_i sign operator equal to 1 if the underlap increases with X_t , -1 otherwise [-]
- X_i underlap of the i orifice [m]
- X_{i0} underlap of the i orifice when the spool is at the hydraulic null [m]
- X_t spool displacement [m]



Figure 2-12: Underlap and overlap spool positions based on (Maré, 1993)

(Maré, 1993) proposed a model of the flow across one valve orifice depending on the spool displacement and the sign of the underlap (negative underlap meaning overlap), for a valve with notched sleeve:

$$Q_i = \begin{cases} C_{qi}(\lambda_i) S_i \sqrt{\frac{2}{\rho} |\Delta P_i| \text{sgn}(\Delta P_i)} & \text{if } X_i > 0 \text{ (underlap)} \\ \frac{n_f l_f c^3}{12 \mu (K_g - X_i)} \Delta P_i & \text{if } X_i \leq 0 \text{ (overlap)} \end{cases} \quad (2-16)$$

where:

λ_i	flow number at orifice i [-]
ρ	fluid density [kg/m ³]
C_{qi}	flow coefficient of orifice i [-]
c	radial clearance between spool and sleeve [m]
K_g	flow continuity coefficient between under and overlap states [-]
l_f	length of a notch [m]
n_f	number of notches in the valve sleeve [-]
ΔP_i	pressure at the orifice bounds [Pa]
S_i	opening section of the valve orifice to flow [m ²]

In order to compute the flow rate through one valve orifice Q_i , some necessary quantities are reminded hereafter from (Maré, 1993):

$$\begin{cases} X_{si} = \sqrt{X_i^2 + (X_0 + c)^2} - X_0 \\ S_i = n_f l_f X_{si} \\ \lambda_i = \frac{2 S_i}{n_f \nu (l_f + X_{si})} \sqrt{\frac{2}{\rho} |\Delta P_i| \text{sgn}(\Delta P_i)} \\ C_{qi} = \begin{cases} \delta_\lambda \lambda_i & \text{if } \lambda_i < \lambda_t \\ C_{q\infty} & \text{if } \lambda_i \geq \lambda_t \end{cases} \\ K_g = \frac{c}{48 \delta_\lambda} \end{cases} \quad (2-17)$$

With:

δ_λ	laminar flow constant linked to the flow number [-]
X_0	rounded corner diameter of the spool edges [m]
X_{si}	generating length of the section i [m]

In Simcenter AMESim, for a valve with orifice holes, the overlapped flow is computed using the following equation:

$$Q_{io} = \frac{2 d_{hole} c^3}{12 \mu (X + K_g)} \Delta P_i \quad (2-18)$$

where d_{hole} is the valve orifice diameter [m]. K_g is defined in equation (2-17), and X is given by the following equation where δ_p is the spool position [m]:

$$X = -\frac{\sqrt{\delta_p(\delta_p + d_{hole})}}{\text{atan}\left(\sqrt{\frac{\delta_p + d_{hole}}{\delta}}\right)} \quad (2-19)$$

For both Maré's and Simcenter AMESim models, the flow equations presented are multiplied by the number of orifices. The main difference between Maré's model and the one implemented within Simcenter AMESim is the geometry of the valve orifices.

As part of her doctoral work, (Attar, 2008) proposed an equation for the continuous valve flow model that works for both underlap and overlap situations. Attar's model is based on the turbulent orifice flow equation (2-3) and a modification of the flow coefficient model:

$$C_{qi}(\forall X_i) = C_{q\infty} \tanh\left(\frac{\lambda_i}{\lambda_{crit}} \frac{1}{1 + \frac{1}{2}K_{rec}(|X_i| - X_i)}\right) \quad (2-20)$$

where:

K_{rec} overlap coefficient [-]

In addition to work in both underlap and overlap situations, this model does not assume the fluid flow state (laminar/turbulent), when most models do. For example, both Maré's and AMESim models considers a laminar flow during overlap and a turbulent flow during underlap.

2.5.1.1.2. Jet forces

When a given fluid domain is considered, the total change of fluid momentum at the domain hydraulic port is directly linked to the external forces applied to the fluid (Euler theorem, or fluid momentum conservation). Consequently, when the flows entering and outing the fluid domain have different velocity magnitude or direction, flow forces are generated on the spool body, which impact its force balance and therefore its motion. This "jet" flow force is shown on Figure 2-13, written as F_j . On said figure, pressure distributions are illustrated. One can see that the increased fluid velocity reduces pressure on face b, creating a hydraulic imbalance which tends to close the orifices.

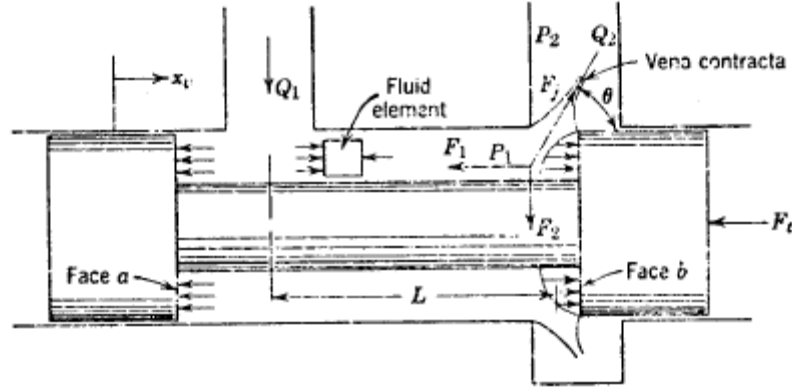


Figure 2-13: Schematics of the fluid forces on a valve spool (Meritt, 1967)

The jet force has both axial and radial components (F_1 and F_2 on the last figure). In the current application, the valve has a symmetrical orifice design which nullifies the overall radial force. The axial component of the steady state jet force during steady state flow is defined in (Meritt, 1967) as (2-21):

$$F_1 = 2C_d C_v S_i (P_1 - P_2) \cos \theta_j \quad (2-21)$$

where:

- θ_j jet angle (θ on Figure 2-13 and Figure 2-14) [rad]
- C_v velocity coefficient [-]

In the said equation (2-21), the jet angle θ_j is function of the orifice opening and the radial clearance (see for example Figure 2-14, for a rectangular orifice with sharp edges) and has values between 0° and 69° . The velocity coefficient C_v is introduced to account for the impact of viscous friction on jet velocity. It is usually around 0.98 and often approximated to one (Meritt, 1967). P_1 and P_2 are the upstream and downstream pressures, respectively. This notation is linked to Figure 2-13.

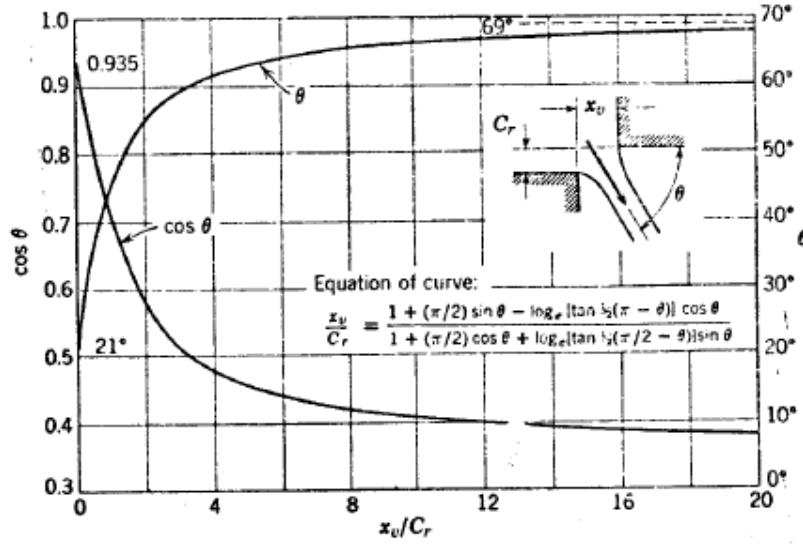


Figure 2-14: Effect of radial clearance on the jet angle (Meritt, 1967)

(Meritt, 1967) also defines transient flow forces due to fluid being accelerated in the annular valve chamber. The transient flow force is written as (2-22), in which the velocity term represents a damping force. The pressure term is usually neglected as “there is little direct evidence that the pressure rate term contributes substantially to valve dynamics” (Meritt, 1967). This equation is valid if and only if $P_1 > P_2$.

$$F_{tr} = LC_d w \sqrt{2\rho(P_1 - P_2)} \frac{dx_v}{dt} + \frac{LC_d w x_v}{\sqrt{2/\rho(P_1 - P_2)}} \frac{d(P_1 - P_2)}{dt} \quad (2-22)$$

with, from Figure 2-13:

- L axial length between incoming and outgoing flows (damping length) [m]
- w orifice area gradient of as a function of spool displacement [m^2/m]
- x_v spool displacement [m] as per Figure 2-13

In Simcenter AMESim, the flow force F_j is written as (2-23), where k_{jet} is a jet coefficient supplied by the user, X_i is the orifice underlap and x_{min} is the underlap for which the flow area is minimum.

$$F_j = F_1 k_{jet} \frac{1}{2} \left[\tanh \left(2 \frac{X_i - x_{min}}{x_{min}} \right) + 1 \right] \quad (2-23)$$

In this software, the jet angle θ_j is computed through interpolation from data of Figure 2-14, as a function of the underlap and the radial clearance between valve and spool. In this case, the addition of the hyperbolic tangent allows for the smooth annulation of the jet force when the orifice when transiting from underlap to overlap configuration.

2.5.1.2. Models of the pump compensation in literature

Complete models of the pump compensation in literature are compared in Table 2-7. This table, which enters a total of 24 physical phenomena, highlights contact management, annular leakage and valve models in literature. A total of 24 phenomena are listed. On average, 37% of the 24 listed effects are taken into account in the cited literature. The more complete references considering the number of physical effects listed in the current study are (Blackman, 2001), with 66.7% of considered effect, and (Aaltonen, 2016) with 58.3%. This table highlights the state-of-the art on lumped-parameters modelling of pump pressure compensators. These models are well established and there is no real improvements to be made in a lumped-parameter approach. Even so, do the listed reference models allow for degradation simulation?

Failure of a pressure compensation mechanism, with design as that of Figure 2-9, is defined through its consequence on the pump regulation: loss of pressure adjustment, instability of discharge pressure, or low response time to flow demand. Normal pump dynamics behaviour is defined for instance in the ATP, which highlight test made on pump upon reception to verify their behaviour. One example of specified pump dynamic behaviour is summarized in Table 2-8 from the ATP of a Super Puma (now H225) H/C pump. Pump discharge pressure outside of this normal behaviour can mean pressure compensator failure.

Degradation is a creeping process leading to failure. All the cited references of Table 2-7 allow for the simulation of a degraded state if proper parameterization is made. However, none of them allow for the temporal variation of said parameters to simulate the degradation process.

One of the main fault considering the pressure compensation in H/C context are the following:

- Wear of the valve;
- Jamming of the valve due to particle in the spool/sleeve clearance;

A way of implementing models for the simulation of the degradation processes leading to both faults is presented in the next section.

Table 2-7: Pressure compensator in lumped-parameter modelling literature

References		(Kavanagh, 1987)	(Manning & Johnson, 1996)	(Blackman, 2001)	(Mancó, et al., 2002)	(Anthony, 2012)	(Aaltonen, 2016)	(Spuri & Goes, 2017)	(Corvaglia & Rundo, 2018)
		Y N Ø	Y N Ø	Y N Ø	Y N Ø	Y N Ø	Y N Ø	Y N Ø	Y N Ø
Spool	Inertia			x	x	x	x	x	x
	Annular leakage			x	x	x	x	x	x
	> Eccentricity			x	x	x	x	x	x
	Friction			x	x	x	x	x	x
	Static friction			x	x	x	x	x	x
	Jet forces								
	> Steady			x	x	x	x	x	x
	> Transient			x	x	x	x	x	x
Swashplate	Inertia	x	x	x	x		x		x
	Friction	x	x	x	x		x		x
	Static friction	x	x	x	x		x		x
Stroking piston	Inertia	x	x	x	x	x	x	x	x
	Annular leakage	x	x	x	x	x	x	x	x
	> Eccentricity	x	x	x	x	x	x	x	x
	Friction	x	x	x	x	x	x	x	x
	Static friction	x	x	x	x	x	x	x	x
	Sporadic contact with swashplate	x	x	x	x	x	x	x	x
Compensating piston	Inertia	x	x	x	x		x	x	x
	Annular leakage		x	x	x			x	x
	> Eccentricity		x	x	x				x
	Friction		x	x	x				x
	Static friction		x	x	x				x
	Sporadic contact with swashplate	x	x	x	x		x	x	x
Fluid	Compressibility	x	x	x	x	x	x	x	x

Legend:

Y	Included	N	Not included	Ø	No explicit mention		Not applicable in the cited study
---	----------	---	--------------	---	---------------------	--	-----------------------------------

Table 2-8: Pump dynamic specification - from ATP (Airbus Helicopters, 2012, p. 137)

Specifications	Full flow to zero flow	Zero flow to full flow
Maximum allowed peak pressure	257bar	N/A
Time to settle	Less than 1s to reach rated zero flow pressure	Less than 1s to reach 60% of rated full flow pressure
Response time	Less than 0.05s	
Pressure oscillation envelope	+/- 20,7 bar	

2.5.2. Compensator model for condition monitoring- implementation proposal

This section aims at showing how time variable parameters have been implemented inside models to simulate time-dependent degradation. The goal is also to show the difference between models made with functionality in mind, compared to those developed for CM. It is however not in the scope to the present work to develop degradation models for the pump pressure compensation, but only to show ways of implementing degradation models. The solutions presented hereafter are described through the Bond-Graph formalism. Partial models focused on the part of interest are introduced in the next two sections. Then a complete model of the pressure compensation mechanism for condition monitoring is described, both in Bond-Graph formalism and implemented in a simulation environment.

2.5.2.1. Valve wear

Valve wear is the result of three main phenomena: erosion, abrasion and cavitation. Erosion wear is due to impact of solid or liquid particles with high velocity against a solid surface. Abrasion wear is defined as the loss of material by passage of a hard particle over a surface. Last but not least, cavitation wear is caused by the local impact of a released dissolved gas bubble against a surface during its collapse. More detailed information on all three wear phenomena can be found for example in (Stachowiak & Batchelor, 2014).

Erosion, caused by the impact of a fluid with high velocity on a surface, tends to appear prior to abrasion on helicopter axial piston pumps. As a matter of fact, in this application, spool valves are designed with sharp edges in order to avoid particle entry in the radial clearance (thus reducing the possibility of abrasion). Cavitation wear, although similar to erosion wear in the process, is much milder (Stachowiak & Batchelor, 2014). For these reasons, the focus of this section is put on valve spool edge erosion. The process of simulation described hereafter can be applied to abrasion without modification.

Modelling such complex phenomenon like erosion is reported in literature with the use of CFD and distributed-parameter approaches (see e.g. (Fang, et al., 2013) for erosion wear simulation in electro hydraulic servo valves). In a lumped-parameter paradigm, a much simpler approach must be used.

Literature shows that erosion and abrasion tends to appear mainly on the spool valve metering edges (Vaughan, et al., 1993). When it happens, valve leakage increases and both pressure and flow gains are affected. As such, timely variations of the valve edges radius seems to be a promising approach to simulate erosion in a lumped-parameter modelling context.

Doing so, erosion is assumed to be homogenous around the edge, which is not representative of reality. However, it is not the aim of the current project to propose detailed models for erosion, but to show ways of implementing solutions for degradation models in a lumped-parameter paradigm. Consequently, the proposed approach detailed hereafter is a compromise between modelling effort and result quality.

At model structure level, erosion can easily be introduced when the variable orifice model explicitly uses the orifice rounded edge radius. In this case, a mean rounded edge value is used for the whole orifice/spool edge pair. It is supposed that erosion is homogenous around the spool edge. Figure 2-15 displays the original model a), and the model b) modified with a modulated hydraulic resistance MR. This modulation allows for the introduction of the time-dependent rounded corner parameter $X_0/2$ in equation (2-17) which is piloted externally.

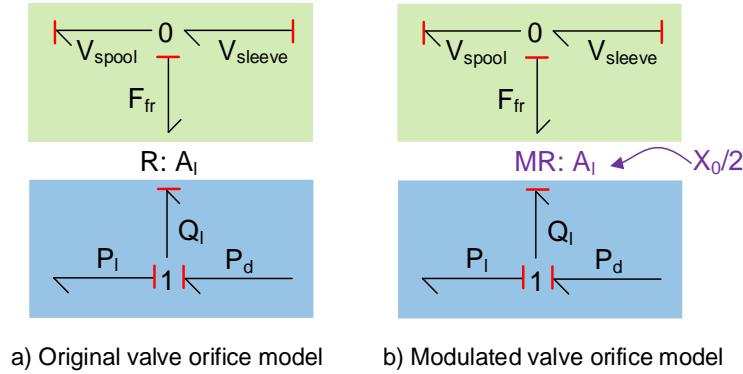


Figure 2-15: Comparison of valve orifice bond-graph models – original vs modulated

On the bond-graphs of Figure 2-15 and all BG that will follow, the same colour-code as in architecture is used: dark blue for hydraulic domain, green for the mechanical domain, and red for the signal domain. Purple is used to highlight additions or modifications from original (or functional) models. This modulation of the flow area does not generate any change of the causality, as also illustrated by Figure 2-15. This figure constitutes another example of an R field in bond-graph theory.

Another proposal for the implementation of CM models is made in the next section which focuses on compensating spool valve.

2.5.2.2. Jamming

Hydraulic fluid particle pollution can cause the valve spool to jam when particles get into the radial clearance between valve spool and sleeve. The valve spool can be stuck momentarily or for a longer time; as a one-time event or as an erratic re-occurrence. Depending on the position in which the spool is jammed, several things can happen:

- 1) Spool blocked in a position where the control port is connected to high pressure. In that situation, the stroking piston is actuated directly by the system pressure, which is only counterbalanced by the compensating spring
- 2) Blocked spool connects case pressure to control pressure. In this case, the stroking piston is not actuated, leaving the swashplate tilted in maximum displacement position whatever the system pressure. If flow demand is low, the system pressure increases uncontrolled due to flow force-feeding by the pump.
- 3) Spool blocked in a closed control orifice position. In that configuration, the control pressure goes down to case pressure (if the jamming duration is long enough) due to leakage around the stroking piston, causing uncontrolled swash plate tilt to maximum displacement position. After that, no further actuation of the swashplate is possible, which drives us back to the effects of point number 2.

Figure 2-16 displays a comparison of functional and CM valve force bond-graph. Figure 2-16-a) shows Newton's second law applied to the spool through the 1-type junction. Spool acceleration is the result of the hydraulic and spring forces applied to the spool. The kinetic energy of the spring is not negligible. Therefore it is considered by adding 1/3 of its mass to that of the spool

It is proposed here to simulate jamming through the introduction in the model of a modulated friction element MR as shown on Figure 2-16-b). In this dissertation, jamming is considered as an event defined by two parameters: the state coefficient ζ , which takes the value of 1 when jamming is happening and of 0 otherwise, and the jamming intensity I_j (here in Newton). The supplied jamming force F is then defined as equation (2-24). Comparison of models with and without jamming on Figure 2-16 shows that, in this case, the introduction of the dissipative element R does not generate causality issues with the neighbouring elements.

$$F = \zeta I_j \quad (2-24)$$

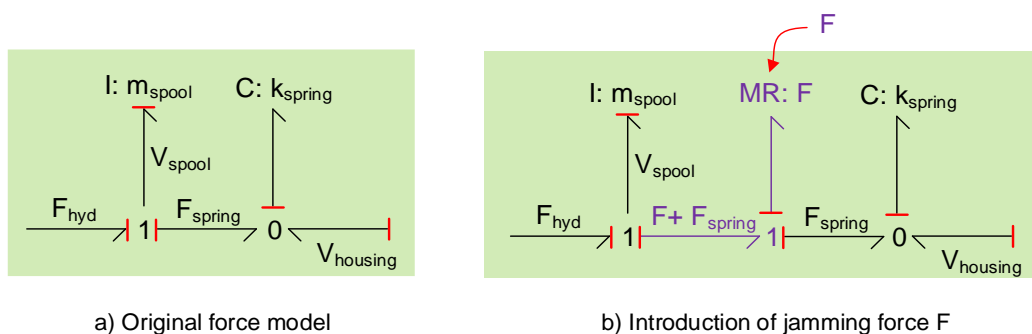


Figure 2-16: Comparison of valve force models: with and without jamming

2.5.2.3. Full model

The complete Bond-Graph model of the pump pressure compensation mechanism is displayed on Figure 2-17. As previously, the proposals made for the implementation of degradation models are written in purple. In order to improve the clarity of the figure, physical domains are not highlighted. The complete compensation considered here has only three interfaces: with the pump discharge port, the pump case volume as well as with the slippers. The same interfaces can be seen on Figure 2-18, which shows the implementation of the model in Simcenter AMESim environment. The bearings resistive effect is considered within the swashplate (yellow) block, with a R element generating the torque $\Gamma_{r/sp}$.

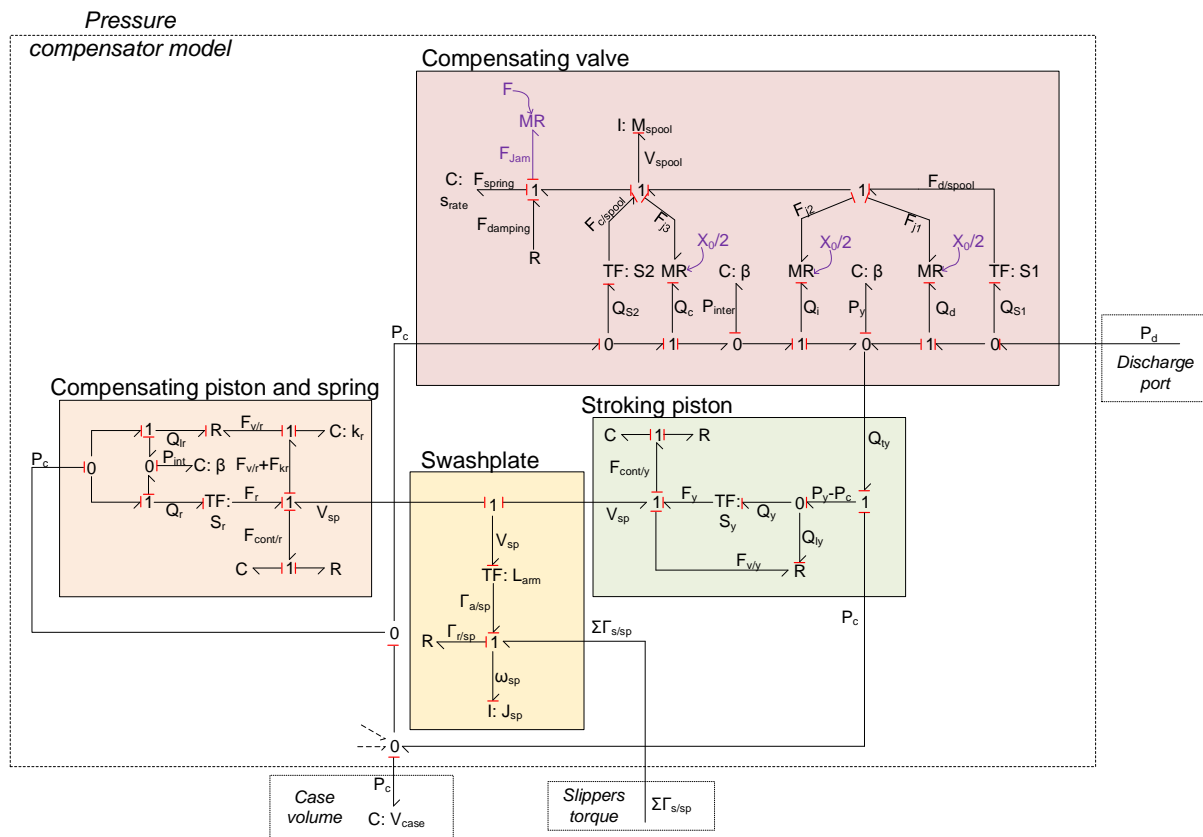


Figure 2-17: CM Bond-Graph of the complete axial piston pump pressure compensator

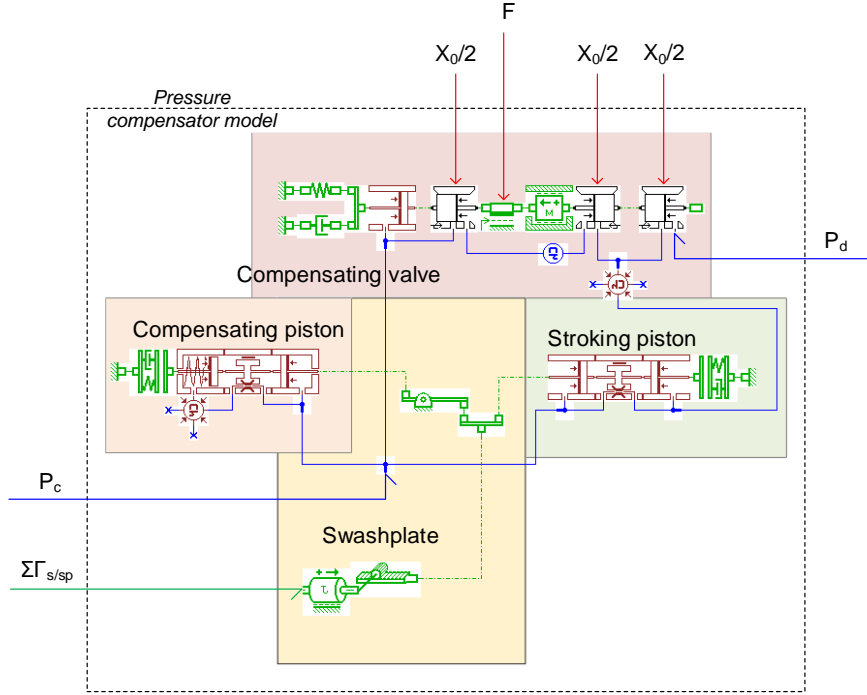


Figure 2-18: AMESim implementation of the pressure compensation mechanism model

In AMESim, the jamming force F is supplied to a controlled variable friction model which translates the jamming force into a physical friction. Rigorously, the spool jamming/friction model should include static friction, pre-sliding displacement, stick-slip motion, as well as Stribeck effect and viscous friction due to lubrication. However, as already stated, it is not the aim of this dissertation to discuss degradation models but to show possibilities for implementation. For this reason it was chosen to apply the hyperbolic tangent Coulomb friction model, despite its low capabilities representing the friction phenomena for low relative velocities. This model allows computing the jamming friction force F_{jam} as per equation (2-25). In order to make a steep variation of the friction force for low relative velocities, the velocity threshold v_0 to obtain the maximum jamming friction in the hyperbolic tangent model is chosen to be at least ten thousand times smaller than the maximum spool velocity in simulation.

$$F_{jam} = F \tanh\left(2 \frac{v_{spool}}{v_0}\right) \quad (2-25)$$

with:

- F jamming force [N]
- v_0 threshold velocity for maximum jamming friction [m/s]
- v_{spool} spool velocity relative to sleeve [m/s]

2.5.3. Verification of compensator model and discussion

The requirements defined from the pump in Table 2-4 (p19) state the model “shall simulate accurate behaviour for internal leakage, as well as suction and discharge pressure and flow”. As a first step of the assessment of the complete pump model “accuracy”, it is then necessary to verify the models developed. In this section, the developed compensator model is first verified in healthy state, then its capabilities in degraded state are highlighted.

2.5.3.1. Healthy state

The developed compensator model is verified in healthy state against ATP specifications. The ATP defines the expected dynamic behaviour of the pump. It is used as a basis for the current project as well as the test conditions for pump dynamic testing. The use document, available in (Airbus Helicopters, 2012) is summarized in Table 2-8 (page 43). It is reminded in Table 2-9 hereafter for a simpler comparison with the simulation results displayed in the last table.

During dynamic tests, the system flow demand is abruptly changed from zero flow to full flow and vice-versa in order to check the response of the tested pump. A virtual test bench is modelled to verify the pressure compensator model in these conditions. The implementation of this model in the AMESim software is displayed on Figure 2-19.

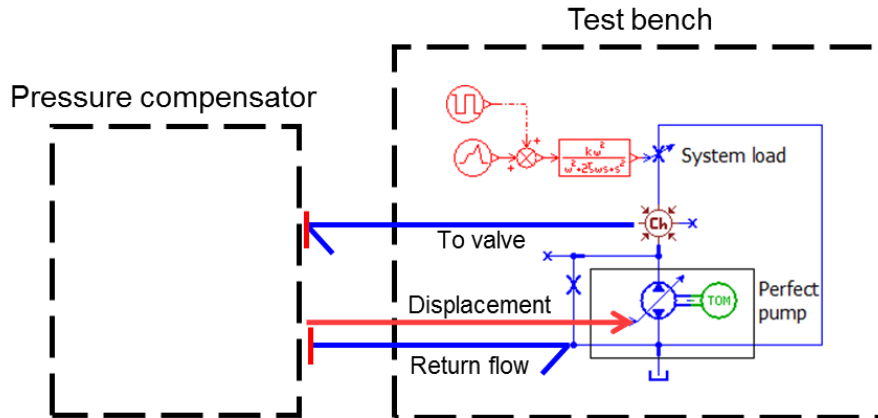


Figure 2-19: Pressure compensator verification virtual test bench

The virtual test bench is composed of a variable displacement perfect pump model (on which leakage is added), and a hydraulic circuit modelled as constant hydraulic capacitance plus a variable hydraulic resistance to change the point of operation. The system load is parameterized to reproduce the conditions of pump dynamic testing. The perfect pump and the leakage orifice are parameterized to generate a flow to the system of 27.17 L/min for a pressure drop across the pump of 160 bar and a leakage of 0.63 L/min (2.25% of maximum rated flow), complying with the H225 pump characteristics of Table 2-1.

The displacement of the AMESim perfect pump model can only be modified through a fraction coefficient. This fraction is varied between 0 and 1, and is supplied through a signal link that gives the percentage of flow the pump should deliver. In order to link the pressure compensator model developed with the perfect pump, it is necessary to sense the swashplate tilt angle, and supply its fraction to the pump model via signal as shown on Figure 2-19.

The pump response to a system load transient is shown on Figure 2-20. On this figure, simulation begins with a non-pressurized hydraulic system, and pump in full flow condition. At time 0.25 s, the modelled hydraulic valve (system load) is abruptly closed. At time 1.25 s, the valve is re-opened in a single step. Figure 2-20 shows the stabilization of discharge pressure and flow as well as pump displacement (swashplate tilt) during the three simulated phases.

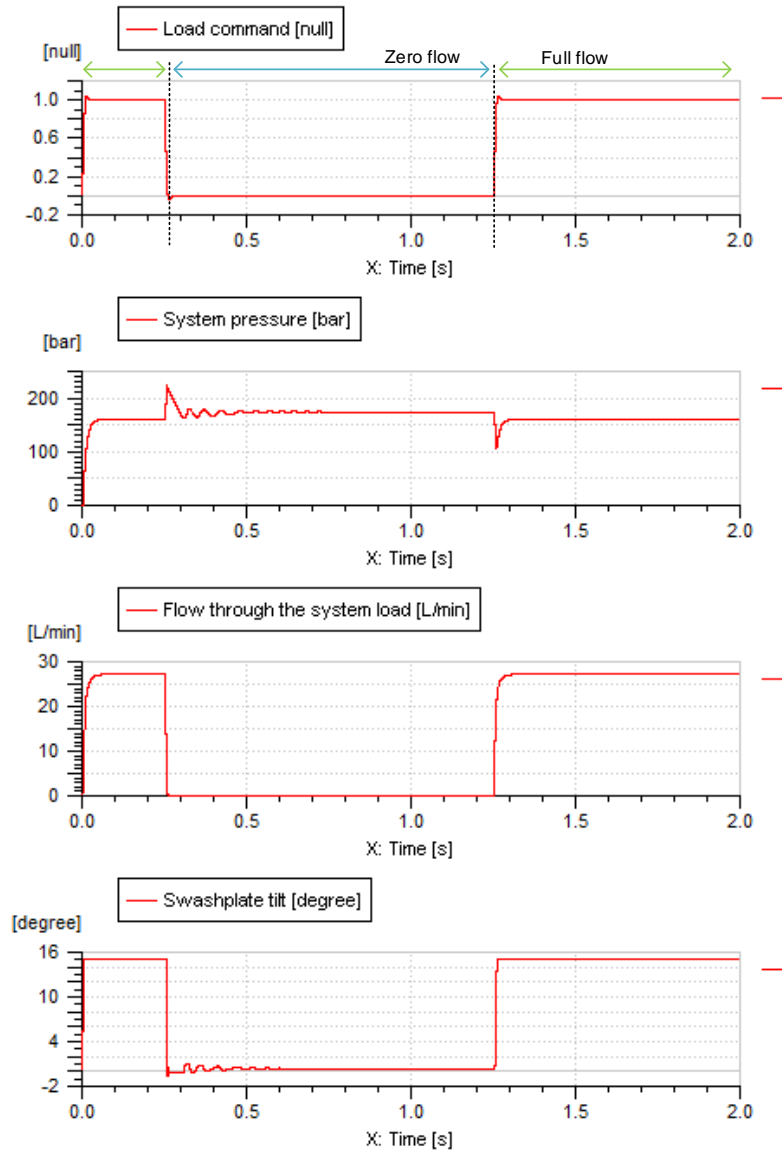


Figure 2-20: Pressure compensator model verification - pump answer to load

The simulation results outlined in Table 2-9 show that the modelled pump meets the ATP specifications. It can be noticed that the model far exceeds the requirements, with a settling time much faster than specification, and very small envelope of oscillations. It must be reminded here that the specification is made to test the complete pump behaviour, while a simplified model of the compensator is tested here. Thus, it is expected for the models to behave better than the specification.

Table 2-9: Complete comparison of compensator models simulation against ATP specifications

	ATP		Model Status	
<i>Specifications</i>	<i>Full flow to zero flow</i>	<i>Zero flow to full flow</i>	<i>Full flow to zero flow</i>	<i>Zero to full flow</i>
Maximum allowed pressure [bar]	257bar	N/A	223	N/A
Time to settle [s]	Less than 1s to reach rated zero flow pressure	Less than 1s to reach 90% of rated full flow pressure	0.35	0.02
Response time	Less than 0.05s		Less than 0.01	
Pressure oscillation envelope [bar]	+/- 20.7 bar		+/- 1 after settling	

After verifying the healthy behaviour of the pressure compensator model, its capabilities in degraded mode must be discussed. This is the aim of the following section.

2.5.3.2. Capabilities in degraded mode and discussion

In the previous sections, proposals were made to implement temporal variation of spool valve wear and jamming. The current section aims at showing the capabilities of the proposed models.

Valve wear

Simulation of spool valve wear through increased rounding of the metering edges can be made with the proposed model. However, it is difficult to show its impact in simulation. Dynamic test cycles simulated on the modelled test bench of Figure 2-19, and with several health conditions of the valve are displayed hereafter.

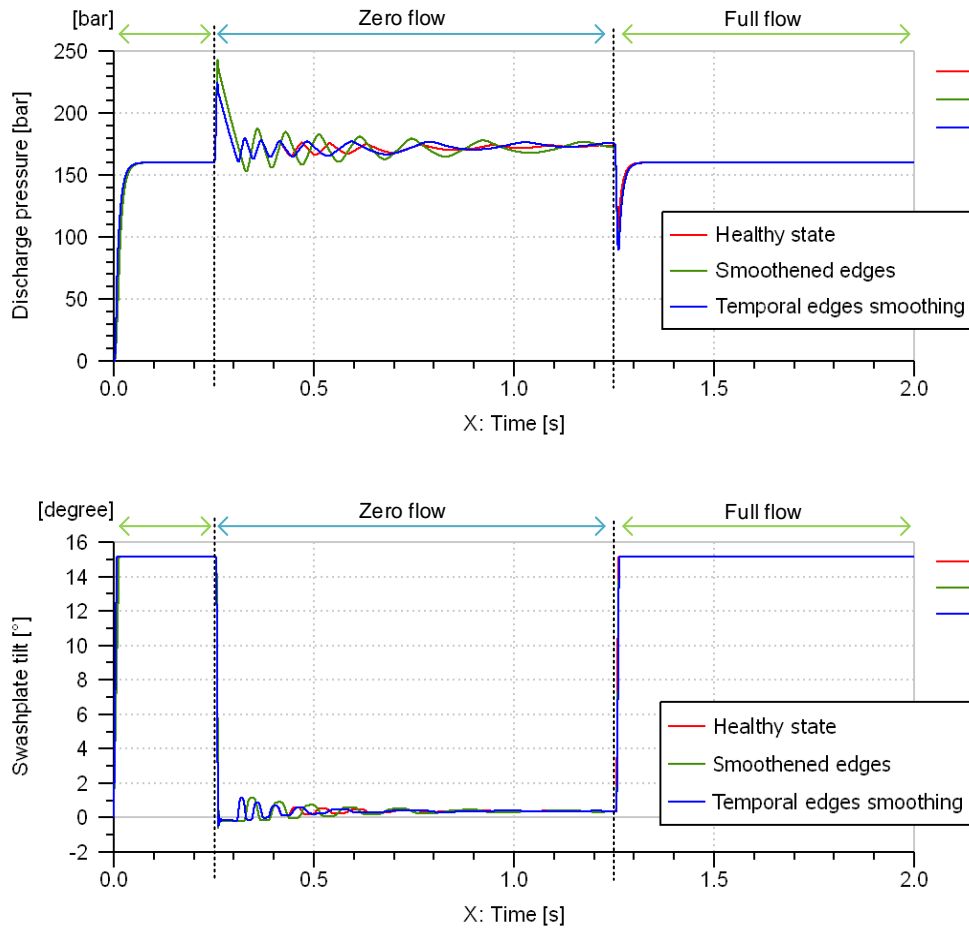


Figure 2-21: Impact of valve wear on pump dynamic response - 3 conditions

Three health conditions were simulated: 1- healthy valve, 2- increased radius of the metering edges ('smoothened edges') and 3- temporal increase of edges smoothing. In practice, Figure 2-21 shows the variation of the pressure gain during simulation: the pressure gain curve slowly diverges from that of the healthy state to approach that of the worn edges. This can be observed for both pump discharge pressure and swashplate tilt. In these simulation, and under the hypotheses taken, one can also see that erosion of the valve metering edge increases the pressure oscillations during zero flow operation. It also increases the response times of both zero to full flow and full to zero flow transitions. This can be understood as any increase in the rounded edges radius augments the valve leakage and reduces its pressure gain, with corresponding consequence of the pressure regulation loop.

Although spool erosion is bound to appear in reality, it is difficult to show the interest of a temporal variation of it. However, the modelling and simulation process itself is interesting as it allows for future implementation of more detailed degradation models.

Spool jamming

As already discussed in the previous section, jamming is considered in this dissertation to be an event defined by its status coefficient ζ and intensity I_j . Figure 2-22 illustrates a dynamic load cycle with sporadic jamming. The simulated jamming is 0.6s long and begins at simulation time 0.5s (highlighted in light yellow on Figure 2-22). Its intensity of 500 N ensures that the spool becomes stuck with the sleeve in normal discharge pressure conditions. On Figure 2-22 are displayed pump discharge pressure, control pressure, swashplate tilt, and spool displacement (not centred on zero).

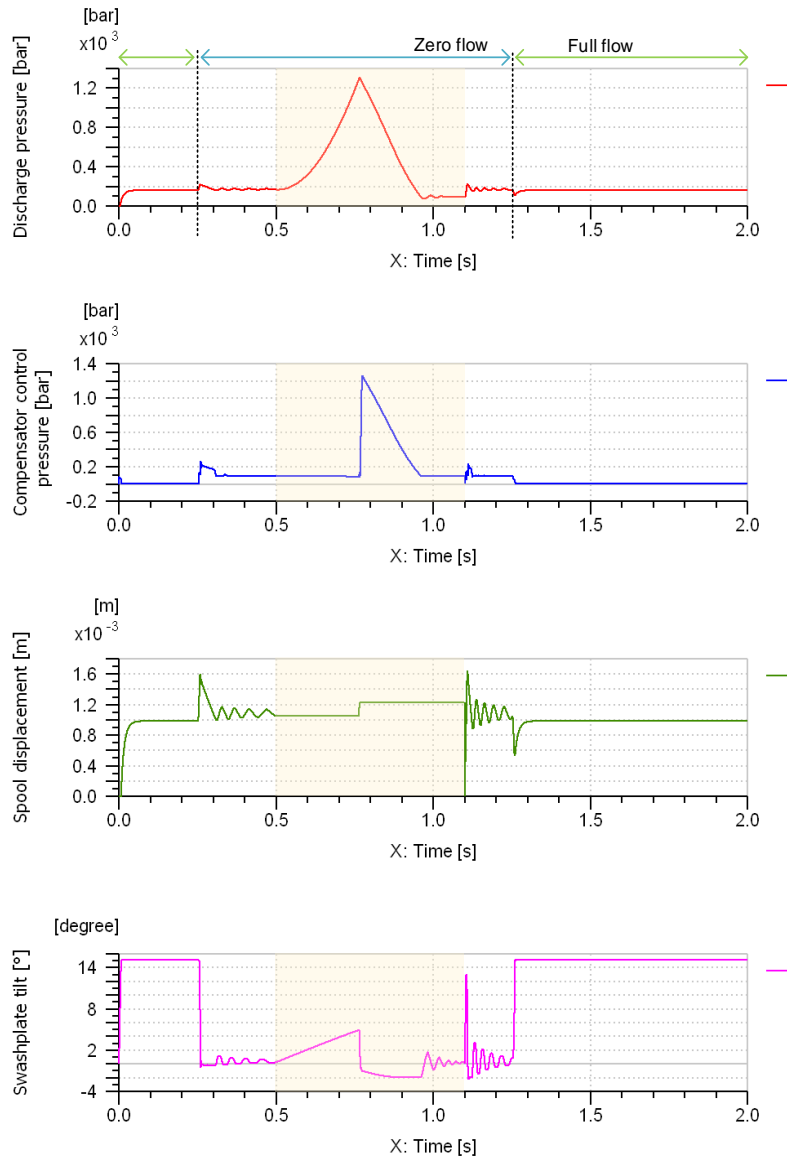


Figure 2-22: Pressure compensator model verification - answer to valve jamming

The shape of the graphs is explained as follows. Jamming happens at 0.5s, within the zero flow phase: the spool is immobilised. Control pressure decreases

due to leakage around the stroking piston, leading to the increase of the swashplate tilt, which, in turn, generate the skyrocketing of the discharge pressure. It should be noted here that any real pump would have been severely damaged by such a pressure overshoot and would not return to normal operation. However, the pressure increase is realistic. In real H/C hydraulic systems, this pressure increase would trigger operation of system safety provisions like pressure limiting valves.

At one point of the simulation (~ 0.75 s) the pilot force generated by the discharge pressure is sufficient to overcome the jamming force, making the spool valve move brutally and connecting discharge pressure to control pressure. Control pressure being high, swashplate tilt is decreased to even negative angles until an equilibrium between compensating piston force and control pressure is reached. During this phase, 0.75 s to 1.1 s, the model behaves more like a healthy compensated pump, as the discharge pressure is connected to control pressure fluid volume. Then, jamming is stopped at 1.1s, the spool is allowed to move and the pumps is again correctly compensated.

It is to be noted that due to the Coulomb friction model used with hyperbolic tangent, the spool is, in practice, not immobilized but only slowed down so that its velocity is at least 10^5 smaller than during normal movement phases.

Jamming showed higher visual impact than spool erosion, and is, in the author's opinion, the most interesting of both effects introduced in the CM model, considered the future possible use of this model at AH. Using such type of model, one would be able to simulate the effects of pressure compensator jamming on the hydraulic system, and, as such, to estimate damage to hydraulic system equipment due to possible jamming cycles.

Using the proposed method, one is able to introduce time variable degradation models to the pump. The capabilities of the proposed approach has been shown for the pressure compensation, for both spool valve erosion and spool jamming. To this end, a high wear rate was set: the rounded radius parameter is increased arbitrarily by twenty in less than half a second. In the same manner, the intensity of the jamming force was set high in order to insure the spool quasi immobilization, without regards to reality. However, as the aim of this section was to propose possible implementations for degradation model but not degradation models themselves, it is considered that the proposed implementation answers its purposes.

2.6. Proposition of a variable slipper/swashplate gap height model

A slipper with its interfaces is shown on the cut-view of Figure 2-23. It is connected to the piston through a ball joint, forcing it to follow the pistons in its rotatory translation. However, the ball joint offers the slipper some degrees of freedom from the pistons. Figure 2-24 defines the local slipper axes. The slipper can tilt around both x_{sl} and y_{sl} directions, and spin around z_{sl} . The slipper can also translate in the z_{sl} direction. This translation is restricted by the swashplate and retainer which are rigidly bound. Piston and slipper being linked through a ball joint, both parts are free to spin relative to each other: the slipper spin can be of different magnitude than that of the piston in its bushing. The combination of these degrees of freedom result in complex dynamic motion of the slipper in real operation.

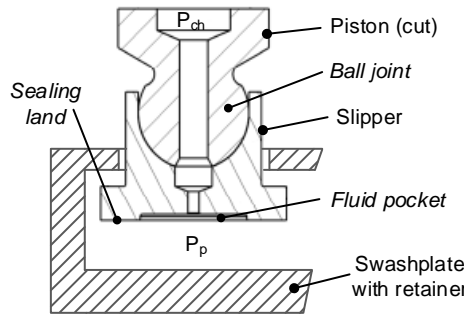


Figure 2-23: Slipper interface schematics, adapted from (Schenk, 2014)

The next section reviews literature considering the modelling of slipper/swashplate interface. Then an improvement of the lumped-parameter state of the art models of the slipper is proposed and described.

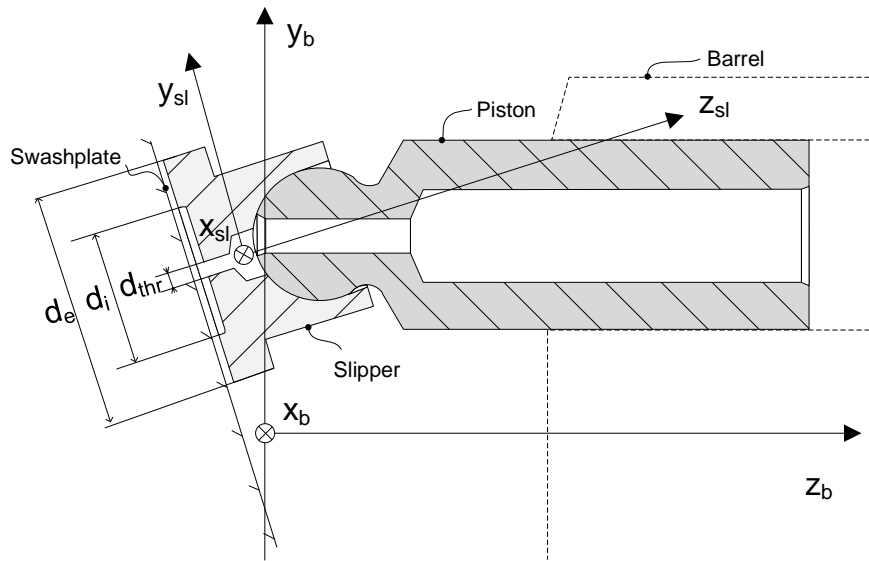


Figure 2-24: Example of slipper local coordinates

2.6.1. Literature review

Rq1 of Table 2-4 (p19) states that the model must simulate an accurate leakage behaviour, but how to model it? The well-established steady-state 0-D models of the leakage flow from slipper to swashplate were presented, e.g. in (Böinghoff, 1977) and (Ivantysyn & Ivantysynova, 2003). This leakage flow is modelled using the hydrostatic slipper theory. It is due to pressure difference between slipper pocket and case pressure, defined as equation (2-26) under the assumption of steady, laminar isothermal flow and parallel planes:

$$Q = \frac{\pi h_{sl}^3}{6 \mu \ln\left(\frac{d_e}{d_i}\right)} (P_p - P_c) \quad (2-26)$$

where

μ	absolute viscosity of the fluid [Pa.s]
d_e	external diameter of slipper sealing land [m]
d_i	internal diameter of slipper sealing land [m]
h_{sl}	slipper/swashplate clearance [m]
P_c	pump case pressure [Pa]
P_p	slipper pocket pressure [Pa]

Equation (2-26) is used to estimate the total leakage due to the slippers, which numerical results are given in Table 2-10. The table highlights the results for steady state computation of the leakage (Q^*) for a single slipper, during both discharge and suction phases, and the mean overall leakage (Q_t^*) over one shaft revolution (9 slippers). The value is calculated for a constant gap height of 17 μm . This value corresponds to the hydrostatic gap induced by a 160 bar discharge pressure on the slippers in the current application. The total leakage is computed for nine times the mean leakage over a rotation. In this computation, it is considered that half the rotation is made at suction pressure (1.8bar) while the other half is made at discharge pressure. From these numerical results, it can be seen that equation (2-26) overestimates the leakage at the interface: the overall mean leakage due to slippers is 30% over the maximum total pump leakage flow rate that is allowed in our application (1.5L/min from supplier specification). In the light of this, it can be said that using the state-of-the-art lumped-parameter model for calculating the slipper/swashplate leakage is not accurate enough in the frame of condition monitoring.

Table 2-10: Total leakage from slipper/swashplate interface using the generic leakage model

Notation	Parameters		Variables			Results	
	d_e/d_i [-]	μ [Pa.s]	P_p [bar]	P_c [bar]	h [μm]	Q^* [L./min]	Q_t^* [L./min]
Value	1.45	0.02	160 1.8	3	17	0.4417 -0.0034	1.960

With that said, the following questions remain: what is the state of the art in slipper/swashplate interface modelling, and how could lumped-parameter models be improved? Twenty-seven scientific documents were reviewed in Table 2-11, sourced over a forty-one-year period of time. Leakage is the focus of the present study but is closely linked to slipper/swashplate clearance. Through this table, the author draws the current knowledge related to slipper/swashplate interface and associated motions impacting the clearance. Both the lumped and distributed parameters approaches as well as the experimental ones are considered.

The lines are grouped versus the way used to get the results: “Analytical” (lumped-parameter), “Numerical” (distributed-parameter), “A&N” for both approaches, and “None” for experimental-only papers. The table columns indicate what effects are addressed: slipper/swashplate motions, including swashplate tilt, relative tangential velocities, variable gap, and slipper tilt, azimuth and spin. This table shows that no reference took all six parameters into account. (Tang, et al., 2016), (Lin & Hu, 2015) and (Ivantysyn & Weber, 2016) are the closest to the aim with five motions over six integrated in their research through modelling.

Table 2-12 provides another analysis of the literature found. Lines are associated with the modelled effect, while columns categorises the sourced communications depending on how the data is obtained (experimentally, through lumped-parameter or distributed-parameter models...). Two metrics are used in this table: 1) a percentage of integration of the physical phenomena in the complete pool of communications sourced, 2) a ratio of papers integrating the physical phenomena in a category of communications.

It can be seen that relative velocity, slipper tilt and gap variation are often addressed in literature. This is less the case for swashplate tilt, and slipper spin and azimuth. It is also interesting to note that only distributed parameter models include slipper spin. Experimental studies tend to integrate the listed motions, which is coherent with their aim.

Table 2-11 and Table 2-12 show how weak the lumped-parameter models are compared to distributed-parameter models of the slipper/swashplate interface. Improvements of the state of the art of axial piston pump slipper gap lumped parameter modelling can be made through the integration of the listed motions: relative velocity, variable gap, spin and tilt. As a first step towards the goal, a variable gap height model using the lumped parameter approach is proposed in the next section.

Table 2-11: Comparison of literature on slipper modelling and physical phenomena considered

		References	Relative velocity			Swashplate tilt			Variable gap			Tilt			Azimuth			Spin		
			Y	N	Ø	Y	N	Ø	Y	N	Ø	Y	N	Ø	Y	N	Ø	Y	N	Ø
Equation resolution	Analytical	(Böinghoff, 1977)	x			x				x		x			x					x
		(Bergada & Watton, 2005)	x			x				x		x			x				x	
		(Mancò, et al., 2002)			x	x				x		x			x				x	
		(Yi & Jiang, 2011)	x			x			x			x			x				x	
		(Li, et al., 2015)			x	x				x		x			x				x	
		(Aaltonen, 2016)			x	x				x		x			x				x	
	Numerical	(Hooke & Li, 1988)	x				x		x			x			x				x	
		(Bergada, et al., 2007)	x					x		x		x			x				x	
		(Kumar, et al., 2009)	x				x			x		x			x				x	
		(Bergada, et al., 2012)	x				x			x		x			x				x	
		(Xu, et al., 2012)	x				x		x			x			x				x	
		(Xu, et al., 2015)	x					x	x			x			x				x	
		(Tang, et al., 2016)	x				x		x			x			x				x	
		(Wang, et al., 2015)	x				x		x			x				x			x	
		(Lin & Hu, 2015)	x			x			x			x				x			x	
		(Ma, et al., 2015)	x					x	x			x			x				x	
		(Schenk & Iwantysynova, 2015)	x					x	x			x			x				x	
		(Iwantysyn & Weber, 2016)	x					x	x			x			x				x	
		(Chao, et al., 2018)-1	x					x		x		x			x				x	
		(Jiang, et al., 2018)	x			x			x			x				x				x
	A&N	(Bergada & Watton, 2002)	x			x				x		x			x				x	
		(Bergada, et al., 2010)	x			x				x		x			x				x	
		(Bergada & Kumar, 2014)	x				x		x			x			x				x	
	None	(Rokala, et al., 2008)	x				x		x			x			x				x	
		(Suzuki, et al., 2011)	x				x		x			x			x				x	
		(Kazama, et al., 2014)	x				x		x			x			x				x	
		(Chao, et al., 2018)-2	x			x			x			x				x			x	

Legend:

Y	Included	N	Not included	Ø	No explicit mention
---	----------	---	--------------	---	---------------------

Table 2-12: Comparison of literature through numbers

Motions	Integration [%]	Ratio: paper with integrated motion / number of paper per category			
		Lumped parameter models [-]	Distributed parameter models [-]	Both approaches [-]	Purely experimental studies [-]
Relative speed	96.0	1/2	1	1	1
Swashplate tilt	44.0	1	1/7	2/3	1/4
Variable gap	60.0	1/6	5/7	0	1
Slipper tilt	76.0	1/6	1	1/3	1
Slipper azimuth	40.0	1/6	3/7	0	3/4
Slipper spin	36.0	0	2/3	0	0

2.6.2. Variable gap model of the slipper/swashplate interface

Most lumped-parameter models of axial piston pump in literature, even the most recent ones, consider constant gap heights, e.g. (Mancò, et al., 2002), (Aaltonen, 2016) and (Maurice, 2019). In this section, a variable slipper/swashplate gap is introduced. This variable gap was calculated as a consequence of the temporal balance of the forces applied on the slipper. The following modelling hypotheses were taken:

- Slipper and swashplate remain parallel (no slipper tilt);
- Hydrodynamic forces are neglected (no spin);
- Only 1-D displacements are considered in the slipper z_{sl} or piston z_b axial directions (see Figure 2-24);
- All forces out of piston or slipper axial direction are neglected (no lateral friction, centrifugal effect...);
- There is no play between slipper and piston at ball point;
- Swashplate tilting axis (D) is parallel to the barrel \vec{x}_b axis (see Figure 2-26);

These hypotheses lead to the model interface given on Figure 2-25, which summarises all external influences applied to the slipper, and are considered in this work:

- From piston chamber (ch) and pump case (c), pressure (P) and flow (Q);
- From the piston (p) and the swashplate (sp), the mechanical force (F) and the piston velocity (V). Force from the piston includes the chamber pressure force on the slipper through the piston and the viscous friction between piston and cylinder bore. Force from the swashplate is divided into hydrostatic force from the pressure in the gap between slipper and swashplate, and contact force of swashplate on slipper.

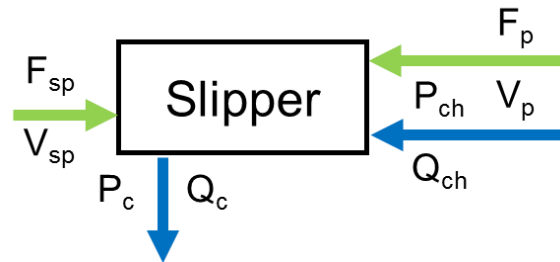


Figure 2-25: Schematics of slipper architecture block interfaces

2.6.2.1. Model

2.6.2.1.1. Slipper kinematics

Motion

The gap height can be seen as the consequence of slipper and swashplate relative movement, which is constrained by the retainer. The kinematics resulting from the made hypotheses is shown on Figure 2-26. On that figure, subscript (*p*) stands for piston, (*sp*) for swashplate, and (*b*) for barrel. The straight line (*D*) is the swashplate tilting axis. The point I is the intersection of (*D*) with axis $\overrightarrow{y_b}$. A is the centre of the ball joint linking slipper to piston. Distance *AB* is the length of the slipper. Distance *BC* is the gap height between slipper and swashplate.

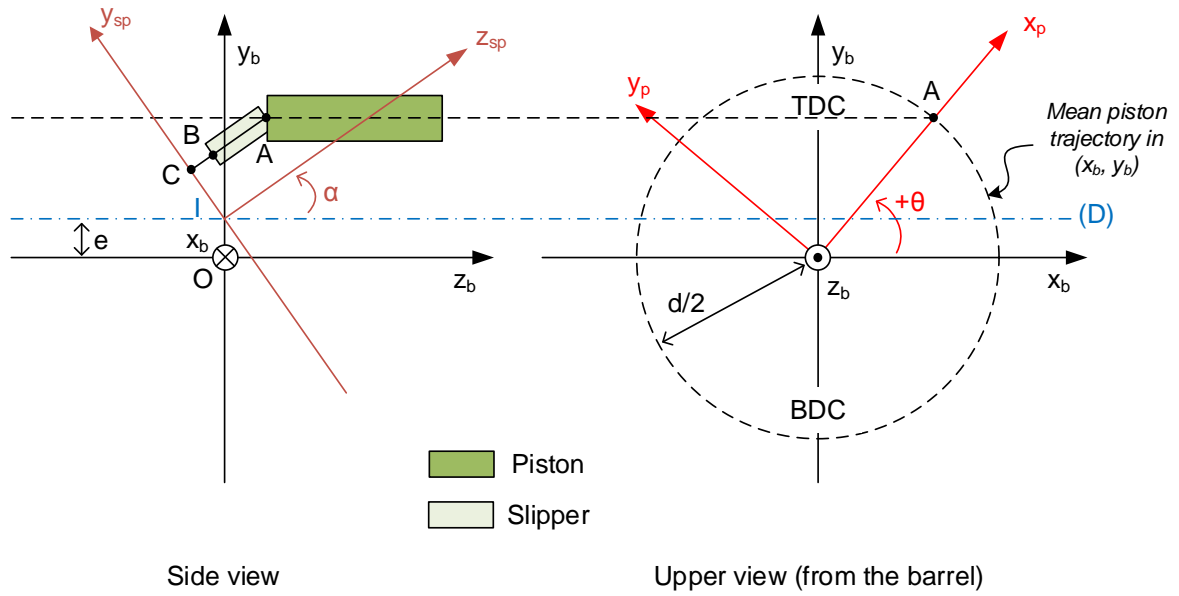


Figure 2-26: Schematics of the slipper kinematics

We are looking for distance $\|\overrightarrow{BC}\|$, the height of the gap between slipper and swashplate. It is possible to define $\|\overrightarrow{AC}\|$: with the hypothesis that slipper and swashplate are parallel, \overrightarrow{AC} is orthogonal to $\overrightarrow{y_{sp}}$ and $\|\overrightarrow{AC}\|$ is the distance from the point A to the *P* plane defined by $(\overrightarrow{x_{sp}}, \overrightarrow{y_{sp}})$. We define *K*, of coordinates (x_k, y_k, z_k) , a point of the plane *P* defined in the $(\overrightarrow{x_b}, \overrightarrow{y_b}, \overrightarrow{z_b})$ coordinate system as:

$$\forall K \in P, \forall x_k, \tan(\alpha) = -\frac{z_k}{y_k - e} \quad (2-27)$$

with

- α swashplate tilt angle [rad]
- e swashplate tilting axis eccentricity [m]

If the Cartesian equation of P is:

$$ax_k + by_k + cz_k + d = 0$$

then we have from (2-27) the following equation.

$$0.x_k + \tan(\alpha) y_k + 1.z_k - e \tan(\alpha) = 0 \quad (2-28)$$

The distance from a point A to a plane P (i.e. to point C) is defined by:

$$d_{A,P} = \frac{|ax_a + by_a + cz_a + d|}{\sqrt{a^2 + b^2 + c^2}} \quad (2-29)$$

With $\overrightarrow{OA} \begin{pmatrix} x_a = \frac{d}{2} \cos(\theta) \\ y_a = \frac{d}{2} \sin(\theta) \\ z_a \end{pmatrix}$, we obtain:

$$\|\overrightarrow{AC}\| = \frac{|\tan(\alpha)R \sin(\theta) + z_a - e \tan(\alpha)|}{\sqrt{\tan(\alpha)^2 + 1}} = \cos(\alpha) \left| z_a + \tan(\alpha) \left(\frac{d}{2} \sin(\theta) - e \right) \right| \quad (2-30)$$

with

- θ piston angular position [rad]
- z_a piston position following $\overrightarrow{z_b}$ [m]
- d Piston trajectory diameter in barrel coordinate system [m]

If we consider that $z_a > -\tan(\alpha) (R \sin(\theta) - e)$, the distance from point A to plane P is:

$$\|\overrightarrow{AC}\| = \cos(\alpha) \left(z_a + \tan(\alpha) \left(\frac{d}{2} \sin(\theta) - e \right) \right) \quad (2-31)$$

As $\|\overrightarrow{AB}\|$ is known and equals the slipper length l_{sl} , the slipper/swashplate gap height is:

$$\|\overrightarrow{BC}\| = h_{sl} = \cos(\alpha) \left(z_a + \tan(\alpha) \left(\frac{d}{2} \sin(\theta) - e \right) \right) - l_{sl} \quad (2-32)$$

Then, deriving $\|\overrightarrow{BC}\|$ with respect to time we obtain the slipper/swashplate gap height velocity \dot{h}_{sl} :

$$\dot{h}_{sl} = \dot{z}_a \cos(\alpha) + \sin(\alpha) \left[\frac{d}{2} \dot{\theta} \cos(\theta) - \dot{\alpha} z_a \right] + \dot{\alpha} \cos(\alpha) \left[\frac{d}{2} \sin(\theta) - e \right] \quad (2-33)$$

When correctly rearranged, equation (2-33) shows the influence of tilt angle variation $\dot{\alpha}$, pump rotating speed $\dot{\theta}$ and piston velocity \dot{z}_a . The influence of each of these three variables can be identified as a perfect transformer, as will be shown in the next section on the example of $\dot{\alpha}$.

Forces

Figure 2-27 displays the free body diagram of the slipper. Considering the hypotheses made, the forces taken into account in the current study are the following: contact forces from the swashplate and retainer F_{cont} , pressure force from the case fluid $F_{c/sl}$, pressure force from the fluid under the slipper F_{HB} and the force applied by the piston on the slipper $F_{p/sl}$. Pressure force from fluid in the gap between piston and slipper at the ball joint is neglected.

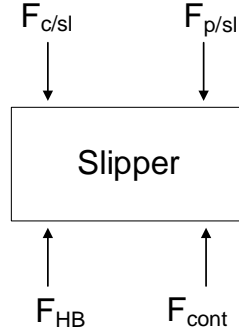


Figure 2-27: Forces on the slipper

Considering the hypotheses taken at the beginning of section 2.6.2, the Newton's second law applied to the slipper gives:

$$m_{sl}\vec{a}_{sl} = \vec{F}_{c/sl} + \vec{F}_{HB} + \vec{F}_{cont} + \vec{F}_{p/sl} \quad (2-34)$$

with

- a_{sl} slipper acceleration [m/s^2]
- m_{sl} slipper mass [kg]

However, it is considered in this study that there is no gap between piston and slipper. The slipper has no mass of its own and is considered, causality wise, as a source of effort for the piston. Then, the component of the slipper/piston force on the \vec{y}_b axis is the following:

$$F_{sl/p} = (-F_{c/sl} + F_{HB} + F_{cont}) \cos(\alpha) \quad (2-35)$$

F_{cont} is the overall contact force acting from the swashplate and retainer on the slipper. It is computed assuming a bilateral elastic end-stop model as described in section 2.4.4 page 32). $F_{c/sl}$ is the pressure force applied by the case fluid on the slipper and is written as:

$$F_{c/sl} = \frac{\pi d_c^2}{4} P_c \quad (2-36)$$

where P_c is the case pressure. If the flow in the gap is laminar, the pressure force F_{HB} on the slipper is (Ivantysyn & Ivantysynova, 2003):

$$F_{HB} = S_{eq} P_p = \frac{\pi(d_e^2 - d_i^2)}{8 \ln d_e/d_i} P_p \quad (2-37)$$

where

S_{eq} equivalent slipper active section for the application of pocket pressure (laminar flow hypothesis) [m²]

The hydrostatic force and contact forces applied at slipper interfaces are also considered to calculate the external torques applied to the swashplate. The torque developed by one slipper on the swashplate is written Γ_{sl/sp_i} and defined hereafter:

$$\Gamma_{sl/sp_i} = L_i (F_{hb_i} + F_{cont_i}) \quad (2-38)$$

Considering Figure 2-26, L_i is the distance following \vec{y}_{sp} between point C and swashplate tilting axis (D), and is defined by the following equation:

$$L_i = |(y_a - \|\vec{AC}\| \sin(\alpha) - e) / \cos(\alpha)| \quad (2-39)$$

Which gives:

$$L_i = \left| \cos(\alpha) \left(\frac{d}{2} \sin(\theta) - e \right) - \sin(\alpha) z_a \right| \quad (2-40)$$

It is to be noted that this result could have been found directly from the Bond-Graph theory. Two power variables denote of the effect of swashplate on the slipper/swashplate gap height: Γ_{sl/sp_i} and $\dot{\alpha}$. Considering this effect as that of a perfect transformation (e.g. across a TF-type transformer), and the energy conservation through such transformer, it was possible to identify L_i , the transformation factor, from (2-33). It corresponds to the factors affecting $\dot{\alpha}$ in the said equation.

Then the total torque $\Gamma_{sl/sp}$ applied by the slippers on the swashplate can be written as equation (2-41). The contact force F_{cont_i} at one slipper can be either negative or positive depending whether the contact occurs at the retainer or the swashplate, respectively. By convention, the torque on the swashplate from the slipper interfaces is positive when helping the compensating mechanism to increase the pump displacement, i.e. to increase the swashplate tilt angle.

$$\Gamma_{sl/sp} = \sum_{i=1}^n L_i (F_{hb_i} + F_{cont_i}) \quad (2-41)$$

The 1-D kinematic lumped-parameter model has been presented. The next section focuses on the hydraulic model that completes the proposed slipper/swashplate variable gap height model.

2.6.2.1.2. Slipper hydraulics

The slipper has interfaces with two fluid domains: the barrel chamber (Ch) and the pump case (C) as illustrated on Figure 2-28. This figure illustrates flows linking the slipper pocket domain (P) (pertaining to the slipper) and the other two fluid domains. Leakage at slipper/piston ball joint interface is neglected as it has been considered that there is no play between both parts.

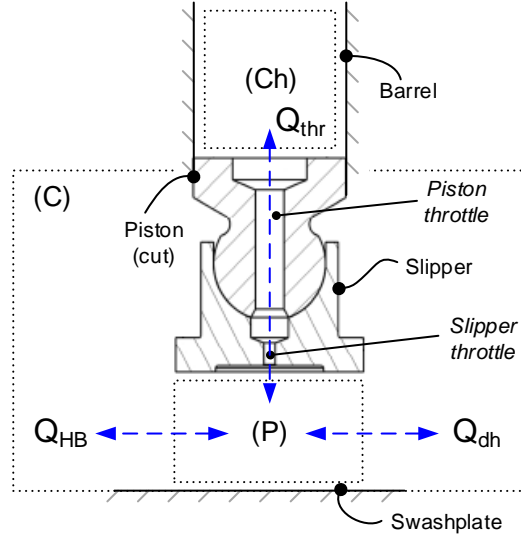


Figure 2-28: Slipper hydraulic interfaces schematics adapted from (Schenk, 2014)

The barrel chamber (Ch) and pocket (P) domains are connected through piston and slipper throttles as shown on Figure 2-28, through which the flow Q_{thr} streams. Considering two short orifices in series generates algebraic loops in simulation due to causality constraints. In order to avoid this, two options are possible: model an equivalent orifice or introduce an intermediary volume between the two throttle orifices. Given the fact that, in the current application, for a given flow rate, the slipper throttle generates about ten times more pressure drop than the piston throttle due to their difference in section, it is chosen to simplify the problem by considering to an equivalent short orifice. Q_{thr} is then computed considering an orifice flow and equation (2-3) reminded hereafter.

$$Q_{thr} = C_d A \sqrt{\frac{2}{\rho} (P_0 - P_1)}$$

On Figure 2-28, two flows link the pump case (C) and the slipper pocket (P) domains. The first one, Q_{HB} is the leakage through the slipper/swashplate gap due to pressure difference. This flow is computed as expressed in (2-26) page 56, given the variable slipper/swashplate clearance outputted by the kinematics model. Equation (2-26) is reminded hereafter:

$$Q_{HB} = \frac{\pi h_{sl}^3}{6 \mu \ln\left(\frac{d_e}{d_i}\right)} (P_p - P_c)$$

The second flow between (C) and (P) domains is the consequence of the slipper displacement, sucking in or pushing out flow from slipper pocket domain, through the clearance. It is modelled as follows:

$$Q_{dh} = S_{eq} \dot{h}_{sl} \quad (2-42)$$

Then the pressure inside the slipper pocket domain (P) is computed using the continuity equation, as a function of those three flows and of the fluid compressibility:

$$\frac{dP_p}{dt} = \frac{B(Q_{thr} + Q_{HB} + Q_{dh})}{V_{(P)}} \quad (2-43)$$

In the last equation $V_{(P)}$ is the domain volume at the current time step, which variation is the consequence of the slipper motion. Depending on the pressure conditions in the pocket, case and chamber domains, the flows Q_{thr} , Q_{HB} and Q_{dh} can be either positive (entering the domain) or negative (leaving the domain).

The slipper motion impacts the case domain (C) just as the pocket domain (P) shown on Figure 2-28: it generates a pumping effect. The consequent pumped flow is the following:

$$Q_{sbp} = \frac{\pi d_e^2}{4} \dot{h}_{sl} \quad (2-44)$$

This pumping motion within the pump case is also introduced at the piston, with equation (2-44) adapted to piston geometry.

The model proposed for both slipper hydraulics and kinematics has now been presented. In the next section, its implementation is analysed using the Bond-Graph formalism and then made in the simulation environment.

2.6.2.2. Model implementation

The slipper/swashplate interface model is shown on Figure 2-29 using the Bond-Graph formalism. This model uses the equations described in the previous section and gathers both kinematics and hydraulics of the slipper/swashplate interface. The three TF-type modulated transformers used to describe the influence of swashplate tilt, piston and pump rotating speeds on the slipper/swashplate gap are visible on the bottom-half of the figure.

The pressure force from the gap is considered through a TF transformer (equivalent to a piston) ❶ with the equivalent area S_{eq} . The gap height is bounded with an end-stop model ❷ that also calculates the F_{cont} force. The influence of

the case pressure on the slipper is taken into account through the TF ③. This component also generates back-pumping from the slipper inside the pump housing. The projection of the forces on the slipper axis is made at ④, through another pure transformer. The leakage from the piston to the case flows through the fixed resistance R ⑤, which corresponds to the slipper throttle, then through the slipper/swashplate gap ⑥ which is implemented as a modulated R (making the orifice area varying as a function of the gap height). The model implemented in the Simcenter AMESim (v14) simulation software is shown on Figure 2-30. The same notation is used on Figure 2-30 and on Figure 2-29 to show the equivalence between both models. Three distinct transformers illustrate the effect of swashplate tilt, rotating speed and piston velocity on the slipper/swashplate gap height in the bond-graph of Figure 2-29. However, only the piston transformer is shown on Figure 2-30, at ④. The absolute viscosity is a variable which depends on pressure. In order to account for that, in AMESim, the absolute viscosity is ‘measured’ at slipper pocket and used at ⑥ for the computation of the isothermal hydrostatic bearing flow.

The model verification, as well as discussion on the simulation results, is made in the following section.

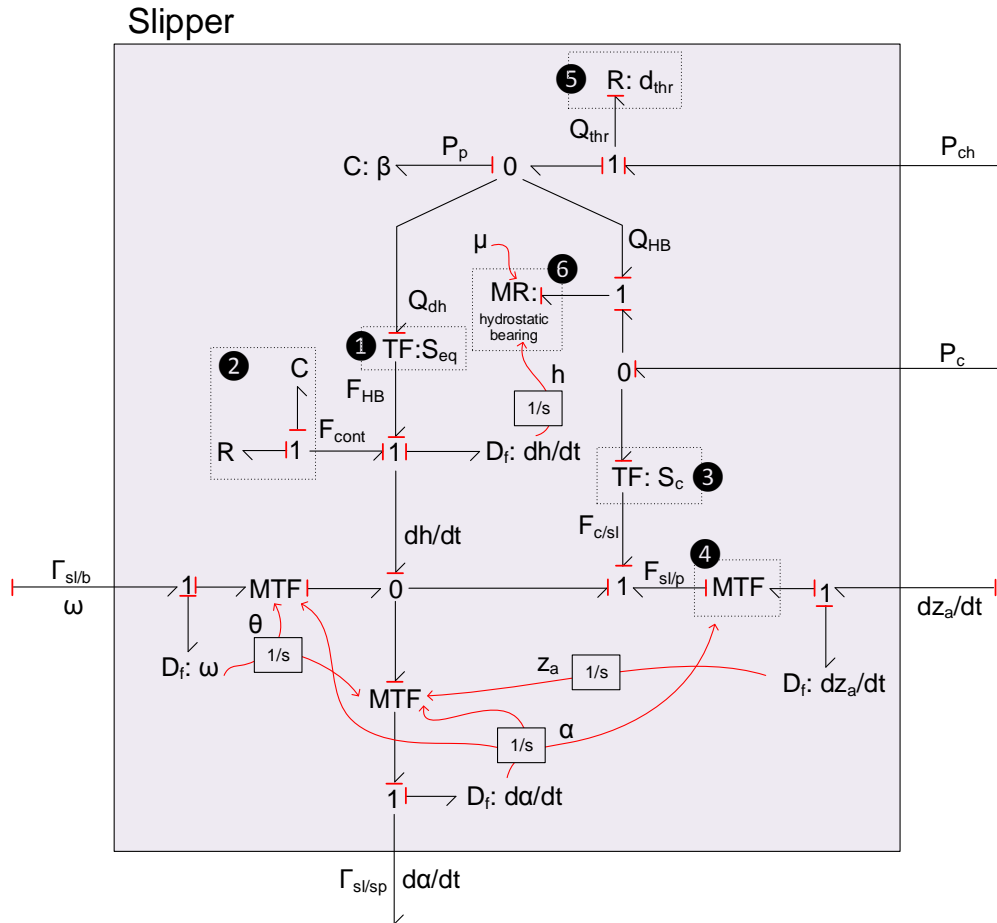


Figure 2-29: Proposed slipper bond-graph model

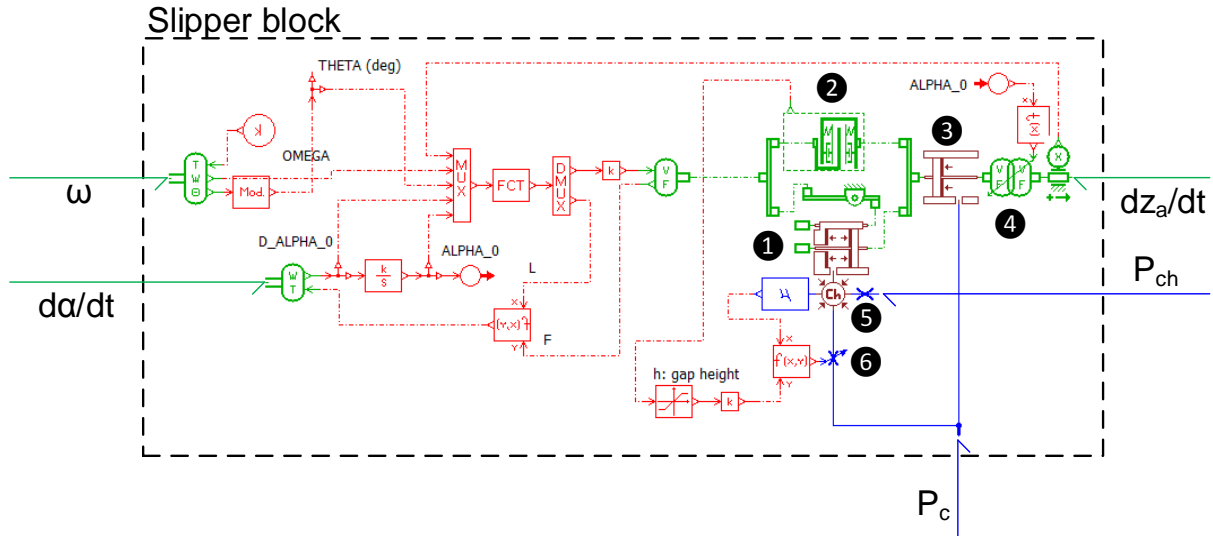
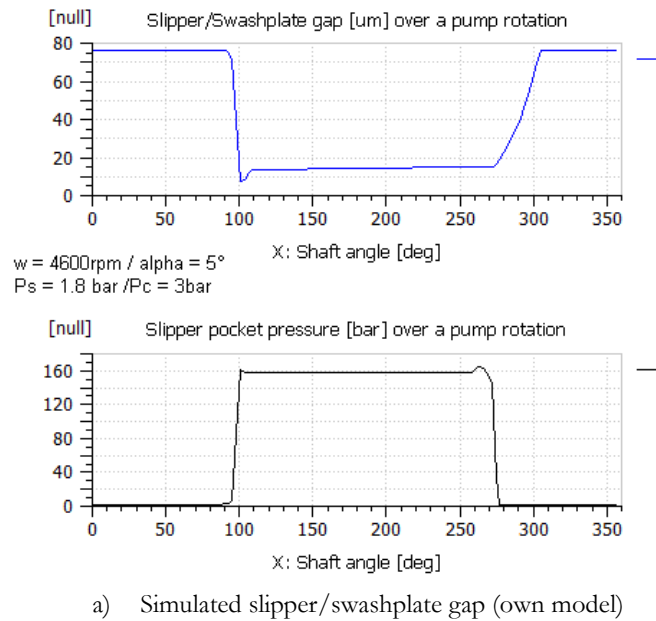


Figure 2-30: Slipper/Swashplate interface model in AMESim

2.6.3. Model verification and discussion

In order to assess the model, it must be first verified that the slipper gap behaviour during a pump cycle is acceptable. To this end, the simulation results from a simple one-piston model (a) are compared qualitatively with 3-D simulations from literature (Ivantysyn & Weber, 2016) (b) and experimental measurements (Chao, et al., 2018) (c) in Figure 2-31. From this comparison, it is verified that simulation reproduces the slipper/swashplate gap height in the same order of magnitude and shape.



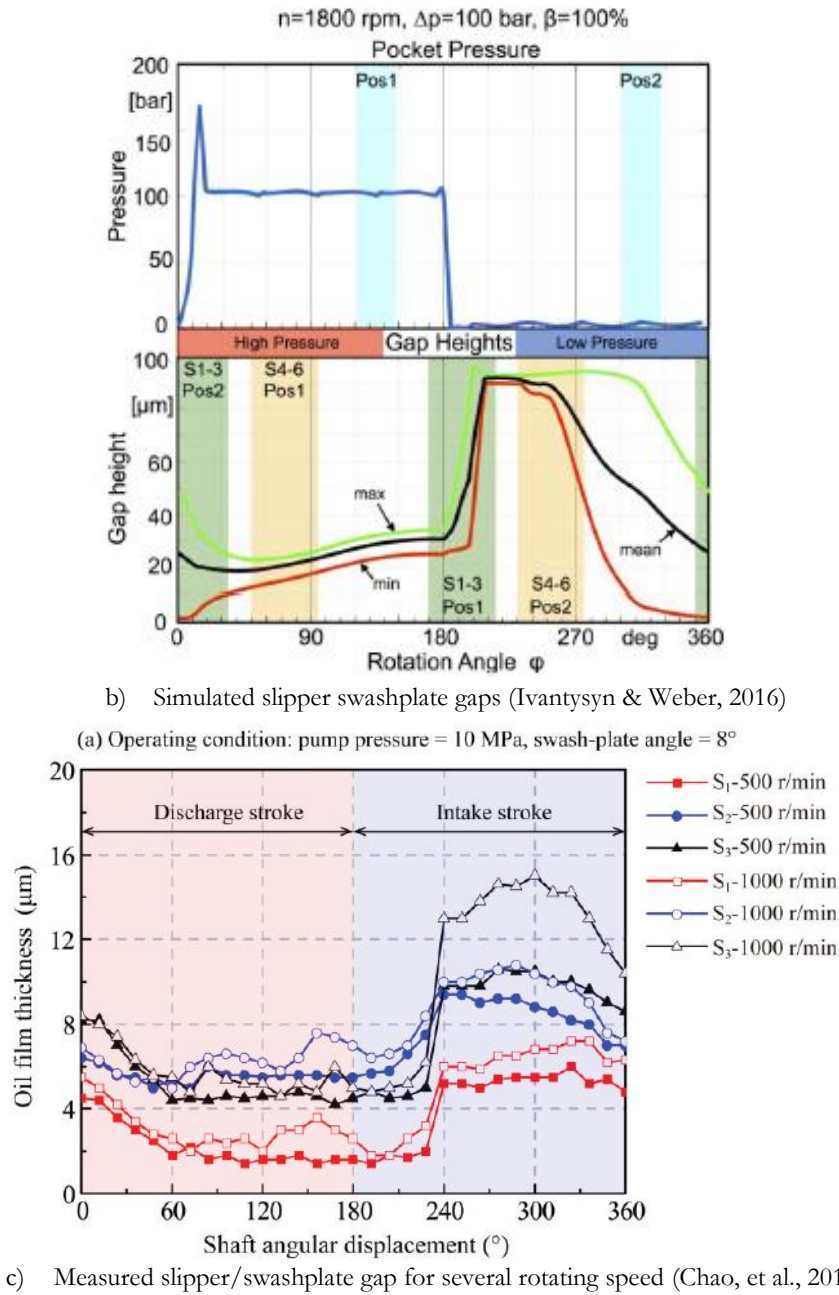


Figure 2-31: Comparison of simulated slipper/swashplate gap with literature

In a second time, the simulation results are compared to that of the generic equations presented in section 2.6.1 (p56). Table 2-13 lists the numerical results for the mean simulated slipper leakage over one pump shaft revolution, computed with the same pressure boundary conditions as in Table 2-10 (p56). The simulated conditions are reminded in the second part of Table 2-13, and Figure 2-32 compares the defined variable in simulated and ideal cases (as per Table 2-10). The relative error, included in Table 2-13, allows for the quantitative comparison of the numerical results. This error is computed as the following:

$$E_r = \frac{Q_t^* - Q_t}{Q_t^*} \times 100 \quad (2-45)$$

Even if in the case of a not tilted swashplate, the leakage is greater than the specified 1.5 L/min (see Table 2-1), the total leakage at slippers Q_t is at least 20% lower than that from the generic model Q_t^* (which is independent from swashplate yoke) whatever the pump displacement. It is interesting to note that at maximal pump displacement, the simulated leakage becomes negative, meaning that the slipper averagely sucks fluid from the pump case.

Table 2-13: Comparison of total leakage at slipper/swashplate interface for 1 rev.

Variable	α [deg]	Q_t^* [L/min]	Q_t [L/min]	E_r [%]
Values	0	1.960	1.567	20.06
	5		0.846	56.84
	15.15		-0.56	128.6

Simulated conditions:

Constant parameters				Variables	
d_e/d_i [-]	P_d [bar]	P_s [bar]	P_c [bar]	P_p [bar]	h_{sl} [μ m]
1.45	160	1.8	3		

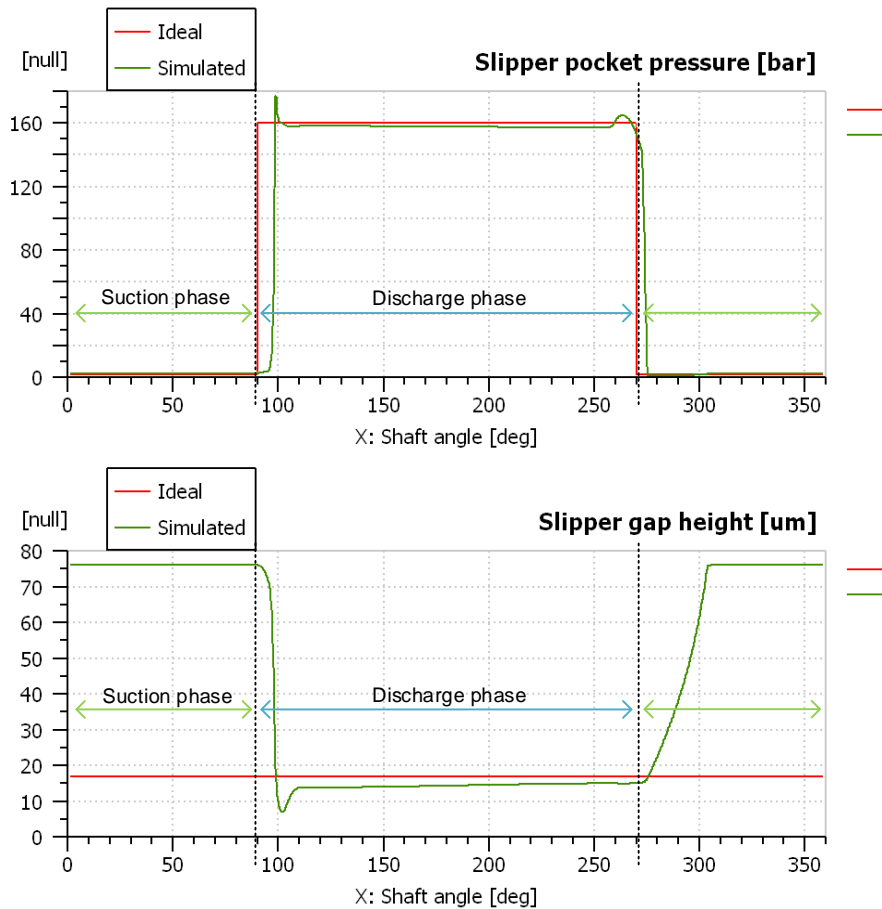


Figure 2-32: Comparison of ideal and simulated variables for slipper leakage computation

One slipper can momentarily suck in fluid from the case, however, a negative average total leakage flow is unrealistic.

In order investigate this simulation result, the simulated slipper/swashplate clearance over two pump shaft revolutions is shown on Figure 2-33, for several operating conditions.

Figure 2-33 highlights two phenomena at low pump displacement. Firstly, the discharge (high) pressure generates slipper lift as predicted by hydrostatic bearings theory. The second phenomena is linked to case pressure. This last point is specific to the present application where forces from case pressure are implemented on slippers and pistons back sections. The parameterized slipper back section is larger than that of the piston, which leads to piston/slipper subassembly displacement towards the swashplate during the suction phase.

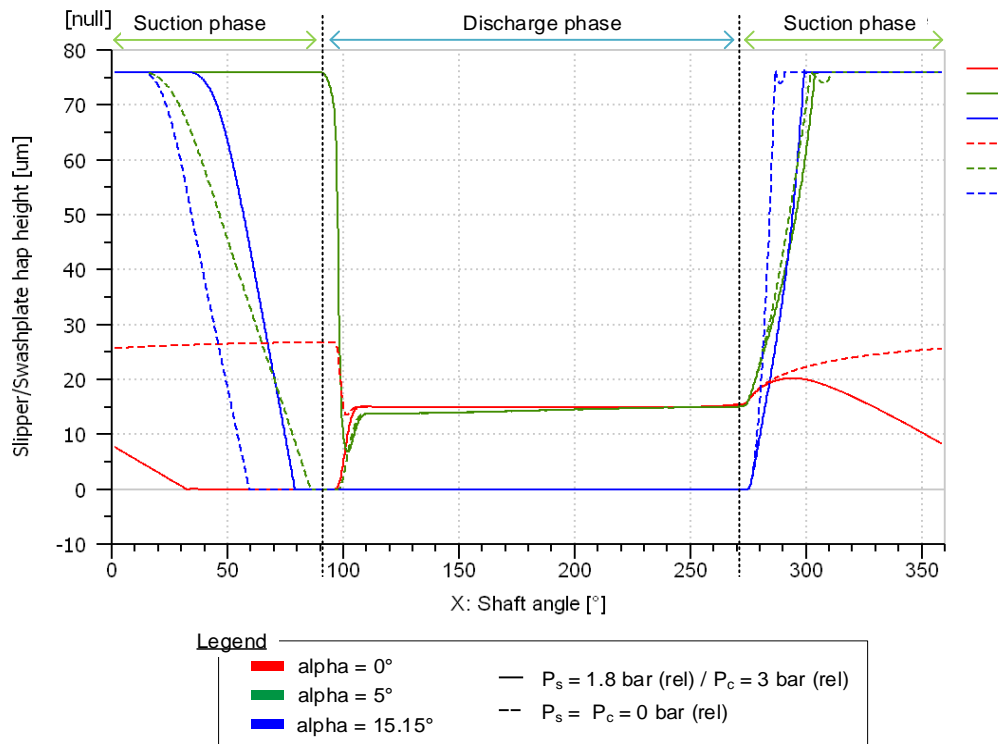


Figure 2-33: Slipper/swashplate gap height over pump rotation in several simulation cases

For high pump displacement, Figure 2-33 shows that the modelled pressure force under the slipper does not allow to lift it hydrostatically during the discharge phase. During the suction phase, the slipper is lifted up until it makes contact with retainer. As the case pressure is greater than the piston chamber pressure in this simulation, this movement leads to fluid intake at slipper. Both facts (no lift at discharge phase and fluid intake during suction phase) explain the overall negative slippers leakage.

The inability of the simulated hydrostatic bearing at the slipper/swashplate clearance to lift the slipper leads to long duration contacts between slipper and swashplate. One of the purpose of the clearance is to maintain lubrication between both parts. Contacts are not desirable as they result in excessive friction, abrasion and wear of the normally lubricated pair, as such, slippers are designed to avoid such contacts. As a consequence, even if slipper/swashplate contact is indeed possible, the duration of the simulated contacts seems excessive and unrealistic. Considering this result and the overall negative leakage at high pump displacement, hints to the need of introducing additional physical effects.

Another limit of the presented model is the equivalent section S_{eq} used to account for the logarithmic decrease of the pressure in the gap along the slipper radius. This section is also used to compute the fluid volume variation under the slipper due to slipper motion. Using the correct section ($\pi d_e^2/4$), the fluid pumping motion of the slipper in the case should be overall compensated: one side (at clearance) of the slipper moves as much fluid as the other side (at case). This is not the case in the current model, and the section unbalance can generate higher flow exiting or entering the pump housing through the case port than in reality.

The behaviour of the slipper is linked to the balance of applied forces. Pressure, centrifugal, contact, friction forces are all playing a role in the slipper attitude, linking slipper tangential speed relative to swashplate, gap, tilt and spin together. The literature gives information about how the effects are coupled. Table 2-14 shows what relations can be pulled out of the source documents, for slipper attitude (gap, tilt, and azimuth) and leakage at interface. Slipper spin in complete pump environment is very little addressed in the literature found but experimental studies showed the reality of slipper spin on test rigs, one example being (Zhang, et al., 2017). Over twenty-seven documents, fifteen give information on slipper/swashplate gap, four on slipper tilt and one on slipper azimuth. Nine out of twenty-five documents show equations or graphs illustrating the leakage at slipper/swashplate interface.

In the current application, we need to be able to describe the (mean) gap height as a function of swashplate tilt, shaft rotating speed, chamber and case pressures, temperature, and piston angular position. The leakage flow must be a function of the (mean) gap height, case and chamber pressures, rotating speed and piston angular position, as well as temperature. None of the information from the gathered literature is that complete. Other ways of improving the presented 1-D lumped-parameter model, not based solely on literature, have to be found.

In this context, there are several possible means of improving the current lumped-parameter model. The first one is to arrange the slipper hydraulic

unbalanced sections. This would mean using a different section for the computation of the hydrostatic force on the slipper F_{hb} than for the flow due to gap variation. In practice, a short term option could be a separation of the hydraulic and mechanical domains by signal in this part of the model. However, this separation of bonds must be realized carefully to keep the modelled physics correct.

A second way of improving the current model is to integrate the squeeze effect that has not yet been completely introduced. Squeezing generates a force that results from slipper motion towards the swashplate, compressing (or sucking) the fluid in the gap. This effect is included in the current model. However, there is also a damping effect due to the fluid around the slipper, which is currently not taken into account in the model. This squeeze effect is discussed in (Adams, 2017) for hydrostatic pads and could be integrated in the current 1-D model.

Table 2-14: Information on slipper attitude and leakage from literature

		References	Slipper attitude description (mathematical or figure)	Slipper leakage description (mathematical or figure)
Equation resolution	Analytical	(Böinghoff, 1977) (Hooke & Li, 1988) (Mancò, et al., 2002) (Bergada & Watton, 2005) (Yi & Jiang, 2011) (Li, et al., 2015) (Aaltonen, 2016)	$h = f_1(\alpha) ; h = f_2(\omega)$ $h = f(\alpha, P)$	$Q/A = f(\omega, \alpha)$ $Q = f(P, \alpha)$
	Numerical	(Bergada, et al., 2007) (Kumar, et al., 2009) (Bergada, et al., 2012) (Xu, et al., 2012) (Xu, et al., 2015) (Tang, et al., 2016) (Wang, et al., 2015) (Lin & Hu, 2015) (Ma, et al., 2015) (Schenk & Ivantysynova, 2015) (Ivantysyn & Weber, 2016) (Chao, et al., 2018)-1 (Jiang, et al., 2018)	$h, \gamma = f(\theta, P)$ $h = f_1(\theta, P) ; h = f_2(\theta, \omega)$ $h, \gamma = f(\theta)$ $h = f(P, \omega)$ $h = f(P, \omega)$ $h = f(\theta)$ $h = f(\theta)$	$Q = f(h, \gamma)$ $Q = f(P, h)$ $Q = f(\gamma, h, P, \omega_s, \theta)$ $Q = f(h, P)$
	N&A	(Bergada & Watton, 2002) (Bergada, et al., 2010) (Bergada & Kumar, 2014)	$h = f(P)$ $h = f(\omega, P)$	$Q = f(P)$ $Q = f(P, \omega, h, \gamma)$ $Q = f(P, \omega, h, \gamma)$
	None	(Rokala, et al., 2008) (Suzuki, et al., 2011) (Kazama, et al., 2014) (Chao, et al., 2018)-2	$h, \gamma = f(\alpha, P)$ $h, \gamma = f(\omega, P, T)$ $h, \gamma, \varphi = f(\omega, P)$ $h = f_1(P, \theta) ; h = f_2(\omega, \theta)$	

Legend:

γ	Slipper tilt	P	Pressure	Q	Leakage flow	φ	Slipper azimuth
α	Swashplate tilt	ω	Shaft velocity	h	Gap height	ω_s	Spin velocity

Slipper load-carrying capability is affected by temperature. As such, a third way would be to introduce thermal effects inside the current lumped parameter model. Doing so, two separated improvement can be made: the inclusion of thermal wedge bearing force to the slipper force equilibrium as done in (Tang, et al., 2018), and the effect of local temperature increase on slipper/swashplate leakage flow due to fluid viscosity variation .

As a fourth option, if one would want to integrate the hydrodynamic effects and to consider slipper tilt, it would be then necessary to make important modifications of the model. One option is to include forces on the slipper on all three axes. This would lead to a 3-D lumped-parameter model. In this direction, the use of co-simulation approaches as in (Rocatello, et al., 2007) can be interesting, but care should be taken to limit the computational burden. Another option is to build *metamodels* of the slipper/swashplate interface. Those metamodels would be built from distributed-parameter models. Compared to a 3-D lumped-parameter model, the last option would allow to keep the simulation time relatively short, as well as to describe accurately the gap behaviour and the consequent leakage.

2.7. Conclusion

A virtual pump was developed to enable the industrial questions to be answered (can we monitor pumps degradation through case pressure measurements alone). It has been discussed that AH does not need very detailed physics-based distributed-parameter models. As such, a lumped-parameter model has been developed. However, it has been shown that lumped-parameter pump models are much less accurate than distributed-parameter models. This observation led to the following scientific questions, drawn in section 1.3 p14:

- Q3. What is the current state of the art for axial piston pump modelling?
- Q4. What improvements can be made from state of the art 1-D pump modelling in the view of condition monitoring and what do those improvements bring?
- Q5. Is the pump model, running a simulated test in given operating conditions, able to reproduce the same result data and patterns as real tests made in the same operating conditions?

The present chapter aimed at answering the first two scientific questions Q3 and Q4, focusing on the pump pressure compensation mechanism and on the slipper/swashplate interface. The question Q5 is answered in the following Chapter 3.

In the current chapter, as a complete 1-D pump model was developed, model architecting were firstly considered. A topology-based architecture has been chosen in order to fulfil the model durability requirements presented in Table 2-4 (p19). Then, the Bond-Graph formalism has been shortly presented in order to facilitate the reader's comprehension of models proposed in the following sections. The said sections focussed on pump pressure compensation mechanism on one part, and on the slipper/swashplate interface on the other part.

It was shown that, although the pressure compensator lumped-parameter modelling is well established in literature, the listed models do not allow for the simulation of temporal degradation processes, but only to simulate degraded states through proper parameterization. As such, a way of implementing models for the simulation of the degradation processes has been proposed, focussing of both processes: valve metering edges erosion and spool jamming.

Both processes have been discussed and a way of implementing them has been proposed through with support of the Bond-Graph formalism. Then the complete model has been presented and implemented in Simcenter AMESim environment. The model has been verified in healthy state against ATP specifications and proved to behave better than specified when tested on a virtual test bench with a perfect pump. The main capabilities of the model to simulate valve erosion and spool jamming have been highlighted, with numerical values chosen arbitrarily. It was however reminded to the reader that the aim of this work was to show ways of implementing degradation models but not the development of degradation models themselves. Degradation models remain a perspective of said work.

The slipper/swashplate interface has a complex physical behaviour which includes several free motions, pressure and centrifugal effects etc. An extensive literature review was performed. It has shown how detailed the distributed-parameter models are compared to lumped-parameter models of this interface. Special consideration to slipper motion and attitude was given in this review. It was concluded that state-of the art 1-D models of the slipper/swashplate could be improved through the integration of additional degrees of freedom. Then a variable dynamic gap height model for the slipper/swashplate clearance has been proposed. This model is based on the introduction of the slipper kinematics perpendicular to the swashplate. The following hypotheses were assumed: no slipper tilt, only 1-D displacements are considered, hydrodynamic forces are neglected, and all forces out of piston or slipper axial directions are neglected. It was shown that the presented model allows for simulation of a qualitatively coherent gap height variation compared to literature.

The simulation results were also compared to a well-established constant gap height leakage models. The introduction of a variable gap reduced the simulated leakage flows, which is much more coherent with the current pump application.

The proposed slipper/swashplate interface model has, however, several shortcomings. Long slipper/swashplate contacts were observed for simulations at high pump displacement which indicates that, in the current application, the hydrostatic forces are insufficient to properly lift the slipper in some conditions.

Solutions to introduce equivalent 1-D models of hydrodynamic effects was searched in the literature. It was found that none of the information from the gathered literature is complete enough to allow for building the model necessary in the current application, in terms of gap height or leakage behaviour. Several ways of improving the current model have been proposed, including the use of metamodels to reproduce a more complete behaviour of the slipper/swashplate gap and leakage in several operating conditions. It is the author's conviction that metamodels of the gaps, generated from real or CFD tests, are the best approach in the current application: they allow for the simulation of very complex phenomena with lighter computational burden.

3. Model assessment

3.1. Introduction

The current research work aims at investigating pump monitoring through pressure measurement at case drain port. As such, and as already discussed in Chapter 1, this dissertation must answer the following industrial questions:

Q1. On H/C, can external case pressure sensors be used to detect pump degradation prior to failure?

Q2. Can pump degradation be isolated from hydraulic system degradation when using one additional case pressure sensor only?

To answer these industrial questions, a pressure compensated axial piston pump lumped-parameter model has been developed. Parts of this model have been described in the last chapter, in which the author presented improvements of the axial piston pump lumped-parameter modelling state of the art (when focusing on condition monitoring). These improvements were proposed to answer some scientific questions linked to modelling. However, one scientific question, Q5, stays unanswered:

Q5. Is the pump model, running a simulated test in given operating conditions, able to reproduce the same result data and patterns as real tests made in the same operating conditions?

This question is linked to the industrial context surrounding the present project and the requirements defined in Table 2.3. Q5 asks for a quantitative answer, based on proper model assessment. As the model must allow simulation of “degradation leading to increased internal linkage” (Rq2 of Table 2.3), it should be assessed both in healthy and degraded states.

In order to answer Q5 and to investigate the model behaviour, it is then necessary to collect real test data with pumps in healthy and degraded states.

It was discussed in Chapter 1 that degraded in-service pumps are normally not available at AH for experimental testing due to the current maintenance process policy and contracts. Thus, it was not possible to gather real data to use for model assessment from an in-service degraded pump.

In such a context, two options - also used in literature - to transform a healthy pump into a degraded one in the frame of laboratory experiments are possible: accelerated degradation processes, or building a pump with parts, which are

especially designed and machined as degraded, based on known degradation modes. The first option relies on a heavily polluted fluid and damaging cycles which increase the pump parts wear rates (see e.g. (Chen, et al., 2016) or (SAE International, 2016)). The representativeness of the obtained degradation compared to that observable on H/C in reality is not certain. As such, it was decided to leave this option out.

The second option simulates a degraded pump through introduction of modified parts (e.g. out of tolerance to increase clearances as in (Bensaad, et al., 2019)). However, this approach is very costly and time consuming. Due to these two reasons and the time frame of the present work, it was not possible to implement such an approach. As a consequence, the topic of built-in degradation in axial piston pumps was also left out of the present research work.

As a straight forward approach under the given constraints, the comparison of the healthy pump model (simulation) against a healthy pump (real test) with resort to simulated and real test data is presented hereafter. In the following sections, the test bench used for data gathering of the healthy hardware pump is described, as well as the model assessment process, which includes the creation of a test bench model, the adaptation of the pump model and the final evaluation of the models combination. The simulation model is compared to the gathered data, and leads to replying the question Q5.

3.2. Experiments

A serial production hydraulic pump from the Super Puma H/C program (now branded as H225), operated with MIL-PRF-83282 hydraulic fluid, was used for the experiment. The said H225 pump has 0 FH (flight hours) and belongs to AH. To make sure that it could be used for the current project, its behaviour was tested using the ATP. The pump passed the test with success (see annex A-4).

In order to realize the hardware data gathering, test campaigns were realised in the facilities of an industrial partner of AH, using a test bench that was available in the partner's facilities. For each test campaign, the author specified the tests (which were non-standard), attended and contributed to the tests and analysed the measurement obtained. In total, three tests campaigns were realised over a period of one year.

The test procedures for the gathering of the pump data as well as the test bench characteristics and behaviour (including sensors and acquisition system) are presented in the following sections.

3.2.1. Test procedure

Both static and dynamic load tests were made. In static load condition, the flow rate demanded by the hydraulic system to the pump is constant throughout the test duration. In dynamic load condition, the system load varies to either increase or decrease the demanded discharge flow.

The full static and dynamic tests list and conditions are described in annex A-1. The following table is proposed as a summary of it. The static load tests were made for several driving speeds, temperatures, pressures at suction port and delivered flows. The dynamic load tests were made under varying hydraulic load (step or ramp), for different suction temperatures. The nominal experimental conditions were: 4600 rpm drive speed, and 0 bar (rel) suction pressure.

The scale of temperature variation is in the working range of the H225 pump on H/C. Rotating speed was varied to investigate the impact of pump rotating speed on case drain pressure and flow variation. The same reason goes for the variation of pump suction pressure. At this point, it is brought to the reader's attention that every pressure value given in this chapter is in bar relative to standard atmospheric pressure (rel).

Table 3-1: Summary of testing conditions for data gathering

Condition Test type	Driving speed [rpm]	Suction pressure [bar relative]	Fluid and climatic chamber temperature [°C]	Load variation
Static	{920; 3545, 4600; 5500}	{0; 2.5}	{50; 100}	N/A
Dynamic	4600	1	{50 ; 100}	{step 0 to 27 L/min ; 27 (L/min)/s ramp}

Five measurement points were defined for each static load test condition, in an attempt to identify the pump static characteristic shown on Figure 3-1. Points (2), (3) and (4) were defined at set pressures of 167, 100 and 50 bar respectively. Points (1), in zero discharge condition, and (5), in full discharge flow condition. They are dependent on pump setting, on the operating conditions (suction pressure, fluid temperature, rotating speed) and on the test bench architecture. The system load can have leakage ('Qmin'), and the hydraulic system generates a minimum pressure drop inherent to its components ('Pmin'). This is the reason why values of discharge flow and pressure are not defined at point (1) nor at point (5).

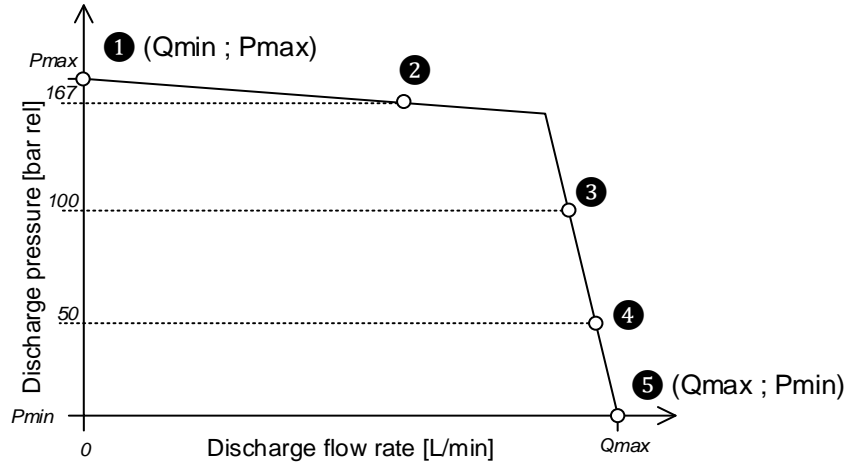


Figure 3-1: Schematics of the pump static operating points to be reproduced in tests

In dynamic conditions, the pump hydraulic load (flow demand) will be controlled to make the pump discharge pressure vary from 0 to 100%, and then from 20 to 80% only. The reason for the latter was to obtain an image of the pressure compensation mechanism without effects introduced by the displacement end-stops.

3.2.2. Test bench set up

International standards can help the definition and realization of experiments and test benches. For example ISO 17559 (ISO, 2003) for electrically controlled pumps, ISO 4409 (ISO, 2019) to test positive displacement pumps steady state performance, or even SAE J745 (SAE International, 2019) for hydraulic positive displacement pumps used on off-road self-propelled work machines. AS19692B (SAE International, 2016) or ISO 8278 (ISO, 2016) define dynamic pump tests for qualifications.

In the present work, an existing test bench was adapted in AH industrial partner facilities for the test campaigns, which allowed for the realization of both steady state and dynamic tests. The industrial partner has defined this test bench to be capable to perform temperature tests on different hydraulic pumps, complying with the various pump performance requirements.

The test bench hydraulic scheme is displayed on Figure 3-2. The test bench is composed of a tank ❶ and the mechanical interface for the test pump (here our H225 pump shown) ❷ which are installed inside a climatic chamber. The loading system and the fluid circulation lines are located outside the climatic chamber. The test pump is driven by a variable-speed electrical motor ❸. The hydraulic pump is loaded by a combination of a manual valve ❹ that is mounted in parallel to pneumatic-operated shut-off valve ❺ followed by a servo-valve ❻ providing

variable hydraulic resistance. Two filters ⑦ and a cooler ⑧ are mounted on the return lines.

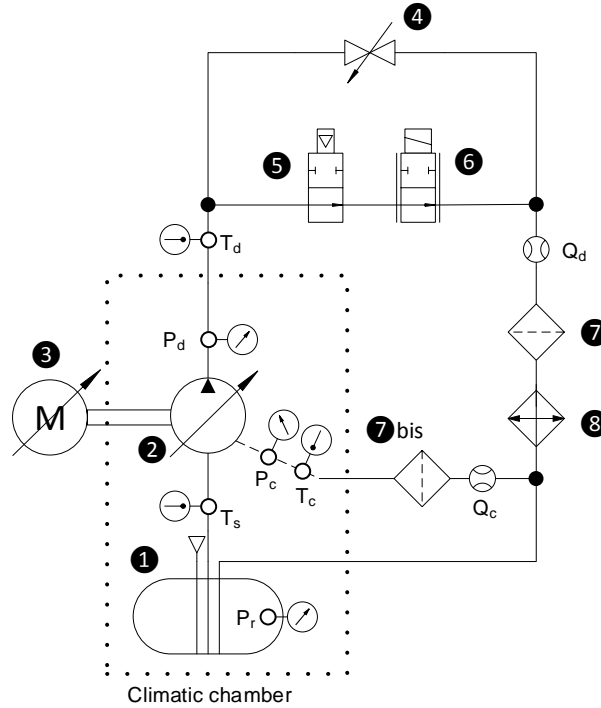


Figure 3-2: Simplified test bench hydraulic scheme

A hard constraint of the present study is not to use intrusive sensors (refer to Chapter 1 for more information) on the axial piston pump. In the test bench proposed by the industrial partner, pressure, flow and temperature can be recorded, as well as ambient temperature, motor torque and motor rotating speed. Figure 3-2 shows the locations of flow (Q), temperature (T) and pressure (P) sensors on the test bench. On this figure and in the rest of the chapter, subscript ‘ d ’ stands for discharge while ‘ s ’ means suction, ‘ c ’ is for case drain and ‘ r ’ is used for reservoir.

Suction pressure was measured inside the tank. Inlet flow rate is considered to be the sum of recorded discharge and case drain flow rates (closed loop) in steady-state conditions, as the test bench has no measureable external leakage. Hose and pipe data as well as sensors detailed location are given in annex (part A-3).

The sensors characteristics are summarized in Table 3-2 hereafter. Unfortunately, the industrial partner could not provide any characteristics for the thermocouple temperature sensors.

As the aim of the project is to assess the usability of the case pressure as monitoring mean, it was of primary importance to get accurate measurements of it. It is for this reason that both high (Kulite) and low (HBM) bandwidth pressure

sensors were used at both case drain and discharge ports. Note that only the locations of the Kulite pressure sensors on the test bench are highlighted on Figure 3-2.

Table 3-2: Sensor data sheets summary

Data \ Sensor	High pressure	Low pressure	High pressure	Low pressure
Type	Kulite HEM-375 (high bandwidth)	Kulite HEM-375 (high bandwidth)	HBM P3 500 (low bandwidth)	HBM P3 50 (low bandwidth)
Full scale	350 bar	17 bar	500 bar	50 bar
Accuracy	+/- 1% FS		+/- 1 % FS	
Compensated / rated temperature range	[+25; +204] °C		[-40; +80] °C	
Sensor type	Piezoresistive		Strain gage	

Data \ Sensor	High flow	Low flow	Speed	Torque
Type	Kem Kueppers HM 009 E	Kem Kueppers HM 005 E	Magtrol TM-311	
Full scale (FS)	29.7 L/min	5.2 L/min	1 to 10,000 rpm	Rated torque 100 N.m
Accuracy	+/- 1% FS		< 0.1% FS	< 0.1% of FS
Compensated temperature range	[0; +200] °C		[-40; +85] °C	
Sensor type	Turbine		Phonic wheel (speed) and strain gauge (torque)	

In order for the measurements to cope with the pump dynamics, a high sampling rate is necessary. The pump basic frequencies are: 1) the pump shaft rotating frequency f_b (in Hz, $f_b = \omega/60$, with ω being the rotating speed in rpm), 2) n pistons times the rotating frequency $f_p = n f_b$, i.e. the pressure pulses due to piston chambers shifting from suction to discharge due to valve plate porting (porting pulsation), 3) f_p second harmonics $f_{2p} = 2n f_b$, generated by the piston number (displacement ripple due to combination of active pistons). Considering the need for about 15 measurements per period to correctly catch the pump dynamics, a sampling rate of 10 kHz was chosen. This sampling rate allows for at least 14 points per piston pressure pulse oscillation, and at least 7 points at the piston pulse frequency first harmonics. For a pure sine wave of frequency f_p and, the error on the measured wave peak to peak amplitude due to the sampling rate of 10 kHz is of 0.75%, and of 4.18% for a frequency f_{2p} .

No information was available on signal conditioners from AH industrial partner. Their range was assumed to be of 0-10V, (or -10;+10 V) and to have a 12-bit resolution. A digital low-pass filter parameterized as a function of the

sampling frequency was used. The filter frequencies for the measured variables are shown in Table 3-3. Flow and temperature were not low-pass filtered.

Table 3-3: Acquisition of sensor signals

Sensor	High pressure (high bandwidth)	Low pressure (high bandwidth)	High flow	Low flow	Tempe- rature	Speed	Torque
Sampling rate	10 kHz						
Filter frequency	1500 Hz	1000 Hz	/	/	/	5 Hz	5 Hz
Quantization (assuming 12- bit full range)	85.4 mbar	4.15 mbar	7.25 cm ³ /min	1.27 cm ³ /min	/	2.44 rpm	2.44 N.cm

Measurements are highlighted in the next section and the test bench set up in the context of modelling is criticized.

3.2.3. Analysis of the measurements

One of the aim of the test campaigns was to gather data for a better understanding of axial piston pump case drain flow and pressure behaviour. The current section, emphasizes on the analysis of case drain pressure measurements as it is poorly documented in literature. Figure 3-3 shows an example of the data obtained at case drain in a nominal configuration (rotating speed $\omega = 4600$ rpm, $P_r = 0$ bar rel.) at 50°C, compared to the discharge pressure measurements, taken at nominal static point n°2 according to Figure 3-1.

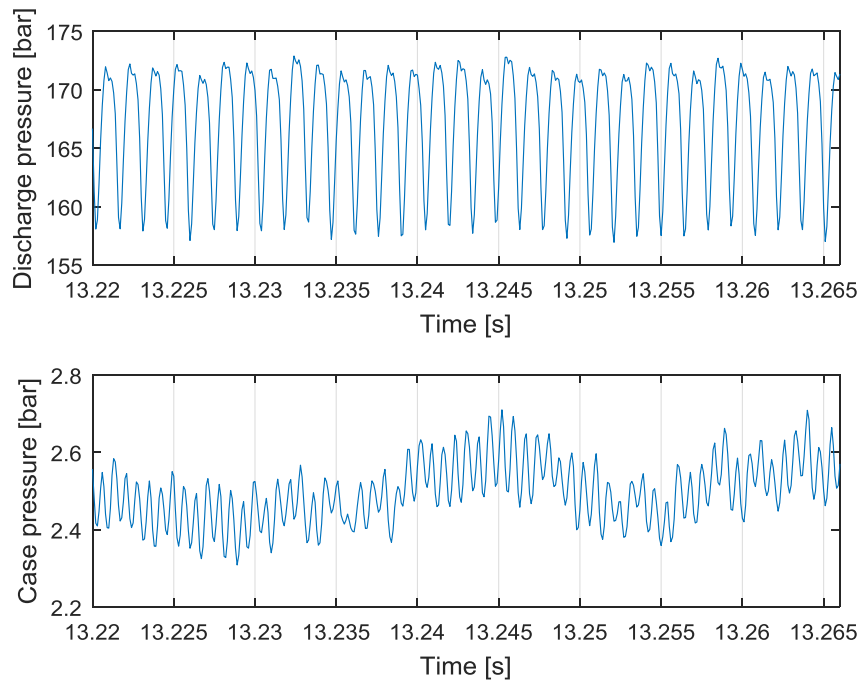


Figure 3-3: Discharge and case pressure during nominal static point n°2 at 50°C

It can be seen that case pressure displays a highly dynamic behaviour with pressure pulses, but which form is different compared to that of the discharge pressure. An evident difference between case and discharge pressure measurements lies with the low frequency oscillation: both signals display it, with a non-negligible amplitude for case pressure. The frequency of this oscillation seems to be the rotating frequency. Although its frequency is identified, the author has no explanation for the oscillation to be happening, except for an unbalance of some rotating parts in the tested pump.

In order to go deeper in the frequency content of the case pressure signal, its Power Spectral Density (PSD) is computed and displayed on Figure 3-4. The PSD is the squared magnitude of the Fast Fourier Transform (FFT), over the spectral bandwidth. It is the image of the energy variation generated by each frequency. As such, the PSD gives information about which frequencies have major or minor impact on the energy variation. Figure 3-4 shows the PSD for discharge and case pressures, computed in MATLAB with Welch's method (Welch, 1967). This method averages the computed PSD over several overlapping time slots, which reduces noise of the plotted graph. The time slots are windowed with specific functions to deal with the non-cyclicity of the data over the considered time slots. In the current work, the Welch's method is applied with a Hanning window, an averaging factor of 16, and a timeslot overlap of 20%.

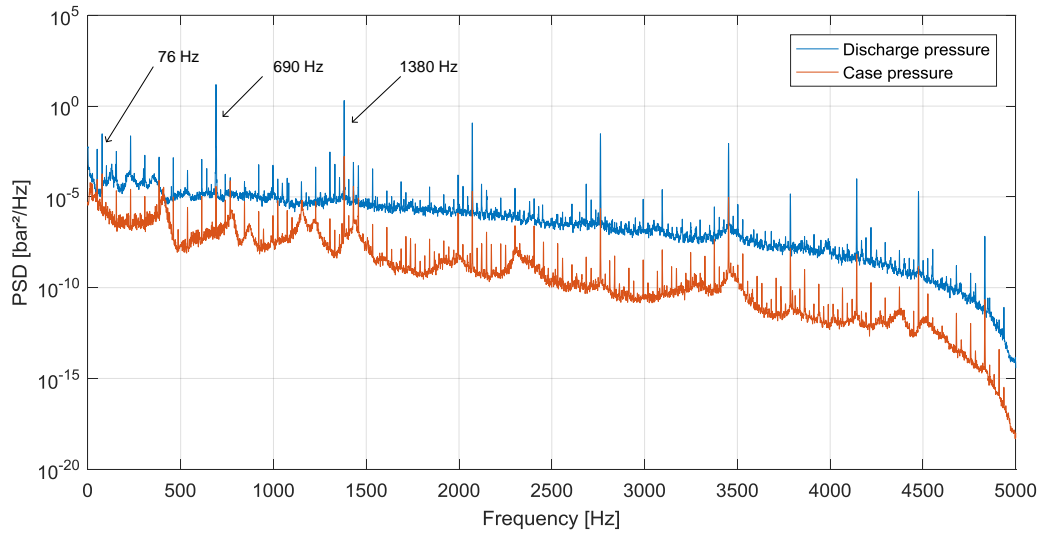


Figure 3-4: Discharge and case pressures PSD - Nominal conditions, 50°C, static point n°2

Figure 3-4 shows that the case pressure signal contains the same base frequencies as the discharge pressure signal: the pump rotating speed (~ 76.6 Hz) with harmonics, and the porting pulsation (690 Hz) with harmonics. It is interesting to remark that the second harmonic of the porting pulsation (1380 Hz, displacement ripple) is the main frequency of the case pressure signal, while the

porting pulsation frequency dominates for the discharge pressure. This observation is also highlighted by Figure 3-7 and Figure 3-8 that are discussed later.

The impact of tank pressure on case drain pressure behaviour is illustrated by Figure 3-5 in time domain and Figure 3-6 in frequency domain. As expected, an increase of tank pressure increases by the same amount the case drain pressure. In terms of frequency, it seems that in our test bench, increasing tank (and suction) pressure, shifts the most important frequency from the displacement ripple (1380 Hz) to the porting pulsation frequency (690 Hz). It also seems to stabilize the case pressure behaviour against system load variation, as will be discussed afterwards.

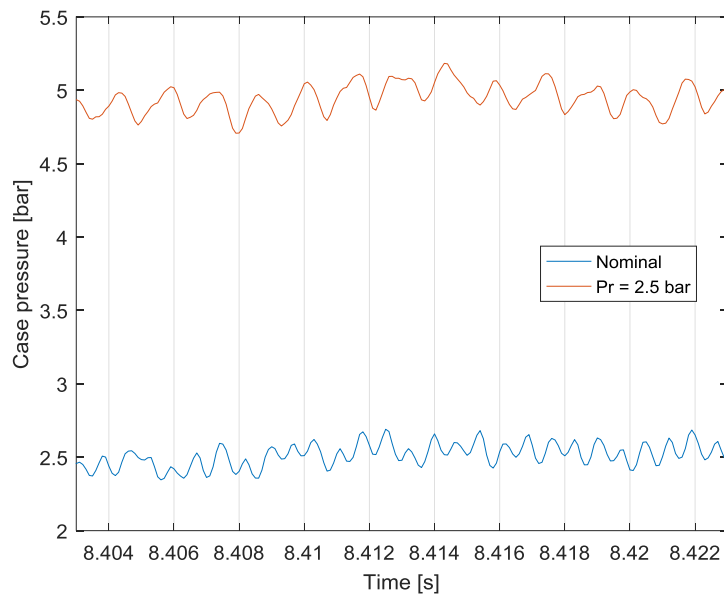


Figure 3-5: Case pressure behaviour depending on tank pressure, 50°C - static point n°2

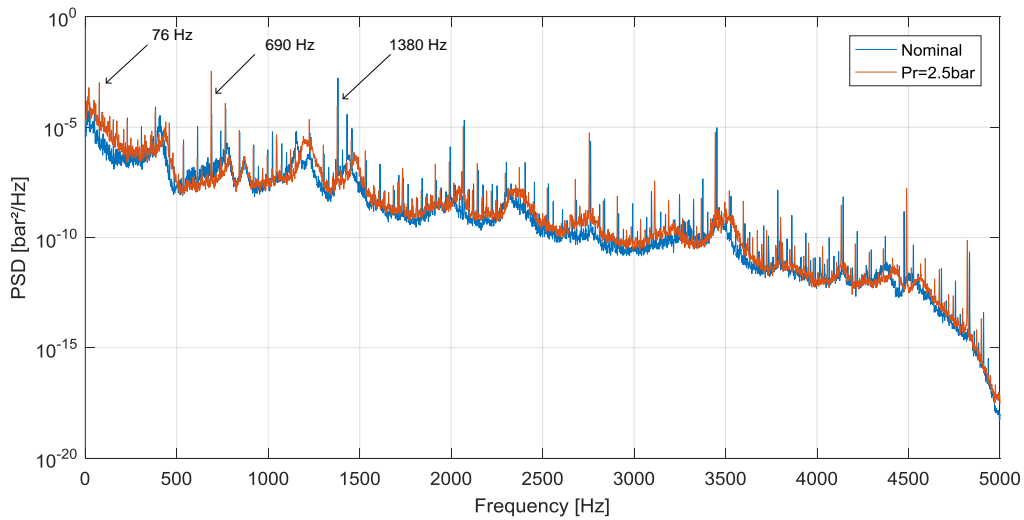


Figure 3-6: Case pressure PSD depending on tank pressure, 50°C- static point n°2

Cumulative PSD (CPSD) plots are used to show the influence of the pump hydraulic load on the frequency content for both case and discharge pressure signals, on Figure 3-8 and Figure 3-7, respectively. CPSD plots facilitate the visualization of the main frequencies in a signal. In this case, the mean values of the signals have been removed in order to clearly identify the impact of frequency. The cumulative sum is normalized in order to facilitate the comparison between several configurations.

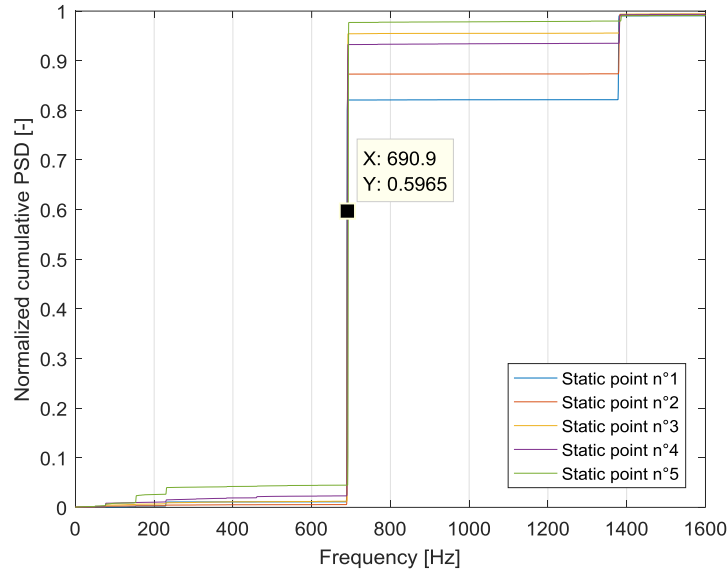


Figure 3-7: Discharge pressure CPSD – 50°C, influence of system load

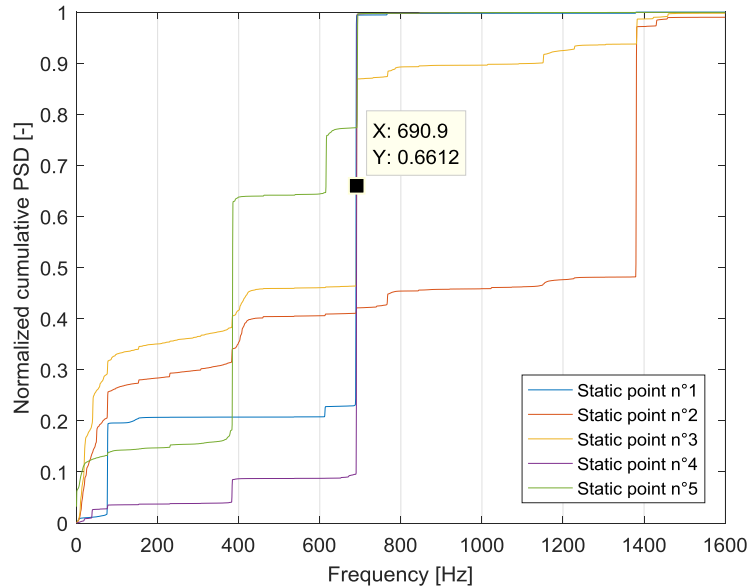


Figure 3-8: Case pressure CPSD – 50°C, influence of system load – $P_r = 0$ bar

Whatever the pump hydraulic load, the two main frequencies of the discharge pressure signal remain the porting pulsation and its second harmonics in nominal conditions (Figure 3-7). We see however, a decrease of the impact of the higher frequencies with lower hydraulic loads: this is because the hydraulic resistance of the loading valve produces a damping effect on the pressure dynamics. The case pressure signal, on its end, seems to be very much dependant on the pump hydraulic load. Focusing on static point n°2, we can see that one of the most important frequencies of the measured signal is around 76.6 Hz, the shaft rotating frequency, which corresponds to the low frequency oscillation of non-negligible amplitude highlighted by Figure 3-3.

Increasing the tank pressure has a stabilizing effect, as can be seen comparing Figure 3-8 (with suction pressure equal to 0 bar) with Figure 3-9 (suction pressure of 2.5 bar). This observation hints that something happens at low suction pressures in the hydraulic system. However, it is not possible to fully explain this phenomenon with the data at hand. One hypothesis is that the delivery flow indirectly impacts the case pressure and flow because of the drain and discharge lines being connected together before reaching the tank.

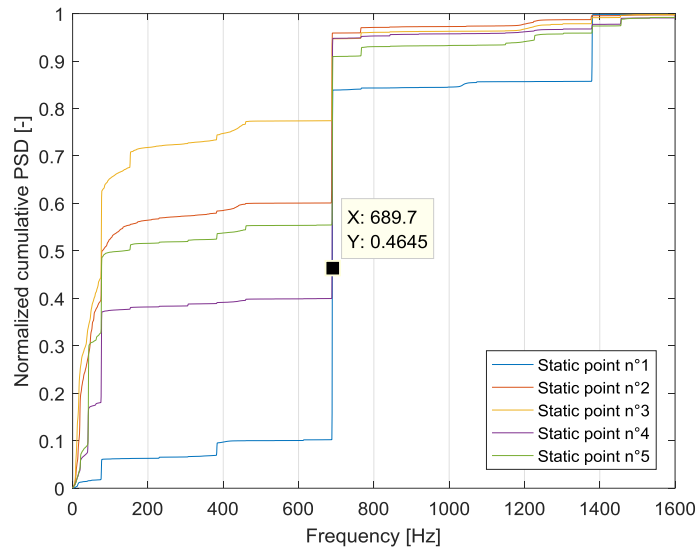


Figure 3-9: Case pressure CPSD – 50°C, influence of system load – $P_r = 2.5$ bar

The influence of rotating speed on pressure behaviour is illustrated for discharge pressure by Figure 3-10 and Figure 3-11, and for case pressure by Figure 3-12 and Figure 3-13, in the configuration of static point n°2.

To facilitate analysis and discussion when comparing measurement made at different rotating speeds, it is proposed to normalise the frequencies used to display the PSD. From Figure 3-10 to Figure 3-13, PSD and cumulative PSD are plotted against the normalized frequency Nf defined hereafter:

$$Nf = f/f_b \quad (3-1)$$

with:

f frequency [s^{-1}]

With this normalized frequency, 1 corresponds to the barrel frequency (i.e the rotating speed in rev/s), 9 is the porting pulsation frequency, etc. This normalization allows for the comparison of several rotating speeds on a single plot. It was found from the measurements that discharge pressure behaviour is independent of pump rotating speed: whatever its configuration, the test brings the same two most impacting frequencies: the porting pulsation frequency and its second harmonic ($Nf = 9$ and 18 , making 690 and 1380 Hz when the rotating speed is 4600 rpm).

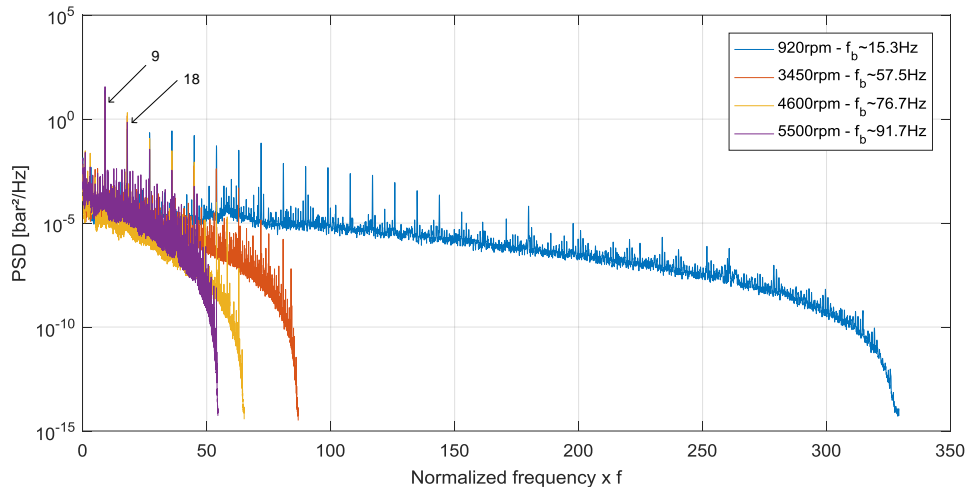


Figure 3-10: Discharge pressure PSD at several pump rotating speed – static point n°2

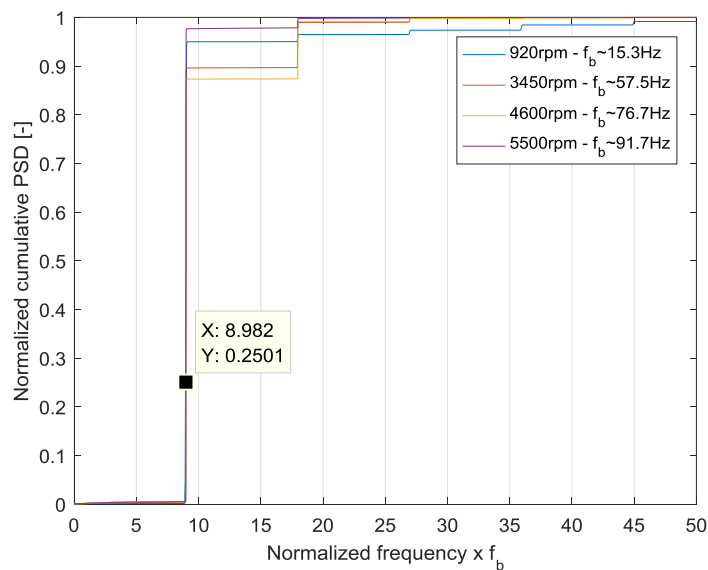


Figure 3-11: Discharge pressure CPSD at several pump rotating speed – static point n°2

Like the pump hydraulic load, the rotating speed seems to have more impact on case pressure, as illustrated by Figure 3-13. At low rotating speeds, the pump is unable to maintain pressure and flow in the hydraulic system as shown on Figure 3-14. As the test bench discharge and drain lines are connected before reaching the tank, it is possible that this inability contributes to the dynamic behaviour of the case pressure signal.

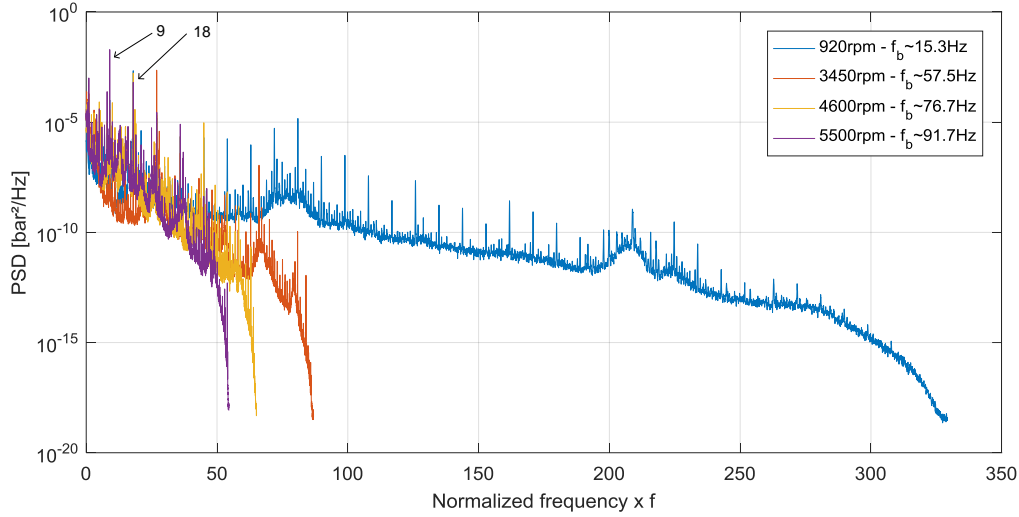


Figure 3-12: Case pressure PSD at several pump rotating speed – 50°C, static point n°2

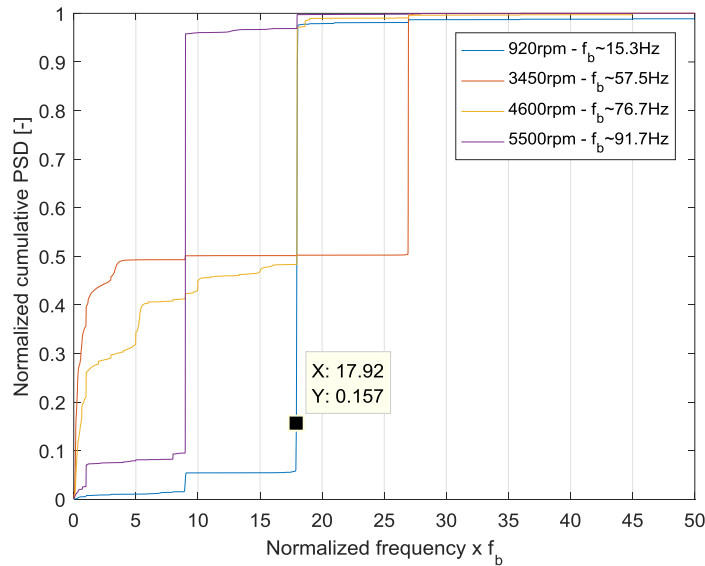


Figure 3-13: Case pressure CPSD at several rotating speed – 50°C, static point n°2

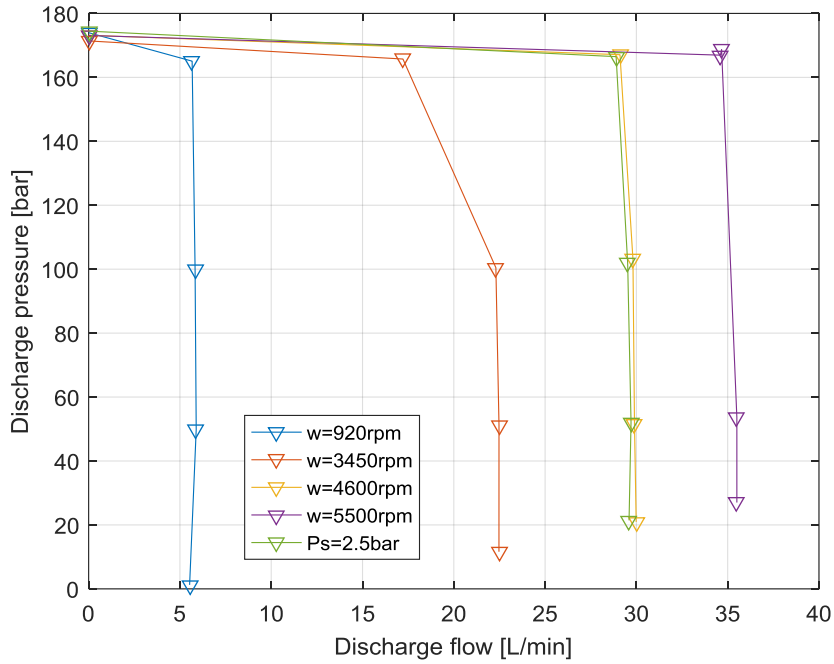


Figure 3-14: Pump pressure static characteristics at 50°C in several test conditions

The observations made lead to the following remark: although the test bench proposed and built by our industrial partner allows us to gain some knowledge on the pump behaviour in the tested conditions, it is not fully suitable for studying the pump case pressure behaviour. As case and discharge lines are connected, it is impossible to make definite conclusions on case pressure behaviour in the tested conditions. However, this hydraulic system configuration is the same as that of most H/C hydraulic system, which can be a benefit for other use of the gathered data, as will be shown in Chapter 4.

Although the main drawbacks of the test bench lie in the case and discharge lines connection, several other points must be highlighted and capitalized for future activities.

One of the said drawbacks lies with the flow sensors used on the test bench. Flow measurement dynamics is expected to be similar to pressure measurements to not introduce phase shifts in the domain of interest. However, this is not confirmed from the measurements due to flow sensors quantification, as shown on Figure 3-15 in the nominal static point n°2 configuration. From flow measurement observation, it seems that both discharge and case drain flow measurements are updated every 13.15 ms which is more than the duration of one pump rotation. The discharge flow sensor seems to have a resolution of 0.05 L/min, while that of the case flow sensor is of about 0.01 L/min. Another point to mention is the maximum viscosity of 100 cSt to get accurate measurements from the flow sensors. With the fluid currently used, MIL-PRF-83282, this

corresponds to 0°C temperature, reducing the range of accurate measurements at low temperature.

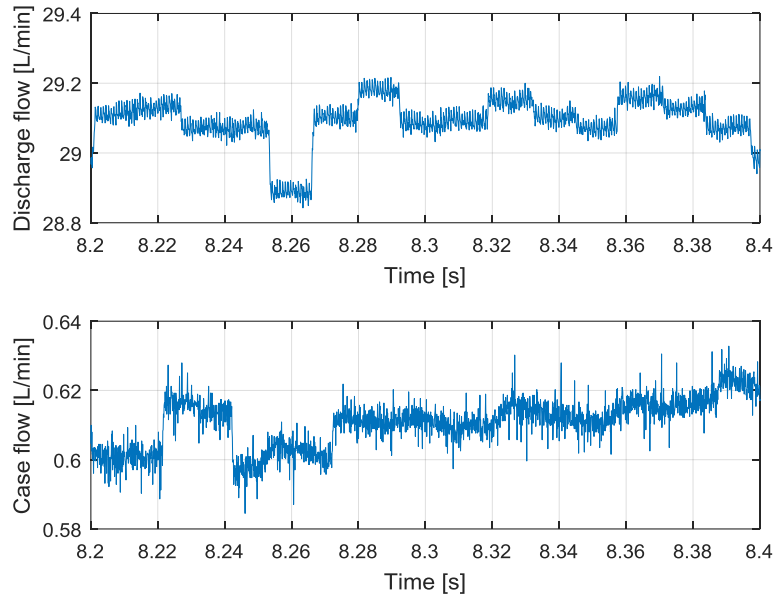


Figure 3-15: Illustration of flow sensors top (measured)

A second point is related to the relation between motor torque and pump rotating speed during load transients: the speed control of the motor that drives the pumps does not have an infinite bandwidth for rejecting the torque load disturbance. Figure 3-16 shows discharge flow, torque and rotating speed during a dynamic test. Rotating speed oscillates in the range of 150 rpm during the tests, being disturbed by the transient pump torque demand due to the rapid change in operating conditions and to the pump displacement compensation. From these measurements, it is concluded that modelling the relation linking pump torque and rotating speed is necessary when simulating pump load variation and comparing the results to measurements.

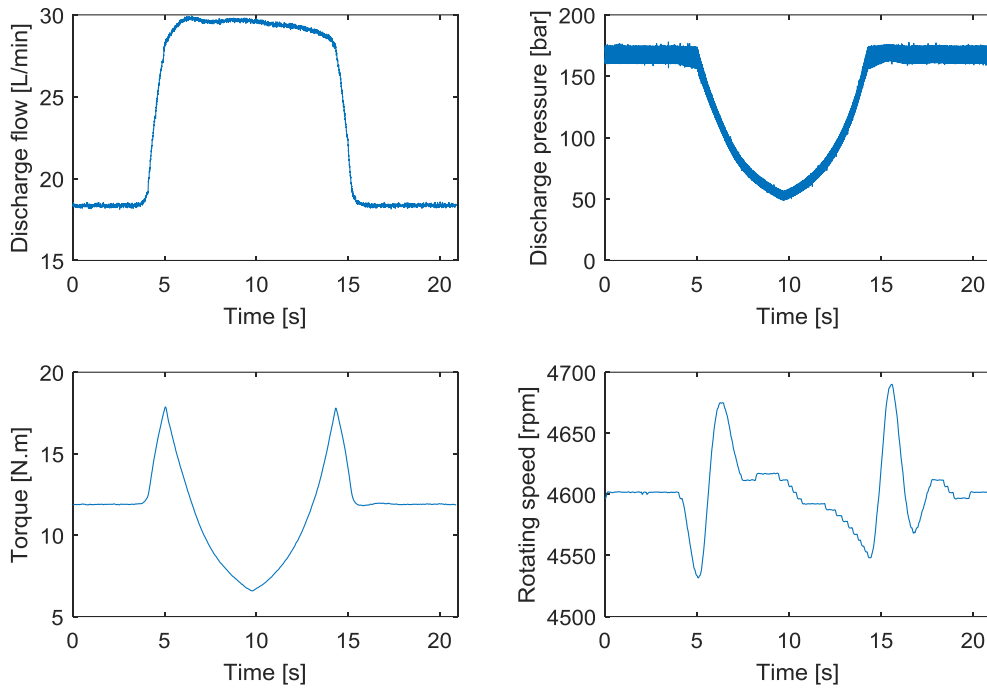


Figure 3-16: Impact of load variation on pump torque and speed

The third drawback concerns the management of temperature during the experiments. Figure 3-17 shows the average temperature during an experiment, at each pump port in addition to the ambient one, and for all experiments made at 50°C. It can be seen that temperature varies in the order of 20°C, although most measurement results are situated between 45°C and 60°C. Using the data plotted on Figure 3-17, standard deviation around mean value and maximum gap between two values are shown on Figure 3-18 for each pump port and the ambient temperature. It is interesting to note that the most scattered temperature measurement is realised on the discharge line, with the only temperature sensor located outside the climatic chamber.

Both figures show the difficulty faced to manage temperature properly. The time frame for the test campaigns was short (about 2 days) on our partner site. Due to this time constraint, it was not possible to wait in each test configuration for a steady-state temperature. Only a small part of the test bench was located inside the climatic chamber (see Figure 3-2), making it even harder to properly manage temperature. This has a high impact on the fluid viscosity that is typically divided by 2 every 20°C temperature increase around 50°C (SAE International, 2000).

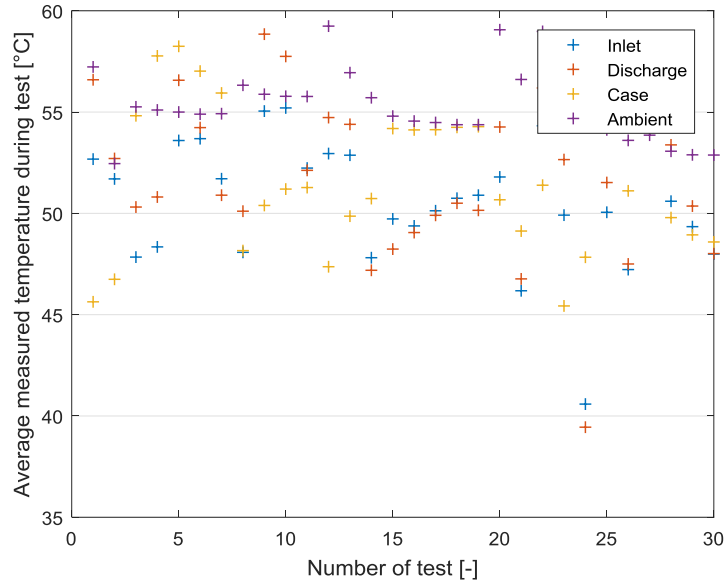


Figure 3-17: Average temperature at each port for every 50°C data set.

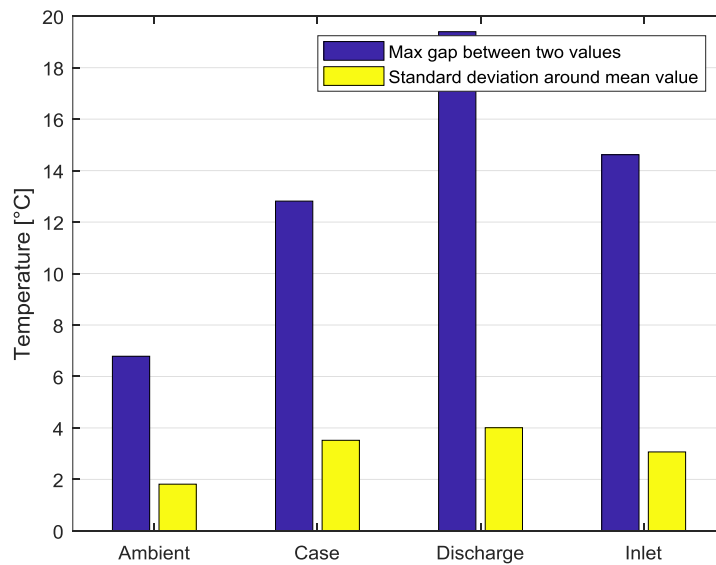


Figure 3-18: Temperature deviation for 50°C tests at each port - average the mean test values

The pump has been tested by the industrial partner, using industrial facilities. The analysis of the test bench design and properties, combined with a detailed analysis of measurements have pointed out significant shortcomings. These shortcomings strongly limit the ability to identify the case drain pressure and flow behaviour versus the pump operating conditions, as initially intended. The main issues have been documented in details to serve as important recommendations for the development of a future test bench to support health monitoring activities.

It is nevertheless a fact that the realised test campaigns allowed for the gathering of some data that are usable in the current study as evaluation material for the model. The model evaluation is discussed in the next section.

3.3. Model assessment

In order to answer the question Q5, it is necessary to evaluate the developed model responses against real pump data. Industrial production, however controlled, generates unique products with geometrical dimensions within tolerances. For example a piston, theoretically cylindrical, is in reality imperfectly cylindrical, with mean diameter of any value within tolerance.

Model parameters generally use the mean value of the tolerance, but there is no proof that the parameter value is the same for the tested pump. To cope for this discrepancy, it is common practice in the modelling field to adjust some model parameters to fit part of the experimental data (parameter identification), and to evaluate the model against the rest of the data (model validation).

Both processes must be made using a simulation model that is also representative of the measurement environment. To this end, it is of prime importance to model the test bench used to gather experimental data.

In the next sections, a model of the test bench is presented to mirror the real hardware, some model parameters are identified to make the simulated pump behaviour fit the test measurements, and the data produced by the combination of both models are then compared to the obtained data sets from section 0.

3.3.1. Test bench model

It is recalled that the aim of the pump model development is to study monitoring approaches, using at least pressure-flow measurements taken in steady-state conditions. Thus, it is mandatory that the virtual test bench developed to assess the model allows the simulation of such tests.

On another hand, as requirement Rq1 of Table 2-4 asks for accurate simulation of the “internal leakage, as well as suction and discharge pressure and flow”, it is required that the test bench model enables the comparison of simulated pressure and flow with real data at each hydraulic port of the pump.

The developed pump model hydraulic interfaces with the test bench are shown on Figure 3-19. The displayed causality of Figure 3-19 is a consequence of the modelling choices made during the development of the pump model. With the current model, pressure is to be supplied at discharge and suction ports, while the model delivers pressure to the hydraulic system model through the case port.

As it is already defined, the pump model causality constrains the creation of a test bench model.

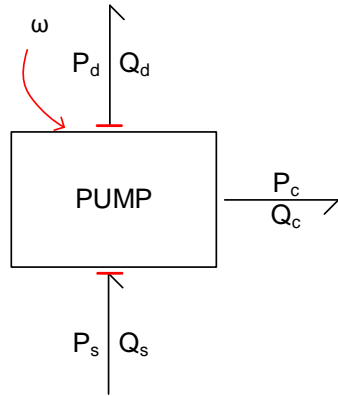


Figure 3-19: Pump model hydraulic interfaces with the test bench

In the current case, thanks to the measured data, it is possible to use either a data-driven or a physics based approach to model the test bench. The pure physics-based lumped-parameter approach consists in reproducing the complete test bench virtually, from pipe lengths, diameters, singularities and so on. The lengths and diameters of the pipes were carefully written down prior the test campaigns. However, necessary data to develop the test bench digital twin are missing: hoses wall compliance, pressure drop across the fittings, elbows, filters and cooler, and acquisition system characteristics. To compensate this lack of data, a mixed data-driven/physics-based approach can be used.

The data measured on the test bench include the acquisition loop. As such, one possible modelling approach for the mixed data-driven/physics-based test bench is to directly inject measured data as excitations to the pump model. However, doing so would also mean injecting measurement errors in the pump model, increasing as a consequence the overall model uncertainty. In addition, this approach would limit the model evaluation to be made on part of the data as the other part must be supplied to the model due to causality constraints (here discharge and suction pressures as well as case drain flow).

As an alternative to a mixed data-driven/physics-based approach, it was decided to identify a simplified test bench model using the measured data. A simplified layout of the test bench displayed on Figure 3-20-a is shown on Figure 3-20-b, where the hydraulic load of the pump is replaced by a proportional variable valve. The corresponding causal Bond-graph is shown on Figure 3-20-c.

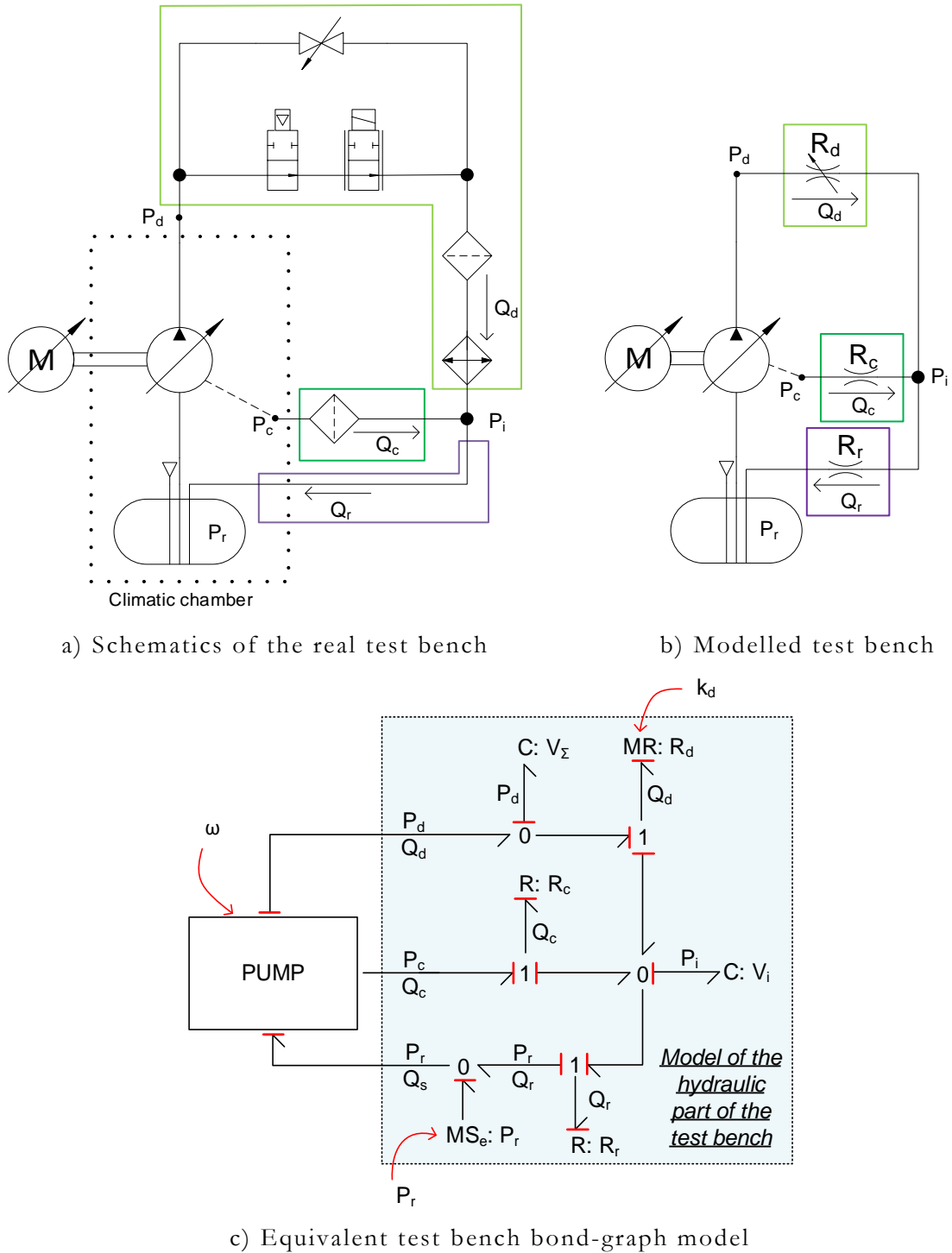


Figure 3-20: Test benches – a) Real hardware, b) Identified model, c) Bond-Graph

The test bench model must allow for the evaluation of the pump model on static pressure-flow points. In steady state conditions, the experimental set up can be modelled as a combination of lumped resistances. Here, three equivalent orifice models are involved: one variable resistance R_d , and two fixed resistance R_c and R_r . However, in order to comply with the pump model causality, two

hydraulic capacitances V_z and V_i are added to the model, to provide the discharge pressure P_d and an intermediate pressure P_i , respectively.

The resistance R_d , which corresponds to the pump hydraulic load (mainly the loading valve, highlighted by the light green boxes on Figure 3-20-a, and Figure 3-20-b), is considered to generate a turbulent flow which pressure drop can be expressed using the simplified equation hereunder:

$$Q_d = \sqrt{\frac{1}{k_d}} |P_d - P_i| \text{sgn}(P_d - P_i) \quad (3-2)$$

with:

k_d	characteristic coefficient for resistance R_d , function of the operating point [Pa/(m ³ /s) ²]
P_d	pressure at pump discharge port [Pa]
P_i	intermediate pressure [Pa]
Q_d	flow at pump discharge port [m ³ /s]

On the drain line, the smaller hose diameter is of 6 mm with a maximum flow of 1.29 L/min. With MIL-PRF-83282 fluid at about 50 °C (kinematic viscosity of $\nu = 15$ cSt), the Reynolds number is $Re = 305$. At 100°C, the fluid viscosity drops to $\nu = 3$ cSt, leading to $Re = 1525$. The computed values being less than the transition Reynolds number (2000) between laminar and turbulent flow patterns, the resistance R_c , associated to the drain line, is modelled as a laminar orifice, which gives the simplified following equation:

$$Q_c = \frac{1}{k_c} (P_c - P_i) \quad (3-3)$$

with:

k_c	case resistance of R_c effect [Pa/(m ³ /s)]
P_c	pressure at pump case drain port [Pa]
Q_c	flow rate at case drain port [m ³ /s]

There is a high uncertainty on the effective transition Reynolds number, which can drop to 1500. In this case, the Reynolds number computed at 100 °C reaches this limit. Knowing this, it is possible that modelling the drain line as a laminar orifice at 100 °C will prove to be not accurate.

The model of the shared return line resistance R_r for discharge and case drain flow is subjected to more uncertainties than the first two. On one hand, at zero flow, discharge flow is null and only case flow passes through R_r , which in this case should be modelled as a laminar orifice. However, at any other operating

point, a simple calculation show that the flow becomes turbulent. The resistance model should then include a laminar/turbulent transition. On the other hand, it is unclear whether the resistance should be modelled as a lumped pressure drop in a singularity or a distributed pressure drop in a hydraulic line. In order to tackle both uncertainties, the resistance R_r is modelled through the following equation. In the said equation, the parameter γ allows for the shift from Hagen-Poiseuille model (laminar, $\gamma = 0$), Blasius model ($\gamma = 0.75$) and turbulent flow in smooth pipe ($\gamma = 1$).

$$(P_i - P_r) = \frac{k_\infty}{\tanh\left(Q_r^\gamma/K\right)} Q_r^{1+\gamma} \quad (3-4)$$

with:

- γ shifting parameter from distributed to lumped pressure drop model [-]
- K laminar/turbulent transition coefficient for resistance R_r [(m³/s) ^{γ}]
- k_∞ return resistance R_r coefficient [Pa/(m³/s)^{1+ γ}]
- P_r hydraulic reservoir pressure [Pa]
- Q_r total return flow from hydraulic system to reservoir [m³/s]

Parameter identification

In steady state operation, the continuity equation applied to the domain at pressure P_i is:

$$Q_r = Q_d + Q_c \quad (3-5)$$

Finally the test bench model is given by equations (3-2) to (3-5) that involve 5 parameters:

- k_d , variable;
- k_c , fixed;
- k_∞ , fixed;
- K , fixed;
- γ , fixed;

In zero discharge flow steady conditions, $Q_r = Q_c$. The hydraulic test bench model can be simplified as a laminar restriction linking the fluid domain at case pressure P_c to that at reservoir pressure P_r . The model gives:

$$P_i = \frac{k_\infty}{\tanh\left(Q_c^\gamma/K\right)} Q_c^{1+\gamma} + P_r \quad (3-6)$$

When $Q_c^\gamma/K \rightarrow 0$, then $\lim_{Q_c^\gamma/K \rightarrow 0} \tanh\left(Q_c^\gamma/K\right) = Q_c^\gamma/K$, which leads to:

$$\lim_{Q_c^\alpha/K \rightarrow 0} P_i = \frac{k_\infty K}{Q_c^\alpha} Q_c^{1+\gamma} + P_r \quad (3-7)$$

$$\lim_{Q_c^\alpha/K \rightarrow 0} P_i = k_\infty K Q_c + P_r \quad (3-8)$$

Combining (3-8) and (3-4) in zero flow conditions, we obtain the following equation:

$$P_c - k_c Q_c = P_r + k_\infty K Q_c \quad (3-9)$$

As a consequence, in zero flow condition, the laminar restriction linking the fluid domain at case pressure P_c to that at reservoir pressure P_r is given by the equation hereunder, linking the test bench model parameters k_c, k_∞ and K .

$$P_c - P_r = (k_c + k_\infty K) Q_c \quad (3-10)$$

In the rest of this chapter, the $(k_c + k_\infty K)$ factor is identified as an additional parameter k_{cr} .

The test bench parameters are identified from the static measurements, using for each test the averaged data. In the rest of the current chapter, measured values are marked with an asterisk (*), to separate them from general and simulated variables. The parameters identification problem is expressed as an optimization problem where the parameter vector $\psi = (k_{cr}, \gamma, K, k_\infty, k_d)^T$ must be found for each temperature so as to minimize the criteria J defined as follows:

$$J(\psi) = \sum_i (Q_{ci}^* - Q_{ci})^2 + (Q_{di}^* - Q_{di})^2 \quad (3-11)$$

with:

i experiment number [-]

It is reminded here that k_d is not a single value but a vector which depends on the operating point, as already stated earlier. In order to simplify the optimization problem, it is broken down in several successive steps, highlighted by Figure 3-21.

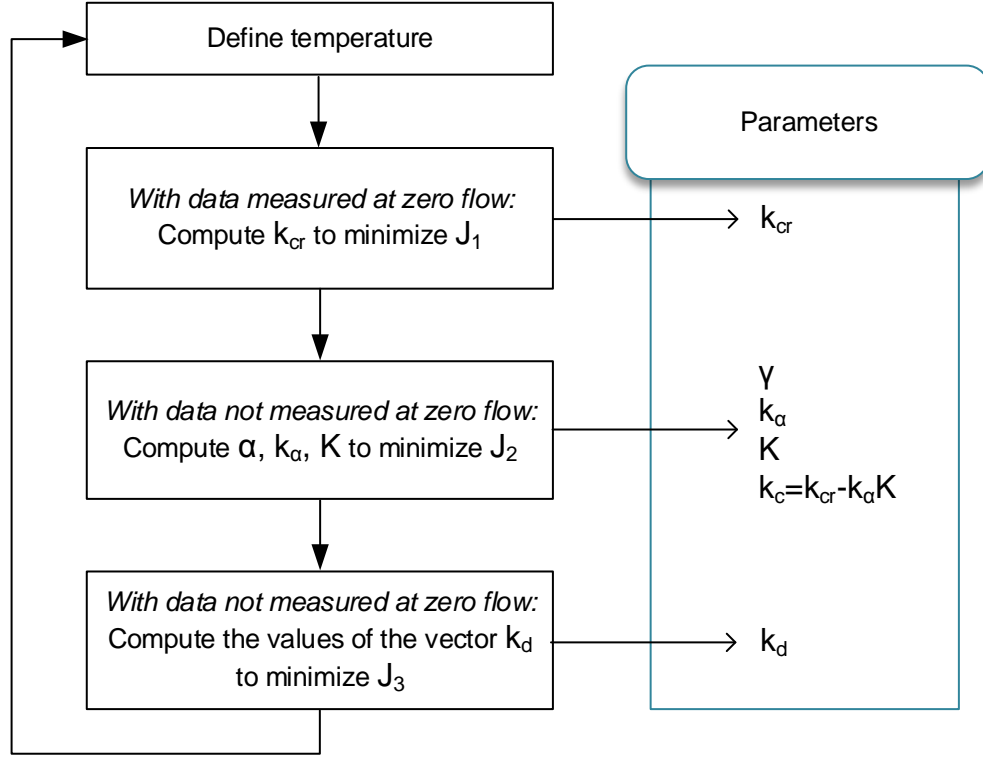


Figure 3-21: Test bench model parameters identification process

The first step consists in identifying the parameter k_{cr} so as to minimize the criteria J_1 defined using equation (3-10) and the measures taken in zero flow conditions:

$$J_1(k_{cr}) = \sum_{i_0} ([P_c^*(i_0) - P_s^*(i_0)] - k_{cr} Q_c^*(i_0))^2 \quad (3-12)$$

with:

i_0 experiment number at zero flow [-]

The second step focuses on identifying the parameters (α, k_∞, K) outside of full flow conditions, minimizing the second criteria J_2 that is defined combining equations (3-3) and (3-4) under the following form:

$$J_2(\alpha, k_\infty, K) = \sum_{i_1} \left([P_c^*(i_1) - P_r^*(i_1)] - \left[k_c Q_c^*(i_1) - \frac{k_\infty}{\tanh\left(\frac{Q_r^*(i_1)^\gamma}{K}\right)} Q_r^*(i_1)^{(1+\gamma)} \right] \right)^2 \quad (3-13)$$

with:

i_1 experiment number not measured at zero flow [-]

The third and final step consists in identifying the parameter vector k_d in order to minimize, for each non-zero flow test condition, the third criteria J_3 defined from equations (3-2) and (3-4) as follows:

$$J_3(k_d(i_1)) = \left([P_r^*(i_1) - P_d^*(i_1)] - \left[k_d(i_1) Q_d^*(i_1)^2 - \frac{k_\infty}{\tanh\left(\frac{Q_r^*(i_1)^\gamma}{K}\right)} Q_r^*(i_1)^{(1+\gamma)} \right] \right)^2 \quad (3-14)$$

Table 3-4 gathers the identified parameters for both data sets measured respectively at 50 °C and 100 °C.

Table 3-4: Test bench model identified fixed parameters

Temperature \ Parameter	k_{cr} [bar/L/min]	k_c [bar/L/min]	γ [-]	k_∞ [bar/(L/min) ²]	K [L/min]
50°C	0.337	0.290	1	0.00206	22.8
100°C	0.352	0.300	1	0.00158	32.8

As every model, the test bench model is a representation of reality, but can never be completely accurate. This is firstly illustrated here with case drain flow. Indeed, in the present research work, it is important that the test bench model allows for the correct simulation of the case drain flow. With the identified parameters, the average error on case drain flow is of 0.3 L/min. This is an important value considering that is it 20% of the maximum measured case drain flow that is about 1.5 L/min.

A second example of test bench model lack of accuracy focuses on viscosity. Increasing temperature from 50 °C to 100 °C, viscosity drops by five times (see (SAE International, 2000) for MIL-PRF-83282 fluid). It was expected for the test bench parameters to display variation of the same order (or to power $1/2$), increasing with temperature. However, it is not the case: they are in reality subjected to factors around 1, and even smaller than 1 for k_∞ .

Nothing was changed in the test bench set up between 50 °C and 100 °C real experiments, so measurements should have no play in this phenomenon. It is then linked to the test bench model, and in particular to the laminar model of the case drain orifice. The computed Reynolds number at 100°C was near the transition value of 1500 that some authors consider, and it could have been a better option to model an orifice with laminar/turbulent transition linked to temperature.

The two listed facts (error on case drain flow and test bench temperature behaviour) establish the limits of the test bench model in terms of accuracy. However, no more data was made available by the partner in charge of the pump tests. This introduced severe limitations in the identification process and deprived us of means to improve the model. Therefore, it was accepted to use the identified test bench model as is. Yet, it was decided to limit the pump model parameter

identification and assessment to 50°C data sets in order to limit possible interpretation errors.

The complete model assessment process is discussed in the next section.

3.3.2. Pump model evaluation process

This chapter aims at answering the question Q5, which is about pump model accuracy and representativeness. In order to evaluate the pump model an environment similar to that of the hardware experiments, a test bench model has been identified. The pump model evaluation process is discussed in this section.

The said process goes in two steps: the first one consists in configuring parameters of the pump model so as to fit part of the experimental results with the simulation. The second one consists in evaluating the fitted model against the rest of the experimental results, which in some fields of research is called model validation.

In the next section, and before identification of the pump model parameters, details about the pump model to be evaluated are given.

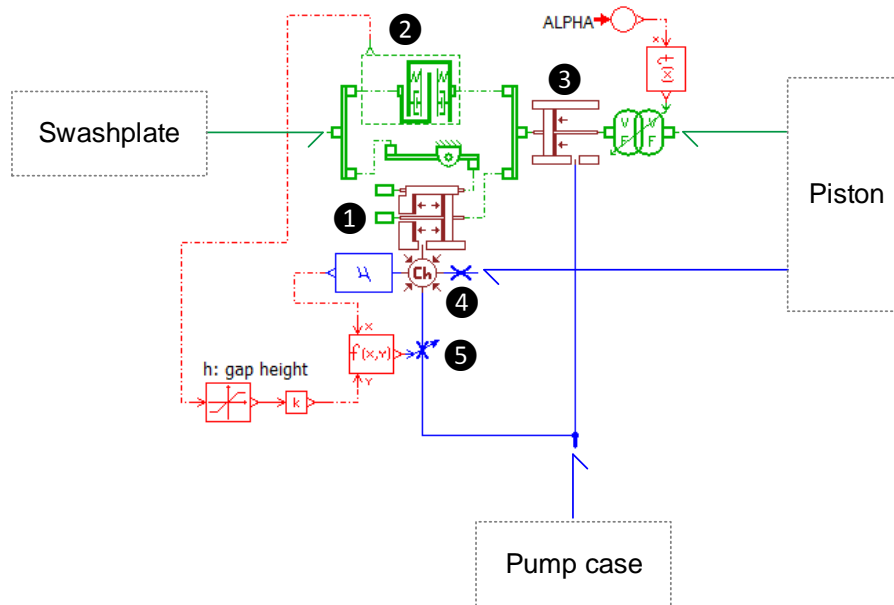
3.3.2.1. Pump model for evaluation

The model initially developed and discussed in Chapter 2 has several shortcomings, especially the slipper/swashplate leakage model with variable gap. Due to these shortcomings, it was chosen to replace the variable gap height by a constant one. However, the model still allows for the simulation of “degradation leading to increased internal leakage” as required in Table 2-4.

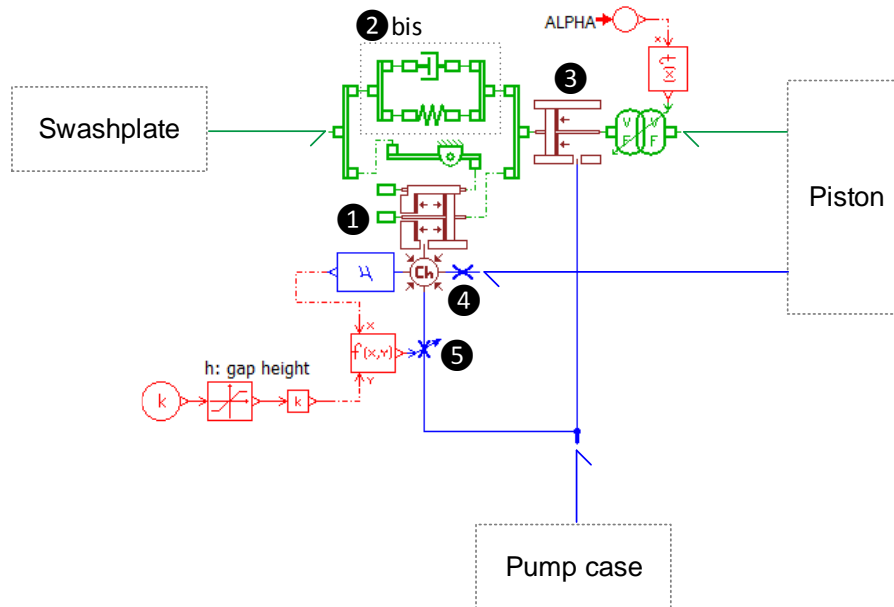
The slipper model is showed on Figure 3-22, where ❶ models the pressure force from the gap on slipper and swashplate, the end-stop ❷ model bounds the gap height and compute the contact force between slipper and swashplate. The influence of the case pressure on the slipper is taken into account through ❸. The leakage from the piston to the case flows through the fixed orifice ❹, which corresponds to the slipper throttle, then through the slipper/swashplate gap ❺ which is implemented as a modulated orifice.

Figure 3-22 shows the differences between the initial model (-a) and the modified model (-b). In terms of hydraulics, introducing a constant gap height means suppling the slipper/swashplate leakage model ❺ a fixed value. In terms of mechanical modelling, it is a bit trickier. The end-stop submodel ❷ that supplies initially the slipper/swashplate gap height also links the piston displacement to the swashplate. Simply removing the submodel would cut that link and the pistons would not be actuated. As such, the end stop submodel is replaced by a spring-damper system (❷bis in Figure 3-22-b) of great stiffness

modelling an anchorage between swashplate and piston. This approach allows also for keeping the developed kinematic model and the associated causalities. Doing so, a few microns of piston displacement are lost, however this does not impact the amount of pumped fluid per revolution.



a) Variable gap height



b) Fixed gap height

Figure 3-22: Simplification of the slipper/swashplate leakage model

Figure 3-23 summarizes and schematises the complete pump model, based on a H225 pump. On this figure, information on the modelled physical effects is also given. Table 3-5 highlights the pump leakage models.

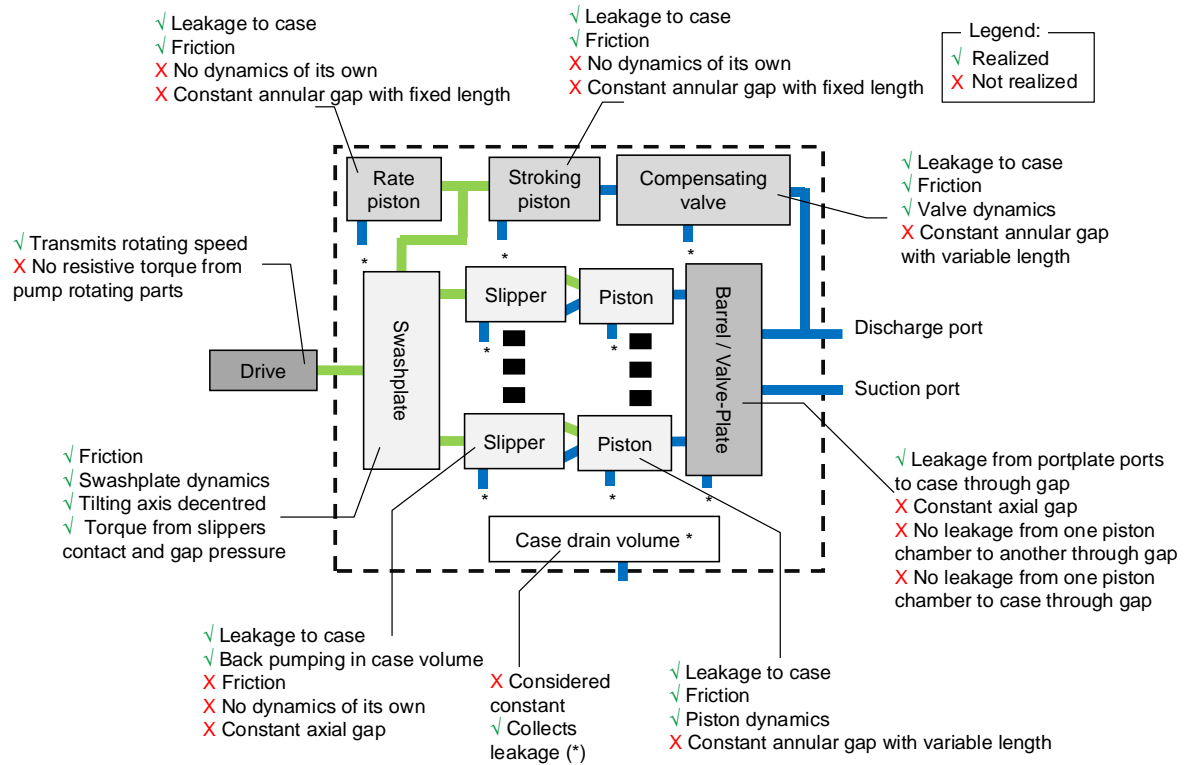


Figure 3-23: Highlight of the complete axial piston hydraulic pump model

Table 3-5: Leakages considered in the complete pump model

Pump part	Modelled leakage
Barrel	/
Portplate	To case through barrel/portplate gap as per (Bergada, et al., 2012) considering a non-tilted barrel, with a fixed gap height.
Piston	To case through piston/barrel clearance as per (2-9), with a fixed gap height and no eccentricity
Slipper	To case through slipper/swashplate constant gap as per (2-26)
Swashplate	/
Compensating valve	To case through spool/sleeve clearance as per (2-9), with a fixed gap height and no eccentricity
Stroking piston	To case through piston/housing clearance as per (2-9) with a fixed gap height and no eccentricity, and a constant length
Compensating piston	To case through piston/housing clearance as per (2-9) with a fixed gap height and no eccentricity, and a constant length

The model adaptation for its evaluation due to the slipper/swashplate variable gap height model has been discussed. Some detailed information about the physical effects considered in the complete healthy pump model has been given. In the next section, the second step of the evaluation process, the model parameter fitting, is discussed.

3.3.2.2. Identification of the pump model geometry parameters

Most geometry parameters of the pump model are supplied by our industrial partner. It was decided to only use the most uncertain ones as parameters to be fitted, which are the listed in Table 3-6.

It was noticed during testing that the maximum measured flow rate exceeded the theoretical capability of the H225 pump. This can originate from pump parts geometry non-conformity, for example of pistons or yoke piston. However, it is not intended for the model to cover all possible root-causes. As a consequence, and in order to introduce the possibility of flow rate exceeding the theoretical limit in simulation, the maximum swashplate tilt angle was added to the list of parameters to be fitted.

Table 3-6: List of parameters to be fitted

Parameter name	Unit	Description
α_{max}	rad	Swashplate maximum tilt angle
h_{th}	mm	Slipper/swashplate gap height (common to all slippers)
h_{bpp}	μm	Barrel/port-plate clearance
P_{yoke}	Pa	Preload for the compensating piston spring

The hydraulic behaviour of the pump in the hydraulic system is defined by the pressure and flow at its ports. The fitting of the above mentioned parameters has been expressed as an optimization problem. The objective function minimizes the average absolute square error between measured and simulated time variable by action on the four model parameters for the n measurement points:

$$O_v(\alpha_{max}, h_{th}, h_{bpp}, P_{yoke}) = \min \left[\frac{1}{n} \sum_{i=1}^n \left(\frac{(I_{v_i}^* - I_{v_i})}{X_{v_i}} \right)^2 \right] \quad (3-15)$$

with:

- O_v objective function of parameters $\alpha_{max}, h_{th}, h_{bpp}$ and P_{yoke}
- v considered variable: P_d, P_c, Q_c , or Q_d
- I_v^* measured reference value [bar] or [L/min]
- I_v average stabilized simulated value [bar] or [L/min]
- X_v normalization factor [bar] or [L/min]
- t_1 initial time for the averaging of the absolute square error [s]
- t_2 final time for the averaging of the absolute square error [s]

Four optimization objectives are defined in the current study, based on pressure and flow at case and discharge ports P_c, P_d, Q_c , and Q_d .

Both real and simulated pump display pressure and flow temporal oscillations. In order to avoid having to match these measured oscillations, which are

temporally different for each recorded experiment, it was decided to average both stabilized measured and simulated variables of interest i , so as to be able to compare them.

As a consequence, the value I_i is obtained by averaging the associated simulated variable. It is made on a stabilized part of the simulation, in order to avoid simulation initialization effects. In the current study, 0.15 s are simulated and the average is computed on the last 10 ms of the simulation, which is a bit less than the duration of one pump revolution at 4600 rpm (~ 13 ms). Normalization factors are used in order to give each objective the same weight in the optimization. Their values are given in Table 3-7.

Table 3-7: Normalization factors used in the optimization objective

Variable	P_d [bar]	Q_d [L/min]	P_c [bar]	Q_c [L/min]
Factor	160	28	2.5	0.8

The fitting of the parameters is made through Simcenter AMESim (v14) optimization module (LMS AMESim, 2015). The module proposes two different optimization methods: Genetic Algorithm (GA) and the NLPQL (for Non-Linear Programming by Quadratic Lagrangian) algorithm.

GA is a computer-based metaphor of Darwin’s theory of natural selection (Holland, 1975). In GA, an individual represents a set of parameter values. A population is generated randomly, the best individuals are kept and their “children” (obtained by randomly picking two parents and giving the child characteristics close to theirs) replace the others population steady. The new population is “mutated”, their characteristics (parameter values) being changed by adding perturbations to their values. Individuals converge to one or several best solutions after several generations.

The NLPQL method is the implementation of a sequential quadratic programming (SQP) algorithm (Schittkowski, 1986). SQP is a standard method, based on the use of a gradient of objective functions and constraints to solve a non-linear optimization problem. A characteristic of the NLPQL method implemented in AMESim optimization module is that it stops as soon as it finds a local minimum. As such, the results obtained depends highly on the starting point given to the algorithm.

In this study, GA has the benefit to be able to find several fitting solutions. However, this method has high computation burden, as an important number of individuals is necessary to study the optimization space. Due to limited computation capabilities, it was chosen to use the NLPQL method in the optimization process.

Five experiments were used to fit the parameters, in nominal conditions (4600 rpm, 0 bar rel. tank pressure, 50 °C fluid temperature). These five experiments reproduced the points of the pump steady state characteristics shown on Figure 3-1. These experiments were numbered from 1 to 5, going from zero flow to full flow conditions.

In theory, it is better to optimize a single set of parameters for all five experiments, however, due to the realized model and software limitations, it was impossible to do so. As such, the NLPQL method was used to optimize a set of parameter for each experiment. Then, the average value of the optimized parameters were used as a global result for the optimization.

Table 3-8 gives the optimized values of the parameters for each experiment, as well as the values of the objectives and the final errors between measures and simulated outputs.

It is to be noted that not all parameters were fitted for all experiments. For example, the maximum swashplate tilt α_{max} was only used in optimization for the experiments n°4 and n°5, in which the pumps should be near (if not at) maximum displacement. The preload of the compensating piston spring was used only in optimizations for experiments n°2 and n°3 where the pump operated in regulation phase. This parameter was left out in experiment n°1 after verifying that it has no impact on the observed variables. Grey cells in the parameters section of Table 3-8 highlight in which optimization schemes the parameters were unused.

In Table 3-8, an error below 10% of the measured value was highlighted by a green cell, an error between 10 and 20% by a yellow cell, and an error above 20% of the measured value was written in an orange cell. It can be seen that the optimizations made for each reference experiments gave satisfactory results.

Table 3-8: Optimization results in each experimental conditions

Steady state operating point number		1	2	3	4	5
Parameters	h_{th} [mm]	8.06e-03	1.11e-02	1.45e-02	1.92e-02	2.54e-02
	h_{bpp} [m]	6.72e-06	3.79e-07	0.00e+00	2.76e-06	7.27e-06
	P_{yoke} [Pa]	7.00e+06	2.72e+07	1.33e+07	7.00e+06	7.00e+06
	α_{max} [rad]	2.64e-01	2.64e-01	2.64e-01	2.60e-01	2.67e-01
Objectives	O_{Pd}	6.01e-04	7.15e-03	7.58e-03	3.15e-03	1.22e-05
	O_{Qd}	2.58e-09	1.86e-03	5.62e-03	9.67e-03	2.21e-04
	O_{Pc}	2.60e-04	1.00e-02	8.99e-03	2.14e-03	1.38e-03
	O_{Qc}	2.23e-02	4.96e-03	7.05e-02	9.09e-02	7.33e-03
Errors	$ P_d^* - P_d $ [bar]	3.92	13.53	13.93	8.98	0.56
	$ Q_d^* - Q_d $ [L/min]	0.00	1.21	2.10	2.75	0.42
	$ P_c^* - P_c $ [bar]	0.04	0.25	0.24	0.12	0.09
	$ Q_c^* - Q_c $ [L/min]	0.12	0.06	0.21	0.24	0.07

Table 3-9 gathers the average values of the optimized parameter, as well as the standard deviation of the parameters from the average value. The values of the parameters in grey cells in Table 3-8 were not used in the computation as they are not a result of the optimization. The same cell colour code is used in Table 3-9 as in Table 3-8, highlighting the optimization results spread around the average values.

Table 3-9: Average and standard deviation of the optimized parameter sets

	Average	Standard deviation	
		Parameter units	Percentage (%)
h_{th} [mm]	1.57E-02	6.13e-03	39.16
h_{bpp} [m]	3.43E-06	3.07e-06	89.56
P_{yoke} [Pa]	2.03E+07	6.97e+06	34.35
α_{max} [rad]	2.64E-01	3.47e-03	1.32

From the computed standard deviations, as high as 89.56% in the case of barrel/port-plate gap height (h_{bpp}), it is expected to lose part of the accuracy obtained through the parameter fitting when applying the average parameters to the pump model. Table 3-10 shows the relative error between measurements and simulation made with the averaged parameters. The cell colours, compared to that of Table 3-8, show indeed a reduction of accuracy, most importantly on case drain pressure and flow. Discharge pressure seems also to be less accurate, while the relative error on discharge flow stays under 10%, except in the conditions of experiment n°1 (zero flow conditions). In these conditions, the measured discharge flow is very small but non zero due to sensor accuracy, leading to an important percentage error.

Table 3-10: Relative errors between measurements and simulation with averaged fitted parameters

Absolute relative error [%]	Steady state operating point number				
	1	2	3	4	5
Discharge pressure	4.53	14.67	14.59	11.45	9.16
Discharge flow	99.77	7.69	7.64	5.92	4.62
Case pressure	130.07	3.22	5.45	4.03	18.22
Case flow	163.73	188.74	37.44	35.34	68.91

Figure 3-24 displays the absolute error on case pressure and flow for each experiment, in different conditions. The blue rays of the histogram show the model errors before any optimization, the orange rays show the error when the best parameters sets are used in simulation (one set per experiments). The grey rays are obtained with the optimized parameters averages. The same kind of histogram are obtained for discharge pressure and flow, but are not displayed here. It is interesting to note that errors on case drain pressure and flow are

greatly reduced for the operation point n°1 (at zero discharge flow) compared to the others. In these operating conditions, sensibility to the altered clearance parameters is high due to the increased pressure at pump discharge port.

Figure 3-24 shows, in a different way than Table 3-10, the loss of accuracy generated by the use of the average optimized parameter values. This loss is consequent, however it is reassuring to see that the simulation results are improved compared to simulations with the initial parameter values. However, both Table 3-10 and Figure 3-24 show that the pump model, in the identified test bench and with the averaged parameters, does not represent accurately the case flow, even if case pressure is globally under the 10% absolute relative error limit.

Due to the lack of possibilities to improve further the results for the case flow, in which the test bench model participates greatly as discussed in section 3.3.1 (p94), it was decided to use the average values of the optimized parameters as initially proposed. In the next section, the behaviour of the described pump model with the set of modified parameters is assessed against experimental data.

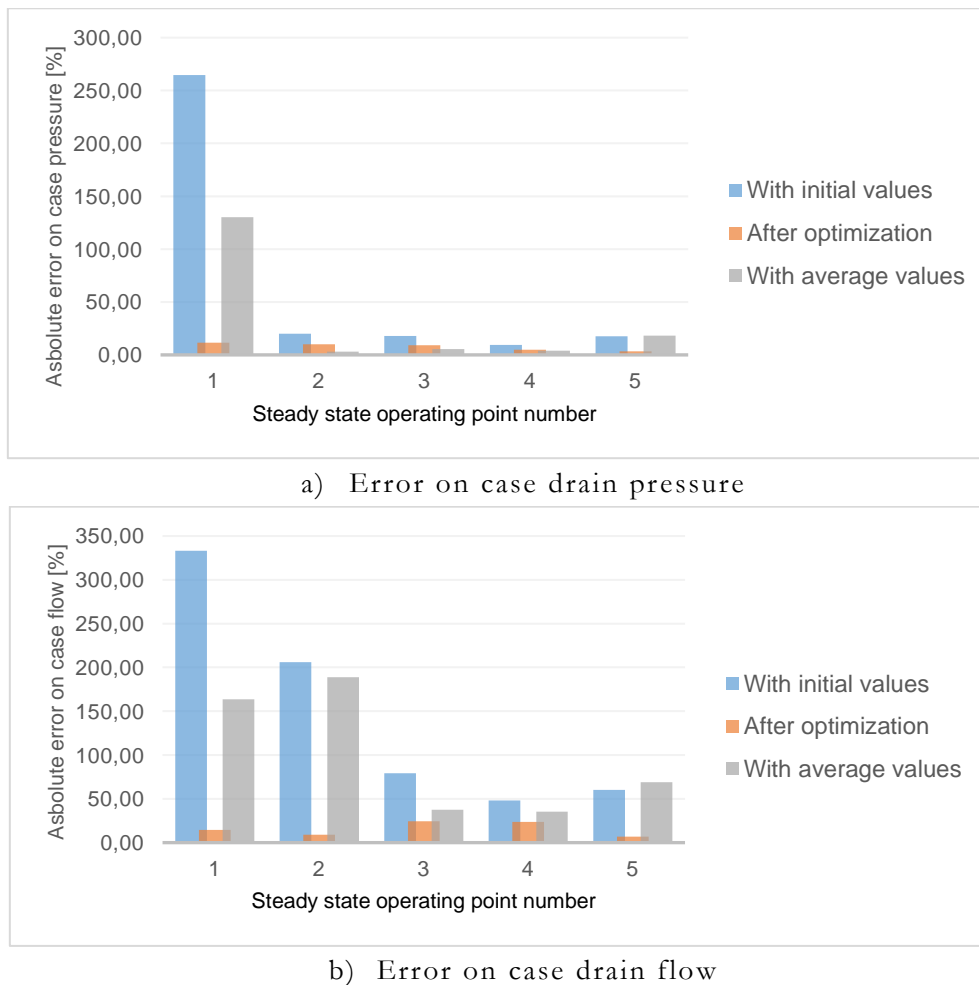


Figure 3-24: Effect of parameters on the virtual pump simulation results

3.3.2.3. Assessment of combined pump and test bench models

As the tested H225 pump nominal speed is 4600 rpm, it was chosen to assess the model against data measured at that speed and 50 °C. As such, from the data gathered experimentally and discussed in part 0, the model accuracy is evaluated against test results from experiments realised with increased suction pressure.

To this end, the simulation model and test bench are put in the same conditions as the experiments with increased suction pressure, and measures are compared with average simulation results in steady state conditions, as done for the parameters optimization.

The results are available in Table 3-11, where the absolute relative error between experimental and simulation results are given for all steady-state operating points and the four observed variables. From this table, it is concluded that the pump model reproduces the test results with the same limitations as in nominal operating conditions: discharge pressure and flow as well as case pressure are globally obtained with less than 20% of error, while the model is unable to reproduce with high accuracy the measured case flow behaviour.

As such, knowing the limits of the model (including the test bench), of the measurements and of the parameter fitting process, it is considered that the pump model is acceptable for operation at 50 °C and 4600 rpm.

Table 3-11: Simulation model errors – {Pr = 2.5 bar, ω =4600rpm, T= 50 °C}

	Steady state operating point number				
Absolute relative error [%]	1	2	3	4	5
Discharge pressure	0.68	13.10	12.24	9.48	6.14
Discharge flow	99.79	6.95	6.53	5.09	3.39
Case pressure	15.77	0.58	3.21	4.16	5.05
Case flow	158.96	324.29	56.40	40.63	71.78

As data is available at different rotating velocities, the opportunity is taken to check the model behaviour at these rotating speeds. It was found that the model loses accuracy when decreasing the rotating speed. This is especially true in the regulation phase (points 1 to 3) of the static characteristics as highlighted by Figure 3-25. This illustration uses the absolute error on case pressure, which is globally well reproduced in nominal conditions except at zero flow (static point n°1). At full flow (points 4 and 5), no tendency from the variation of rotating speed can be highlighted.

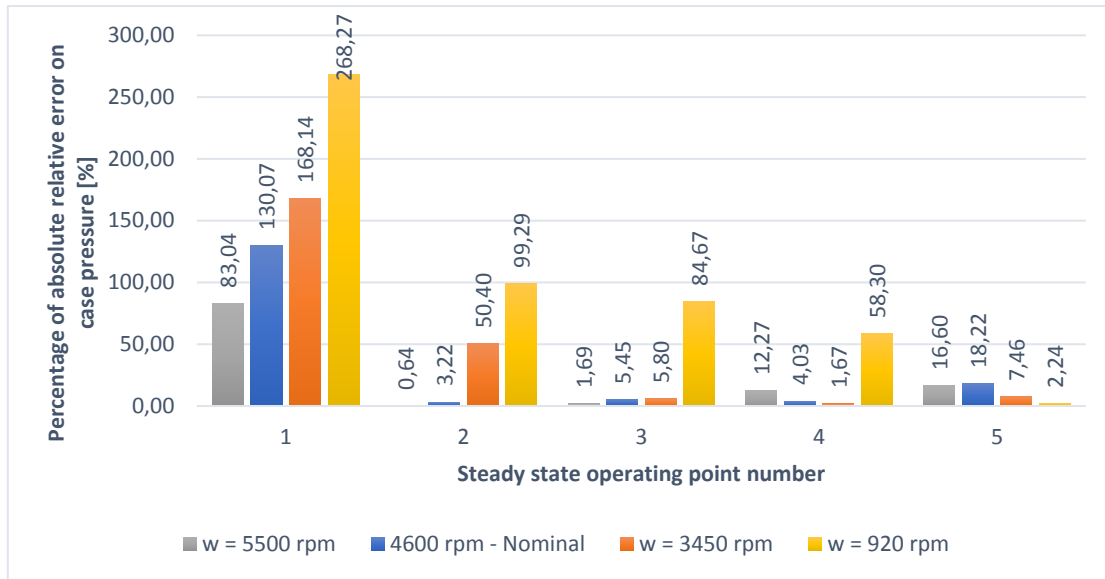


Figure 3-25: Effect of rotating speed on model accuracy - depending on static points

3.4. Conclusion

At the beginning of the chapter, a question relative to the developed model accuracy has been defined. The question was:

Q5. Is the pump model, running a simulated test in given operating conditions, able to reproduce the same result data and patterns as real tests made in the same operating conditions?

The present work focused on evaluating the developed model in steady state conditions, with a pump in healthy state.

In order to provide the answer to the question Q5, several tests campaigns were realized on a H225 pump in the facilities of an industrial partner. Then, the test bench set up was modelled so as to assess the developed pump model in a similar environment to the real tests. Finally the pump model parameters were identified and the model evaluated against the experimental results.

The first aim of these experiments was to gather hardware data and to compare it to the pump simulation results. However, the opportunity was taken to measure case drain pressure with a high bandwidth sensor, so as to increase the knowledge on the case drain pressure behaviour under several operating conditions.

The experimental results were analysed both in time and frequency domains. It was found that case pressure frequency content is similar to that of discharge pressure, with a shift in more impacting frequency, which depends on the

reservoir pressure. When it increases, the frequency content of case drain pressure signal gets closer to that of the discharge pressure signals.

It was thought that the measurements would help the understanding of the pump behaviour, in particular concerning pressure and flow at case drain port. Unfortunately, the industrial partner's test bench was realized in a way that connects the case and discharge return lines before reaching the tank. This introduced an external coupling between the hydraulic power variables at case and discharge ports. This deprived the author of the possibility of accurately identify the influence of the rotating speed and suction pressure on the case drain pressure and flow behaviour. Nevertheless the measurements provided numerous data that allowed for the evaluation of the developed pump model. The main issues related to the design and exploitation of the experimental test bench (e.g. test bench architecture, flow sensors quantization, temperature management) have been documented in details in section 0 to serve as stepping stone for future development of test benches for health monitoring.

A test bench model was developed to simulate the pump model in a test environment similar to the real world. Due to incomplete physical data information, the test bench was modelled using a mixed physics-based/data-driven approach: physics based for model structure, data-driven to identify the model parameters. Although identified from measurements, the test bench model parameters did not reproduce totally the influence of high temperatures. As such, it was decided to evaluate the pump model only on experimental data measured at 50 °C.

The simulation of the very detailed pump model gave access to numerous variables of interest. However a few shortcomings remain, especially concerning the variable slipper/swashplate gap height model. Knowing the limits of this model, the pump model has been adapted to use a fixed gap height, but it still allowed for the simulation of degraded states.

Through the model evaluation process, it was found that the developed pump model allows for the accurate simulation of steady state discharge pressure and flow as well as case pressure, at a fluid temperature of 50 °C and a rotating velocity of 4600 rpm. The error on the three hydraulic variables is in average below 20%. However, the accuracy of the model was significantly worse for the case drain flow, which represents the limit of the developed model: the case flow simulation absolute error is over 40% (related to the 0.8 L/min normalization factor used) for each simulated static points.

As pressure and flow are correlated, it is surprising to have such discrepancy between case pressure and flow simulation accuracies. However, it is to be remembered that the model is evaluated on a virtual test bench, with its own

modelling error. It was highlighted that on average, the error realized on case drain flow due to the test bench is about 0.3 L/min, which means that the test bench can contribute to overall simulation error up to 37.5% (compared to 0.8 L/min).

In order to improve the results, several approaches can be implemented. The first one lies with experiments and a better design of the test bench, with segregated case and return lines. It would facilitate the analysis of the pump case drain pressure behaviour with limited external influences. Introducing a tilt sensor for the swashplate and/or a displacement sensor for the compensating valve would generate rich additional data which could help to evaluate pump models more deeply.

A second one focuses on the improvement of the developed models. Several ways for further improvements of the pump model have been listed in Chapter 2. The one that seems most promising consists in developing meta-models fed from CFD simulations. This would allow for the numerous multi-physical coupled effects to be better considered while limiting the computational burden.

4. Helicopter axial piston pump monitoring

Note: Due to confidentiality reasons, parts of the current chapter have been removed. The removed parts have been highlighted for the reader to be aware of the missing content.

4.1. General considerations

Axial piston pumps can experience several failure mechanisms. These mechanisms are detailed on Table 4-1, which includes the affected parameters and the overall effect of each mechanism. The instigator of the current study, AH is interested in a method to *detect* and *isolate* pump degradation in H/C hydraulic systems, which is the focus of the current research. In this dissertation ‘hydraulic system’ refers to the entirety of the hydraulic circuit components except the pump and the reservoir.

Table 4-1: Axial piston pump failure mechanisms and effects (Paulmann & Mkadara, 2018)

	Failure mechanism	Affected parameters	Effect
1	Wear in compensator valve. Fracture or jam of compensator valve.	Supply pressure, swash plate position, flow rate.	Loss of pressure adjustment.
2	Defective tilting mechanism of swash plate (friction / jam in bearing of swash plate).	Supply pressure, swash plate position, flow rate.	Loss of pressure adjustment and/or flow displacement rate, loss of pressure compensation capability.
3	Friction / wear of pistons / sliding piston surfaces in cylinder block.	Case drain leakage rate, debris in case drain and supply pressure line, (case fluid) temperature.	Increase of (case fluid) temperature, degradation of pressure / flow rate, pollution of filter.
4	Alignment error of internal or external shaft, leading to excessive wear in shaft bearings. Pre-damage of external drive shaft. Friction / jam of drive shaft bearings.	Case drain leakage rate, debris in case drain and supply pressure line, (case fluid) temperature, drive shaft speed.	External droplet leakage at drive shaft seal, jam of internal rotating parts (cylinder block, pistons), increase of (case fluid) temperature, fracture or damage of external drive shaft, pollution of filter.
5	Wear/loss of seal function at compensator adjustment screw.	None.	External droplet leakage.
6	Loss of seal functions at plugs/housing seals/pressure port O-rings.	None.	External leakage.

One of the study constraints is to use only external sensors so as to limit the cost of the approach implementation. Such type of sensors include pressure, flow, temperature or vibration sensors, which allow for the monitoring of the failures

listed in Table 4-1. It was intentionally decided in the very first stages of the study to focus on hydraulic parameters, leaving out the study of pump vibrations.

The research work described and detailed in the present dissertation aims at investigating the benefits of pump case pressure measurement as a mean of axial piston pump monitoring on H/C. Two industrial questions were raised initially, which are reminded hereafter:

Q1. On H/C, can external case pressure sensors be used to detect pump degradation prior to failure?

Q2. Can pump degradation be isolated from hydraulic system degradation when using one additional case pressure sensor only?

The current chapter answers these questions. In a first section, Q1 is answered from the literature and simulation results. A tool is proposed for the isolation of pump degradation from that of the hydraulic system, answering Q2. Then, the feasibility of the proposed approach is studied in a second section.

4.2. Case pressure as a monitoring means

4.2.1. Theoretical considerations

Literature shows that case drain flow is of interest in the Fault Detection and Diagnosis (FDD) field of research. For example, pump case drain flow, associated with discharge pressure and case temperature, is utilised in (Byington, et al., 2003) and (Amin, et al., 2005). In these studies, both high and low frequency contents of the measured signals are used to build features for classification of axial piston pumps health status. The approach described in (Kwan, et al., 2003) is based on the noise level (i.e. high frequency content) of case drain flow measurement only. In (He, et al., 2012), (Wang, et al., 2016) and (Li, et al., 2018), the “return oil flow” is used as a feature for the proposed computation methods of the *remaining useful life*.

Although new technologies of sensors are being developed, see e.g. (Massarotti, et al., 2020), most current flow sensors use turbines placed in the stream. Such type of sensors can lead to unsafe situations for the H/C crew (see section 1.3). As a consequence, flow measurements are generally not implemented on helicopters hydraulic systems.

As pressure and flow are correlated, it is acceptable to conclude that pressure sensors can be use as alternative to flow sensors, and that pump degradation is observable through case pressure measurement. However, no explicit mention of case pressure used as a feature for FDD has been found in literature. The following question can then be raised: can case drain pressure measurement

provide as much information as case drain flow for pump monitoring? The simulation model evaluated in Chapter 3 in steady state is used as a tool to answer this question.

4.2.2. Pump model simulations

The third pump failure mechanism of Table 4-1, which includes wear of pistons and leads to increased leakage flow, is simulated. The simulation conditions are listed in Table 4-2. The load conditions of the pump and hydraulic system are that of the static point n°2 defined in Chapter 3 (p80), which generates in practice and in nominal health condition a discharge pressure of 160 bar for a 29 L/min delivered flow rate.

Table 4-2: Simulated pump degradation conditions

Modified parameter	Piston/barrel clearance
Number of affected pistons	3 (pistons n°1, n°2 and n°3)
Clearance increase percentage	50%, 100%, 150%
Fluid temperature	50 °C
Rotating speed	4600 rpm
Static point n°	2

The average steady state simulation results for both case drain flow and case pressure are displayed in Table 4-3. Results for the nominal state as well as a 50%, 100% and 150% increase of piston/barrel clearance are given. The deviation between the nominal state and each increased clearance one, is also supplied. It is computed subtracting the simulation result with increased clearance to the nominal one. Table 4-3 shows that, as expected, degradation can be observed through case pressure, and that deviation from the nominal state increases with clearance enlargement.

Table 4-3: Simulation results with increased piston clearance - average steady state values

	Nominal	Increased clearance					
		+50%		+100%		+150%	
	Simulation result	Simulation result	Deviation	Simulation result	Deviation	Simulation result	Deviation
Case flow Q_c [L/min]	1.766	1.772	-0.0055	1.782	-0.0163	1.800	-0.0343
Case pressure P_c [bar]	2.498	2.500	-0.0022	2.504	-0.0061	2.510	-0.0122
$\Delta P = P_c - P_i$ [bar]	0.511	0.513	-0.0016	0.517	-0.0047	0.522	-0.0099

In this simulation, case drain flow deviation due to degradation is greater than that of case pressure in steady state. This is due to the flow model used in the test bench identified model, which gives $P_c - P_i = k_c Q_c$ (equation (3-3) p97) with k_c less than 1 bar/(L/min) (see Table 3-4 p101). It is to be noted that the deviation of case drain pressure does not equal that of the pressure drop across the laminar orifice modelling the case drain line. This is due to the test bench

model architecture, which uses an intermediate fluid domain at variable pressure P_i between the fluid domain at case drain pressure P_c and the reservoir P_r (see Figure 3-20).

Even when the clearance increase is substantial, the resulting simulated deviations of case pressure and flow are small: +0.49% and +1.94% respectively, for a clearance increase of +150%. Taking for example the sensors defined in Chapter 3 (Table 3-2 p82), the simulated deviation of both case drain pressure and flow is smaller than the sensor accuracy (0.17 bar and 0.052 L/min respectively): none of the simulated degradation could have been observed with a case drain flow or pressure measurement. Nonetheless, it is to be reminded here that pump degradation should happen in several zones of the pump even if in different amount. So, the degradation would grow in time and, with adequate sensors, would be detected both from case drain flow or pressure signals.

To conclude, simulation showed that even if case drain pressure deviation from nominal value is smaller than that of case drain flow, deviation exists and could be measured and detected with appropriate sensors. Such sensors must be defined through experiments with pumps in several degraded states (from healthy to severely degraded), to define the amount of deviation which must be measurable with accuracy. It was not possible to answer this question during the PhD due to degraded pump not being available for testing at AH (see section 3.1 for more information). However, it is estimated that a pressure sensor with 5 bar full scale and 1% accuracy, with bandwidth and sampling rate allowing for the accurate characterization of the pressure mean value, would fit the monitoring need.

In the next section, the possibility of isolating pump degradation from that of the hydraulic system using case drain pressure is discussed.

4.2.3. Pump vs. hydraulic system degradation

Content removed for reasons of confidentiality.

Content removed for reasons of confidentiality.

Content removed for reasons of confidentiality.

Content removed for reasons of confidentiality.

4.3. Feasibility study of the proposed approach

Content removed for reasons of confidentiality..

Content removed for reasons of confidentiality.

Content removed for reasons of confidentiality.

Content removed for reasons of confidentiality.

Content removed for reasons of confidentiality.

Content removed for reasons of confidentiality.

Content removed for reasons of confidentiality.

Content removed for reasons of confidentiality.

Content removed for reasons of confidentiality.

Content removed for reasons of confidentiality.

4.4. About implementation on helicopter

Initially, the AH need is to reduce maintenance costs for the client, to improve H/C availability. To this end, predictive maintenance, as defined in Chapter 1, is advantageous. For hydraulic pumps, implementing predictive maintenance has the benefits of removing TBOs and limiting the number of maintenance tasks.

Predictive maintenance is based on condition monitoring. The authors of (Paulmann & Mkadara, 2018) defined two maturity levels for condition monitoring:

- The Level B allows to detect and isolate failures of a component/equipment/system/process at an early stage under operation and environmental conditions to avoid un-scheduled repairs/exchanges.
- The Level A, based on data and experience accumulated in level B, allows for predicting and forecasting the remaining useful life of a component/equipment/system/process until major failure. It takes into account the evolution trend of the failure mechanisms governing parameters and the individual influencing environmental conditions.

Implementation of a level B condition monitoring can improve mission and dispatch availability of equipment, which has a direct positive impact on operational costs. This level of maturity leads to condition-based maintenance. There are two options for the maturity level A: either the condition monitoring system is certified, which means that it can be implemented H/C and be used to insure crew safety, or it is not. Aeronautical certification is a tedious process that requires a high technology readiness level (TRL). Before it is certified, the level A CM system can provide the basis for a predictive maintenance service to customers.

The current study proposed a way to progress towards the CM maturity level B, i.e. towards condition-based maintenance. The author proposed a tool to isolate pump degradation to that of the hydraulic system. However, several points have yet to be dealt with concerning practical implementation on H/C. The first one, discussed in next section, lies with measurement conditions.

4.4.1. Measurement conditions on H/C

The problem lies with the timing when to make such measurement during an H/C mission, and the reproducibility of the measurement flow conditions. The initial thought is to take advantage of the existing pre-flight check procedures. Two checks are made for flight controls:

- 1) The pilot check, where the pilot verifies that there is no blocking point on the flight control chain by making control movements in each direction (longitudinal, lateral and yaw axes).
- 2) The autopilot check, where the authority of the autopilot is verified. During this test, small displacements of the actuators are realised at constant speed.

In pilot checks, the speed and amplitude of the control movements depends on the pilots. As such, this pilot check does not produce reproducible pump steady-state discharge flow. The constant speed travel of the actuators during the autopilot check generates a constant flow demand in the hydraulic system. However, the stable phases of this pre-flight check are too fast to allow for a steady-state measurement. As none of the two existing procedures can be taken advantage of, the pump monitoring time must be defined outside of it.

In the current case, measurements in zero flow condition have been preconized, i.e. but without any pilot or autopilot action. To insure steady-state of the hydraulic system, these measurements could be made prior to any check, as long as rotor is turning with stable speed, and fluid temperature is steady.

In the case where measurements with constant, non-zero, discharge flow are proven to be necessary, it is proposed to take advantage of H/C tied down ground runs. When helicopter is tied down, important flight control movements can be made without safety issues. In practice, it makes possible to generate a high constant flow demand for the pump.

4.4.2. Other considerations

A tool has been proposed to help pump isolation of pump degradation from that of the hydraulic system. Nevertheless, it is still a theoretical work which lays the foundation of TRL 3 (theoretical proof of concept) for a condition monitoring approach. For AH to consider real implementation of a condition monitoring approach, its maturity must reach TRL 4 (experimental validation of the approach), and the economic benefits of such implemented approach must be confirmed.

To reach the condition monitoring approach TRL 3, a detection algorithm must be designed. Then, this algorithm must be tested experimentally against both healthy and degraded pumps, so as to insure low probability of false, or missed, alarms. Doing so, TRL 4 could be demonstrated, prior implementation on H/C prototypes or iron bird for further testing in representative environmental conditions.

A way to gather the data on H/C and to retrieve it from clients must also be proposed and tested. A Health and Usage Monitoring System (HUMS) has already

been implemented on several AH H/C families, including that of the H225. Measurement realized through the HUMS can be retrieved by AH and analysed. However, this retrieval is constrained by contracts with the clients owning the helicopters and the clients' agreement to supply the measured data. Integrating the pump degradation detection algorithm and the necessary associated hardware (e.g. case drain pressure sensor) in the already existing HUMS seems to be the best approach for efficient condition monitoring. Nevertheless, such integration requires a transversal planning and realization, with conjoint work of several AH departments.

All the previously listed points (detection algorithm definition, experimental investigation for increased TRL, implementation on H/C through HUMS) will come at an effort which must be assessed both in terms of time and money. An additional cost to be considered is that of sensor certification. Characteristics of a case drain pressure sensor which fit the monitoring need have been proposed (see §4.2.2). However, the availability of an aeronautically certified pressure sensor of these characteristics has yet to be confirmed. Nevertheless, the condition monitoring approach proposed is based on a single additional non-intrusive pressure sensor, which limits unavoidable added costs.

4.5. Conclusion

This chapter aimed at answering both following questions:

- Q1. On H/C, can external case pressure sensors be used to detect pump degradation prior to failure?
- Q2. Can pump degradation be isolated from hydraulic system degradation when using one additional case pressure sensor only?

A literature study showed that measuring the pump leakage flow has been used as a mean to isolate the pump fault or to computation of remaining useful life in laboratory studies. As pressure and flow are correlated, it was found acceptable to use case drain pressure a monitoring variable in a new approach. The worth of case pressure compared to that of case drain flow has been assessed through simulation, in steady-state operation. It was found that although case pressure deviation from nominal state due to pump degradation was smaller than that of case drain flow, pump degradation could be monitored with a case pressure sensor of appropriate range and accuracy.

A graphical representation (also referred hereafter as 'solution') was proposed to facilitate the diagnosis of pump degradation against hydraulic system degradation.

The feasibility of the solution has been analysed [*content removed for confidentiality reasons*]. To this end, both simulation and experimental results, as well as AH standardized test procedures, were used.

It was found that, as expected, both fluid temperature and pump rotating speed should be fixed and steady during the measurements on and off H/C.

[*Paragraph removed for confidentiality reasons*]

Pump and hydraulic system behaviour variability due to their uniqueness has been discussed. The realised study, based both on pump ATP and simulation in the case of the hydraulic system, found that making measurements in zero discharge flow conditions limits greatly the variability of the results.

As a conclusion, the answer to both risen questions is yes: case pressure can be used to monitor the pump degradation, and using a case pressure sensor allows for the segregation of pump degradation against hydraulic system degradation, with the proposed solution.

[*Paragraph removed for confidentiality reasons*]

In the end, a tool has been proposed to help the diagnosis of pump degradation compared to hydraulic system degradation. However, detection of pump degradation has never been discussed. The proposed solution can be used for detection. Nonetheless, experiments must be realized to define a proper limit for healthy/degraded behaviour, in each hydraulic system of interest.

5. General conclusion

The aim of the current study was to propose and evaluate a low cost solution for axial piston pump monitoring. The research focused on the use of case pressure measurement in a monitoring scheme, and the following industrial questions were identified:

- Q1. On H/C, can external case pressure sensors be used to detect pump degradation prior to failure?
- Q2. Can pump degradation be isolated from hydraulic system degradation when using one additional case pressure sensor only?

The industrial context raised the need for developing the lumped-parameter model of an axial piston pump. The following scientific question relative to pump modelling were identified:

- Q3. What is the current state of the art for axial piston pump modelling?
- Q4. What improvements can be made from state of the art 1-D pump modelling in the view of condition monitoring and what do those improvements bring?
- Q5. Is the pump model, running a simulated test in given operating conditions, able to reproduce the same result data and patterns as real tests made in the same operating conditions?

In order to answer these questions, the dissertation has been separated in three main chapters (numbered from 2 to 4).

In Chapter 2, an axial piston pump model was developed following requirements, for an existing in-service pump. Initially, a model architecting process has been presented to answer the defined industrial durability requirements. A literature review was realised to answer Q3. Then, considering condition monitoring and modelling, two ways of improving the detailed state-of-the-art in axial piston pump lumped-parameter modelling have been detailed, answering Q4. The first one focuses on pressure compensating mechanism. An approach to simulate time variable clearances and part jamming has been suggested, based on bond-graphs. The second way deals with the swashplate/slipper interface. A slipper/swashplate variable gap height model has been proposed in order to improve the leakage representativeness of lumped-parameter axial piston pump models. The model, based on a kinematic representation of the gap height, allows for the simulation of the clearance

variation during a pump cycle, due to the hydraulic and mechanical forces applied on the different pump parts. The limits of the gap height model were highlighted. The long slipper/swashplate contacts observed for simulations at high pump displacement is one of them. This simulated behaviour leads to unrealistic leakage flow. Despite the numerous solutions tested to improve the slipper/swashplate model, it was not possible to reduce this effect within the time frame of the PhD. The use of metamodels for the further improvement of the pump model has been proposed for further research activities. This type of models, based on CFD simulations, will enable taking in to account more complex phenomena (e.g. slipper tilt, squeeze effect, localized temperature effects on fluid viscosity), without the computational burden of CFD.

Chapter 3 focused on answering question Q5. Experiments were realised in order to gather data for the pump model evaluation as well as study the case drain pressure versus operating conditions. The author specified the experimental test program and the analysed the results, which were obtained on an already existing test bench with a pressurized reservoir, and a partially common return line for the case drain and discharge flows. The analysis showed that the frequency behaviour of the case drain pressure measured signal depends greatly on the reservoir pressure. However, the architecture of the test bench prevented the identification of the influence of rotating speed on case drain pressure and flow. For future research, a test bench must be designed with separated discharge and case drain lines. This will allow the study of case drain pressure and flow both in temporal and frequency domains, without other influence than the pump itself.

The coupling of case and discharge lines in the experiments increased the need for a test bench model on which to evaluate the pump model. A parametric test bench model has been developed. Its structure was based on the physics, and its parameters were identified from experimental measurements. It was estimated that the modelled test bench, alone, generates an error on case drain flow of about 0.3 L/min in average. To put this value in perspective, this error amounts to 20% of the 1.5 L/min maximum pump leakage allowed in practice. In addition to that, the temperature evolution of the identified model parameters was found unrealistic. This test bench model was nonetheless considered sufficiently accurate to be used to evaluate the developed axial piston pump model (with fixed gap height) in nominal conditions (fluid temperature 50°C, rotating speed 4600 rpm, and reservoir pressure 0 bar rel.). Coupling the pump and test bench models (after pump model parameter identification) allowed for the accurate simulation of discharge pressure and flow as well as case drain pressure in nominal conditions, with an absolute error below 20%. However, the accuracy of the model was significantly worse for the case drain flow: the absolute error was over 40% in all simulations made in nominal conditions. Two distinct approaches can

be suggested to improve the overall model representativeness. The first one focuses on the test bench model. A better data gathering during experiments, and the change of the case drain orifice model (from laminar orifice to an orifice with laminar/turbulent transition) will generate significant improvements of the test bench model accuracy. The second approach is linked to the inclusion of metamodels in the pump model, as already discussed.

Chapter 4 focused on answering the industrial question Q1 and Q2. Q1 has been answered favourably thanks to literature. Then, a solution [*removed for confidentiality reasons*], has been proposed. This solution enables pump degradation to be isolated from hydraulic system degradation. A special attention has been paid to the feasibility of this approach regarding its robustness against variations of reservoir pressure, fluid temperature, and rotating speed. It was also considered of major importance to account for production variability at both hydraulic system and pump levels. It was suggested to realize the comparative measurements in zero flow conditions to mitigate the impact of this variability. In practice this can be achieved e.g. taking measurements on H/C during a pre(or post)-flight test, when no pilot command is applied. It was also suggested to characterise the reference curve from measurements taken on AH “iron birds” (H/C system hardware test bed).

In order increase the maturity level of the proposed pump monitoring approach, several points remain to be addressed:

- This PhD has addressed the interest and feasibility of tracking the pump degradation through the solution. However the detection of the pump degradation itself was not dealt with. This will require further research to design, implement and evaluate a detection algorithm.
- It is necessary to launch an experimental campaign so as to demonstrate the feasibility of the proposed approach, through the increase of the technology readiness level from level 3 to level 4.
- For measuring the pump case pressure, the sensor to be added should have a range of 5 bar. However, attention must be paid to the availability and cost of such a certified pressure sensor.
- Last but not least, the implementation of the proposed approach on H/C (e.g. introduction of a monitoring automatic routine) remains a key point that requires a huge transverse work between numerous AH departments.

References

- 20-sim, n.d. *Bond-Graphs*. [Online]
Available at: <https://www.20sim.com/features/model-libraries/bondgraphs/>
[Accessed 5th May 2018].
- Aaltonen, J., 2016. *Interaction of Bootstrap Reservoir and Hydraulic Pump in Aircraft Hydraulic Systems*. Tampere University of Technology: Ph.-D. Thesis dissertation.
- Adams, M. L., 2017. *Bearings : Basic Design and Design Applications*. Boca Raton: CRC Press, Taylor & Francis Group.
- Airbus Helicopters, 2012. *AER-AH-1368*. s.l.:s.n.
- Amin, S., Byington, C. & Watson, M., 2005. Fuzzy inference and fusion for health state diagnosis of hydraulic pumps and motors. *NAFIPS 2005 - 2005 Annual Meeting of the North American Fuzzy Information Processing Society, Detroit, MI, USA*, pp. 13 - 18.
- Anthony, A., 2012. *Modeling and Analysis of Hydraulic Load Sensing Strategies in Off Highway Equipment*. Università degli Studi di Parma: Ph.-D. Dissertation.
- Attar, B., 2008. *Modélisation réaliste en conditions extrêmes des servovalves électrohydrauliques utilisées pour le guidage et la navigation aéronautique et spatiale*. Institut National des Sciences Appliquées (INSA) de Toulouse: Ph.-D. Thesis dissertation.
- Bayer, C. & Enge-Rosenblatt, O., 2011. *Modeling of hydraulic axial piston pumps including specific signs of wear and tear*. Dresden, Germany, Proceedings of the 8th Modelica Conference, March 20-22, 2011.
- Bensaad, D., Soualhi, A. & Guillet, F., 2019. A new leaky piston identification method in an axial piston pump based on the extended Kalman filter. *Measurements*, Volume 148.
- Bergada, J. M. & Kumar, S., 2014. *Fluid Power, Mathematical design of several components*. First ed. New-York: Nova Science Publishers.
- Bergada, J. M., Kumar, S., Davies, D. L. & Watton, J., 2012. A complete analysis of axial piston pump leakage and output flow ripples. *Applied Mathematical Modelling*, Volume 36, pp. 1731-1751.
- Bergada, J. M., Kumar, S. & Watton, J., 2007. Towards an analytical solution for axial piston pump leakage and output flow ripple. *Proceedings of the 9th International Symposium on Fluid Control Measurement and Visualization (FLUCOME 2007)*, pp. 35-43.
- Bergada, J. M. & Watton, J., 2002. A direct leakage flow rate calculation method for axial pump grooved pistons and slippers, and its evaluation for a 5/95 fluid application. *Proceedings of the JFPS International Symposium on Fluid Power*, pp. 259-264.

References

- Bergada, J. M. & Watton, J., 2005. Optimisation of the lift characteristics of an axial piston pump grooved slipper. *Proceedings of the JFPS International Symposium on Fluid Power*, pp. 700-704.
- Bergada, J. M., Watton, J., Haynes, J. & Davies, D., 2010. The hydrostatic/hydrodynamic behaviour of an axial piston pump slipper with multiple lands. *Meccanica*, Volume 45, pp. 585-602.
- Blackburn, J. F., Reethof, G. & Shearer, J. L., 1960. *Fluid Power Control*. New York: John Wiley & Sons.
- Blackman, L. D., 2001. *Detailed Dynamic Model for Variable Displacement Pumps - a new Approach with Simulink*. Recent Advances in Aerospace Actuation Systems and Components, June 13-15, Toulouse, France.
- Böinghoff, O., 1977. Untersuchungen zum Reibungsverhalten der Gleitschuhe in Schrägscheiben-Axialkolbenmaschinen. *VDI-Forschungsheft*, Volume 584, pp. 1-46.
- Byington, C., Watson, M., Edwards, D. & Dunkin, B., 2003. In-line health monitoring system for hydraulic pumps and motors. *IEEE Aerospace Conference Proceedings*, Volume 7, pp. 3279 - 3287.
- Chao, Q., Zhang, J., Xu, B. & Wang, Q., 2018. Discussion on the Reynolds equation for the slipper bearing modeling in axial piston pumps. *Tribology International*, Volume 118, pp. 140-147.
- Chao, Q., Zhang, J., Xu, B. & Wang, Q., 2018. Multi-position measurement of oil film thickness within the slipper bearing in axial piston pumps. *Measurement*, Volume 122, pp. 66-72.
- Chen, J., Zhang, J. & Li, J., 2016. RESEARCH ON LOAD SPECTRUM OF AERO HYDRAULIC PUMP BASED ON ACCELERATED DEGRADATION TESTING. Deajon, South Korea, Proceedings of the 30th Congress of the International Council of the Aerospace Sciences (ICAS).
- Coïc, C., 2017. *Model-Aided Design of a High-Performance Fly-By-Wire Actuator, Based on a Global Modelling of the Actuation System using Bond Graphs*. Institut National des Sciences Appliquées (INSA) de Toulouse, France: Ph.-D. Thesis dissertation.
- Corvaglia, A. & Rundo, M., 2018. *Comparison of 0D and 3D Hydraulic Models for Axial Piston Pumps*. 73rd Conference of the Italian Thermal Machines Engineering Association (ATI 2018), 12-13 September, Pisa, Italy.
- Dauphin-Tanguy, G., 2000. *Les bond-graphs*. Paris: HERMES Science.
- Deléchelle, O., 2019. *From CAD to Simulation - A Smooth Workflow to Model Axial Piston Pumps for EDP/EHA systems*. SIEMENS Digital Industry Software: Presentation at SAE A-6 meeting, October 2019.
- Eaton Corporation, 2000. *A Descriptive Summary of Vickers Inline Pumps and their Applications*. [Online] Available at: http://www.eaton.com/Eaton/ProductsServices/Aerospace/Hydraulics/PCT_249150#tabs-2 [Accessed 16 10 2017].
- Fairlie-Clarke, A. C., 1999. Force as flow variable. *Proceedings of the Institution of Mechanical Engineers (IMechE) Part. I: Journals of Systems and Control Engineering*, Volume 213.
- Fang, X. et al., 2013. Physics-of-failure models of erosion wear in electrohydraulic servovalve, and erosion wear life prediction method. *Mechatronics*, 23(8), pp. 1202-1214.

References

- He, Z., Wang, S., Wang, K. & Li, K., 2012. Prognostic analysis based on hybrid prediction method for axial piston pump. *IEEE 10th International Conference on Industrial Informatics, Beijing, 2012*, pp. 688-692..
- Holland, J., 1975. *Adaptation in natural and artificial systems*. Ann Arbor: University of Michigan Press.
- Hooke, C. J. & Li, K. Y., 1988. The Lubrication of Overclamped Slippers in Axial Piston Pumps - Centrally Loaded Behaviour. *Proceedings of the IMechE Part C: Journal of Mechanical Engineering Science*, 1 July, 202(4), pp. 287-293.
- Isermann, R. & Ballé, P., 1997. Trends in the application of model-based fault detection and diagnosis of technical processes. *Control Engineering Practice*, 5(5), pp. 709-719.
- ISO, 2003. *ISO 17559:2003(en) - Hydraulic Fluid Power - Electrically controlled hydraulic pumps - Test methods to determine performance characteristics*. s.l.:s.n.
- ISO, 2016. *ISO 8278:2016(en) - Aerospace series — Hydraulic, pressure compensated, variable delivery pumps — General requirements*. s.l.:s.n.
- ISO, 2019. *ISO 4409:2019(en) - Hydraulic fluid power — Positive-displacement pumps, motors and integral transmissions — Methods of testing and presenting basic steady state performance*. s.l.:s.n.
- Ivantysyn, J. & Ivantysynova, M., 2003. *Hydrostatic Pumps and Motors: Principles, Design, Performance, Modelling, Analysis, Control and Testing*. s.l.:Tech Books International.
- Ivantysynova, M. & Baker, J., 2009. Power Loss in the Lubricating Gap between Cylinder Block and Valve Plate of Swash Plate type Axial Piston Machines. *International Journal of Fluid Power*, 10(2), pp. 29-43.
- Ivantysyn, R. & Weber, J., 2016. "Transparent Pump": An Approach to Visualize Lifetime Limiting Factors in Axial Piston Pumps. *Proceedings of the ASME 2016 9th FPNI Ph.D. Symposium on Fluid Power. V001T01A006*.
- Jiang, J. H., Wang, Z. B. & Wang, K. L., 2018. Power loss of slipper/swashplate based on elastohydrodynamic lubrication model in axial piston pump. *IOP Conference Series: Earth and Environmental Science*, Volume 188.
- Kavanagh, G. P., 1987. *The Dynamic Modelling of an Axial Piston Hydraulic Pump*. Department of Mechanical Engineering ed. Saskatoon, Sask., Canada: University of Saskatchewan.
- Kazama, T., Suzuki, M. & Suzuki, K., 2014. Relation between Sliding-Part Temperature and Clearance Shape of a Slipper in Swashplate Axial Piston Motors. *JFP International Journal of Fluid Power System*, Volume 8, pp. 10-17.
- Khemliche, M., Ouid Bouamama, B. & Haffaf, H., 2004. Optimal Sensor Placement Using Bond-Graph Model for FDI Design. *IFAC Proceedings Volumes*, 37(5), pp. 79-84.
- Kumar, S., Bergada, J. & Watton, J., 2009. Axial piston pump grooved slipper analysis by CFD simulation of three-dimensional NVS equation in cylindrical coordinates. *Computer & Fluids*, 38(3), pp. 648-663.
- Kwan, C., Xu, R. & Zhang, X., 2003. *Fault Detection and Identification in Aircraft Hydraulic Pumps using MCA*. Washington, D.C., USA, s.n.

References

- Li, H. et al., 2015. Energy-loss mechanism and load capacity analysis of slipper pair in an aerial axial piston pump. *Proceedings of the 2015 IEEE International Conference on Advanced Intelligent Mechatronics (AIM)*, pp. 396-400.
- Linköping University, 2008. *Formula Book for Hydraulics and Pneumatics*. Linköping: Linköping University.
- Lin, S. & Hu, J., 2015. Tribo-dynamic model of slipper bearings. *Applied Mathematical Modelling*, Volume 39, pp. 548-558.
- Li, T., Wang, S., Shi, J. & Ma, Z., 2018. An adaptive-order particle filter for remaining useful life prediction of aviation piston pumps. *Chinese Journal of Aeronautics*, 31(5), pp. 941-948.
- LMS AMESim, 2015. *Design of Exploration - User's Guide*. Available in: AMEHelp.
- LMS AMESim, 2015. *Hydraulic Component Design library: BAO043 component*. Available in: AMEHelp.
- LMS AMESim, 2015. *Mechanical library: elastic collision in LMS AMESim*. Available in: AMEHelp.
- MacLellan, G. D., Mitchell, A. E. & Turnbull, D., 1960. Flow characteristics of piston-type control valves. *Proceedings of the Symposium on Recent Mechanical Engineering Developments in Automatic Control*, pp. 13-30.
- Ma, J. et al., 2015. Wear analysis of swash plate/ slipper pair of axix piston hydraulic pump. *Tribology International*, Volume 90, pp. 467-472.
- Mancò, S., Nervegna, N., Lettini, A. & Gilardino, L., 2002. Advances in the simulation of axial piston pumps. *Proceedings of the Fifth JFPS International Symposium on Fluid Power*, pp. 251-258.
- Manring, N. D. & Johnson, R. E., 1996. Modeling and Designing a Variable-Displacement Open-Loop Pump. *Journal of Dynamic Systems, Measurement, and Control*, Volume 118, pp. 267-271.
- Maré, J.-C., 1993. *Contribution à la modélisation, la simulation, l'identification et la commande d'actionneurs électrohydrauliques*. Université Claude Bernard - Lyon 1: Ph.-D. Thesis Dissertation.
- Maré, J.-C., 2015. *Modelling and Simulation (of end-mechanical systems) - Lecture notes*. Toulouse: Institut National des Sciences Appliquées.
- Maré, J.-C., 2019. Best practices for model-based and simulation-aided engineering of power transmission and motion control systems. *Chinese Journal of Aeronautics*, 32(1), pp. 186-199.
- Maré, J.-C. & Akitani, S., 2018. *Foundation for Virtual Prototyping of Mechanical Power Management Functions in Actuators*. Bath, UK, Proceedings of the BATH/ASME 2018 Symposium on Fluid Power and Motion Control FPMC2018, September 12-14, 2018.
- Massarotti, G., Ferrari, C., Codina Macià, E. & Ruggeri, M., 2020. *MEMS sensors in hydraulics, an opportunity to creat smart components*. Dresden, Germany, Proceedings of the 12th International Fluid Power Conference, March 9-11.
- Maurice, F., 2019. *Développement et mise en œuvre de plans d'expériences numériques en modélisation et simulation système : application à l'hydraulique de puissance*. Université de Technologie de Compiègne: Ph.-D. Thesis Dissertation.
- Mc Cloy, D., 1968. Discharge Characteristics of servovalves orifices. *Proceedings of the Fluid Power International Conference*, pp. 43-50.

References

- Meritt, H. E., 1967. *Hydraulic Control Systems*. 1e ed. New York: John Wiley & Sons, Inc..
- Mkadara, G. & Maré, J.-C., 2020. *Development of a lumped parameter model of an aerospace pump for condition monitoring purposes*. Dresden, Germany, Proceedings of the 12th International Fluid Power Conference, October 12-14.
- Modelica Association, n.d. *ElastoGap*. [Online] Available at: build.openmodelica.org/Documentation/Modelica.Mechanics.Translational.Components.ElastoGap.html [Accessed 27 March 2019].
- Nesci, A., De Martin, A., Jacazio, G. & Sorli, M., 2020. Detection and Prognosis of Propagating Faults in Flight Control Actuators for Helicopters. *Aerospace*, 7(20).
- Paulmann, G. & Mkadara, G., 2018. *Condition Monitoring of hydraulic pumps - lessons learnt*. Aachen, Germany, Proceedings of the 11th International Fluid Power Conference, March 19-21.
- Paynter, H. M., 1961. *Analysis and Design of Engineering Systems - Classe Notes for M.I.T., Course 2.751*. Cambridge: M.I.T. Press.
- Pelosi, M. & Ivantysynova, M., 2009. *A Novel Fluid-Structure Interaction Model for Lubricating Gaps of Piston Machines*. Southampton, Proceedings of the Fifth Fluid Structure Interaction Conference.
- Poole, K., Raeth, M., Thielecke, F. & Mädige, C., 2011. *Leakage Diagnosis for Electric Motor Pumps in Aircrews Hydraulic Systems*. Bremen, Germany, Deutscher Luft - und Raumfahrtkongress, September 27-29.
- Raetz, R., 2009. *Théorie Elementaire de l'Hélicoptère - 2e édition*. Collection aviation éd. s.l.:Cepadues Editions.
- Rocatello, A., Mancò, S. & Nervegna, N., 2007. Modelling a Variable Displacement Axial Piston Pump in a Multibody Simulation Environment. *ASME J. Dyn. Sys, Meas., Control.*, 129(4), pp. 456-468.
- Rokala, M., Caloni, O., Koskinen, K. & Pietola, M., 2008. Study of the lubrication conditions in slipper-swashplate contact in water hydraulic axial piston pump test rig. *Proceedings of the JFPS International Symposium on Fluid Power*, pp. 91-94.
- SAE International, 2000. *Aerospace Hydraulic Fluids Physical Properties (AIR 1362B)*. s.l.:s.n.
- SAE International, 2016. *AS19692B - Aerospace Standard - Aerospace military type variable delivery, Pressure compensated hydraulic pump*. [Online] Available at: <https://doi.org/10.4271/AS19692B> [Accessed 05 05 2019].
- SAE International, 2019. *SAE J745_201911 Hydraulic Power Pump Test Procedure for hydraulic positive displacement pumps used on off-road self-propelled work machines*. s.l.:s.n.
- Schenk, A., 2014. *Predicting lubrication performance between the slipper and swash-plate in axial piston hydraulic machines*. Purdue University: Open Access Dissertations. 359.
- Schenk, A. & Ivantysynova, M., 2015. A Transient Thermoelastohydrodynamic Lubrication Model for the Slipper/Swashplate in Axial Piston Machines. *Journal of Tribology*, Volume 137.

References

- Schittkowski, K., 1986. NLPQL: A FORTRAN subroutine for solving constrained nonlinear programming problems. *Annals of Operations Research*, Volume 5, pp. 485-500.
- Sidoroff, F., 2010. Lois de comportement. In: *Mécanique des milieux continus*. Engineering School: Ecole centrale de Lyon, pp. 43-56.
- Spuri, F. & Goes, L., 2017. *Modeling and Parametric Identification of a Variable-Displacement Pressure Compensated Pump*. Linköping, Sweden, s.n.
- Stachowiak, G. W. & Batchelor, A. W., 2014. Chapter 11 - Abrasive, Erosive and Cavitation Wear. In: *Engineering Tribology (4th edition)*. Oxford: Butterworth-Heinemann, pp. 525-276.
- Succi, G. P. & Chin, H., 1996. *Helicopter Hydraulic Pump Condition Monitoring Using Neural Net Analysis of the Vibration signature*. Dayton, Ohio, USA, Presented at the 1996 SAE Aerospace Atlantic Conference, May 1996, Dayton, OH, Paper No. 961307.
- Suzuki, M., Akita, H., Saito, T. & Kazama, T., 2011. Experiment on slippers behavior in swashplate-type axial piston motors. *Proceedings of the 8th JFPS International Symposium on Fluid Power*, pp. 157-162.
- Tang, H., Yin, Y. & Li, J., 2016. Lubrication characteristics analysis os slipper bearing in axial piston pump considering thermal effect. *Lubrication Science*, 28(2), pp. 107-124.
- Tang, H. et al., 2018. Impact of the thermal effect on the load-carrying capacity of a slipper pair for an aviation axial-piston pump. *Chinese Journal of Aeronautics*, 31(2), pp. 395-409.
- Thoma, J. U., 1975. *Introduction to Bond Graphs and their applications*. s.l.:Pergamon Press.
- Torikka, T., 2011. *Evaluation of Analysis Methods for Fault Diagnosis on Axial Piston Pumps*. Tampere, Finland, Proceedings of the Twelfth Scandinavian International Conference on Fluid Power, May 18-20, 2011.
- Vaughan, N. D., Tiley, D. G. & Pomeroy, P. E., 1993. *Erosive Wear Measurement in Spool Valves*. Peoria, IL, United States of America, Proceedings of the Annual Earthmoving Industry Conference, pp. 93-99.
- Viersma, T. J., 1961. *Investigation in the accuracy of hydraulic servomotors*. Delft University of Technology: Ph.-D. Thesis Dissertation.
- Wang, Q.-n., Xu, B. & Zhang, J., 2015. Optimization design of the inner radius of the sealing surface of slipper. *Proceedings of the 2015 IEEE International Conference on Advanced Intelligent Mechatronics*, pp. 388-395.
- Wang, X. et al., 2016. Remaining useful life prediction based on the Wiener process for an aviation axial piston pump. *Chinese Journal of Aeronautics*, 29(3), pp. 779-788.
- Welch, P., 1967. The use of fast Fourier transform for the estimation of power spectra: A method based on time averaging over short, modified periodograms. *IEEE Transactions on Audio and Electroacoustics*, 15(2), pp. 70-73.
- Wieczorek, U. & Ivantysynova, M., 2002. Computer Aided Optimization of Bearing and Sealing Gaps in Hydrostatic Machines - The Simulation Tool CASPAR. *International Journal of Fluid Power*, 3(1), pp. 7-20.
- Xu, B., Wang, Q.-n. & Zhang, J., 2015. Effect of case drain pressure on slipper/swashplate pai within axial piston pump. *Journal of Zhejiang University SCIENCE A (Applied Physics & Engineering)*, 16(12), pp. 1001-1014.

References

- Xu, B., Zhang, J. & Yang, H., 2012. Investigation on structural optimization of anti-overturning slipper of axial piston pump. *Science China Technological Sciences*, 55(11), pp. 3010-3018.
- Yi, S. & Jiang, J., 2011. Study on oil film characteristics of slipper within axial piston pump under different working conditions. *Proceedings of the 8th JFPS International Symposium on Fluid Power*, pp. 534-539.
- Zhang, J. et al., 2017. Experimental investigations of the slipper spin in an axial piston pump. *Measurement*, Volume 102, pp. 112-120.

Abbreviations

AH	Airbus Helicopters
ATP	Acceptance Test Procedure
BG	Bond Graph
CFD	Computational Fluid Dynamics
CM	Condition monitoring
CPSD	Cumulative Power Spectral Density
DIC	Damage Identification Curve
FDD	Fault Detection and Diagnosis
FH	Flight hours
FFT	Fast Fourier Transform
FS	Full Scale (of a sensor)
GA	Genetic Algorithm
H/C	Helicopter
HUMS	Health and Usage Monitoring System
ICA	Institut Clément Ader
NLPQL	Non-Linear Programming by Quadratic Lagrangian
PSD	Power Spectral Density
SQP	Sequential Quadratic Programming
TBO	Time Between Overhaul
TRL	Technical Readiness Level

Definitions

Durability	The ability of the model to last a long time in the company, being used as is by several employees or being the foundation of other models through total or partial reuse.
Failure	“A permanent interruption of a system’s ability to perform a required function under specified operating conditions.” (Isermann & Ballé, 1997)
Failure mechanism	A deviant physical state or condition leading to a failure mode.
Failure mode	An event triggered by deviant behaviour or function of a component, product, system or process.
Fault	“An unpermitted deviation of at least one characteristic property or parameter of the system from the acceptable / usual / standard condition.” (Isermann & Ballé, 1997)
Fault detection	“Determination of the faults present in a system and the time of detection.” (Isermann & Ballé, 1997)
Fault diagnosis	“Determination of the kind, size location and time of detection of a fault. Follows fault detection. Includes fault isolation and identification.” (Isermann & Ballé, 1997)
Fault identification	“Determination of the size and time-variant behaviour of a fault. Follows fault isolation.” (Isermann & Ballé, 1997)
Fault isolation	“Determination of the kind, location and time of detection of a fault. Follows fault detection.” (Isermann & Ballé, 1997)
Life	Time between product fabrication and failure, often written in Years.
Metamodel	Metamodels, or surrogate models, are approximation of models that reproduce the simulation model behaviour as accurately as possible, while being much cheaper computationally.
Remaining useful life	A prediction of the time to failure of a component, product, system or process done by assessing the extent of its deviation or degradation from the expected normal operating conditions.
Service	Cumulated time of product usage. In aerospace, amount of service is written in Flight Hours (FH).

Nomenclature

α	[rad]	swashplate tilt angle
α_{max}	[rad]	swashplate maximum tilt angle – simulation parameter
β	[Pa ⁻¹]	compressibility coefficient
γ	[-]	shifting parameter from distributed to lumped pressure drop model
$\Gamma_{sl/sp}$	[N.m]	total torque on swashplate due to slippers
Γ_{sl/sp_i}	[N.m]	torque on the swashplate due to slipper i contact and fluid pressure in the gap
θ	[rad]	piston angular position
θ_j	[rad]	jet angle
ψ	[-]	identification parameter vector
δ	[m]	contact deformation
δ_λ	[-]	laminar flow constant linked to the flow number
δ_0	[m]	reference contact deformation at which d_{eff} reaches 95% of d_{effm}
δ_p	[m]	valve spool position
δ_{Re}	[-]	the laminar flow coefficient of the orifice, dependent on geometry
ϵ_i	[-]	sign operator equal to 1 if the underlap increases with X_t , -1 otherwise
ζ	[-]	jamming state coefficient
λ	[-]	flow number
λ_{crit}	[-]	critical flow number at which flow changes from laminar to turbulent
μ	[Pa.s]	fluid absolute (dynamic) viscosity
ν	[m ² /s]	fluid kinematic viscosity
ρ	[kg/m ³]	density
ω	[rpm]	pump rotating speed
A	[m ²]	orifice flow passage area
a_{sl}	[m/s ²]	slipper acceleration
B	[Pa]	fluid bulk modulus
b	[m]	radial clearance between piston and bushing
C_d	[-]	orifice discharge coefficient
$C_{d\infty}$	[-]	limit discharge coefficient
C_q	[-]	flow coefficient
$C_{q\infty}$	[-]	limit flow coefficient
C_v	[-]	velocity coefficient
c	[m]	radial clearance between spool and sleeve
d	[m]	piston trajectory diameter in barrel coordinate system
d_b	[m]	bushing diameter
d_e	[m]	external diameter of slipper sealing land
d_{eff}	[N/(m/s)]	damping coefficient

d_{effm}	[N/(m/s)]	maximum value of d_{eff}
d_{hole}	[m]	valve orifice diameter
d_i	[m]	internal diameter of slipper sealing land
d_p	[m]	piston diameter
e	[m]	swashplate tilting axis eccentricity
e_p	[m]	eccentricity of the piston in the bushing
F	[N]	jamming force
F_1	[N]	axial component of the jet force
$F_{/p}$	[N]	frictional losses on the moving body– flow in annular passage
F_c	[N]	contact force
$F_{c/sl}$	[N]	pressure force applied by the case fluid on the slipper
F_{cont}	[N]	contact force between slipper and swashplate/retainer
F_d	[N]	damping force
F_e	[N]	elastic force
F_{HB}	[N]	pressure force of the fluid in the slipper/swashplate gap
F_j	[N]	jet force
F_{jam}	[N]	jamming friction force in AMESim
$F_{p/sl}$	[N]	force from the piston on the slipper
$F_{sl/p}$	[N]	force from the slipper on the piston
F_{tr}	[N]	transient flow force on the spool
f	[Hz]	frequency
f_{2p}	[Hz]	displacement ripple frequency
f_b	[Hz]	pump rotating frequency
f_p	[Hz]	porting pulsation frequency
h_{bpp}	[μm]	barrel/port-plate clearance– simulation parameter
h_d	[m]	hydraulic diameter
h_{sl}	[m]	slipper/swashplate clearance
\dot{h}_{sl}	[m/s]	slipper/swashplate gap height velocity
h_{th}	[mm]	slipper/swashplate gap height (common to all slippers)– simulation parameter
I_j	[N]	jamming intensity
I_v	[bar, L/min]	average stabilized simulated value
I_v^*	[bar, L/min]	measured reference value
i	[-]	experiment number
i_0	[-]	experiment number at zero flow
i_1	[-]	experiment number not measured at zero flow
J	[(L/min) ²]	optimization criteria
J_1	[bar ²]	optimization criteria depending on k_{cr}
J_2	[bar ²]	optimization criteria depending on (α, k_∞, K)
J_3	[bar ²]	optimization criteria depending on k_d
K	[(m ³ /s) ^γ]	laminar/turbulent transition coefficient for resistance R_r
K_g	[-]	flow continuity coefficient between under and overlap states

K_{rec}	[-]	overlap coefficient
k	[N/m]	elastic coefficient
k_{∞}	[Pa/(m ³ /s) ^{1+γ}]	return resistance R_r coefficient
k_c	[Pa/(m ³ /s)]	case resistance of R_c effect
k_{cr}	[Pa/(m ³ /s)]	other name of the $(k_c + k_{\infty}K)$ factor
k_d	[Pa/(m ³ /s) ²]	characteristic coefficient for resistance R_d , function of the operating point
k_{jet}	[-]	AMESim user supplied coefficient for jet flow force computation
L	[m]	axial length between incoming and outgoing flows (damping length)
L_i	[m]	distance from slipper i centre to swashplate tilting centre
l	[m]	length of the piston in the housing
l_f	[m]	length of a notch
l_{sl}	[m]	length of the slipper
m_{sl}	[kg]	slipper mass
Nf	[-]	normalized frequency
n	[-]	pump number of pistons
n_f	[-]	number of notches in the valve sleeve
O_v	[-]	objective function of parameters α_{max} , h_{th} , h_{bpp} and P_{yoke}
P_0	[Pa]	upstream pressure
P_1	[Pa]	downstream pressure
P_c	[Pa, bar]	pressure at pump case drain port
P_d	[Pa, bar]	pressure at pump discharge port
P_i	[Pa, bar]	test bench intermediate pressure
P_p	[Pa]	slipper pocket fluid domain pressure
P_r	[Pa, bar]	reservoir pressure
P_s	[Pa]	pressure at pump suction port
P_{yoke}	[bar]	preload for the compensating piston spring– simulation parameter
ΔP_i	[Pa]	pressure at the valve orifice bounds
Q_c	[m ³ /s, L/min]	flow at pump case drain port
Q_d	[m ³ /s, L/min]	flow at pump discharge port
Q_{dh}	[m ³ /s]	flow sucked in the slipper pocket domain from pump case due to gap height variation
Q_{HB}	[m ³ /s]	flow from piston domain to slipper pocket domain
Q_i	[m ³]	volumetric flow rate in/ing/outing the fluid domain
Q_r	[m ³ /s, L/min]	total return flow from hydraulic system to reservoir
Q_{sbp}	[m ³ /s]	pumping flow of slipper in the pump case due to gap height variation
Q_{thr}	[m ³ /s]	flow from slipper pocket domain to case through hydrostatic bearing
Re	[-]	Reynolds number
Re_t	[-]	the transition Reynolds number
S_i	[m ²]	opening section of the valve orifice to flow
S_{eq}	[m ²]	equivalent slipper section for the application of pocket pressure (laminar flow hypothesis)
T_c	[°C]	temperature at pump case port
T_d	[°C]	temperature at pump discharge port

T_s	[°C]	temperature at pump suction port
t	[s]	time
t_1	[s]	initial time for the averaging of the absolute square error
t_2	[s]	final time for the averaging of the absolute square error
Vol	[m ³]	current fluid volume in the domain
v	[-]	considered variable in pump model parameter optimization
v_0	[m/s]	threshold velocity for maximum jamming friction
v_b	[m/s]	piston housing velocity
v_p	[m/s]	piston velocity
v_{spool}	[m/s]	valve spool velocity
w	[m ² /m]	orifice area gradient of as a function of spool displacement
X_0	[m]	rounded corner diameter of the spool edges
X_i	[m]	underlap of the i orifice
X_{i0}	[m]	underlap of the i orifice when the spool it at the hydraulic null
X_{si}	[m]	generating length of the section i
X_t	[m]	spool displacement
X_v	[bar, L/min]	normalization factor
x_{min}	[m]	valve orifice underlap for which flow area is minimum
x_v	[m]	valve spool displacement
z_a	[m]	piston position following $\vec{z_b}$

List of figures

Figure 1-1: Maintenance types as schematics.....	8
Figure 1-2: Illustration of mechanical linkage from pilot stick to rotor swashplate, adapted from (Raletz, 2009, p. 49)	10
Figure 1-3: Example of a typical H/C hydraulic system (Coïc, 2017)	11
Figure 2-1: Cut scheme of an axial piston pump, based on (Eaton Corporation, 2000)	15
Figure 2-2: Pump block illustration	21
Figure 2-3: Architecting process proposal.....	22
Figure 2-4: Proposition of architecture structures	23
Figure 2-5 : Illustration of a “matryoshka” block	24
Figure 2-6: Examples of bonds used throughout the dissertation	27
Figure 2-7: Schematics of an eccentric piston in a bushing with annular leakage	32
Figure 2-8: Annular gap model as an "R field" in Bond-Graph theory.....	33
Figure 2-9: Schematics of a hydro-mechanical pump displacement compensation mechanism.....	35
Figure 2-10: Swashplate type axial piston pump compensation process schematics	36
Figure 2-11: Example of a two-land three-way valve	37
Figure 2-12: Underlap and overlap spool positions based on (Maré, 1993)	37
Figure 2-13: Schematics of the fluid forces on a valve spool (Meritt, 1967)	40
Figure 2-14: Effect of radial clearance on the jet angle (Meritt, 1967)	41
Figure 2-15: Comparison of valve orifice bond-graph models – original vs modulated	45
Figure 2-16: Comparison of valve force models: with and without jamming.....	46
Figure 2-17: CM Bond-Graph of the complete axial piston pump pressure compensator.....	47
Figure 2-18: AMESim implementation of the pressure compensation mechanism model	48
Figure 2-19: Pressure compensator verification virtual test bench	49
Figure 2-20: Pressure compensator model verification - pump answer to load.....	50
Figure 2-21: Impact of valve wear on pump dynamic response - 3 conditions	52
Figure 2-22: Pressure compensator model verification - answer to valve jamming.....	53
Figure 2-23: Slipper interface schematics, adapted from (Schenk, 2014).....	55
Figure 2-24: Example of slipper local coordinates.....	55
Figure 2-25: Schematics of slipper architecture block interfaces.....	59
Figure 2-26: Schematics of the slipper kinematics	60
Figure 2-27: Forces on the slipper.....	62
Figure 2-28: Slipper hydraulic interfaces schematics adapted from (Schenk, 2014).....	64
Figure 2-29: Proposed slipper bond-graph model	66
Figure 2-30: Slipper/Swashplate interface model in AMESim	67
Figure 2-31: Comparison of simulated slipper/swashplate gap with literature.....	68
Figure 2-32: Comparison of ideal and simulated variables for slipper leakage computation.....	69
Figure 2-33: Slipper/swashplate gap height over pump rotation in several simulation cases.....	70
Figure 3-1: Schematics of the pump static operating points to be reproduced in tests	80
Figure 3-2: Simplified test bench hydraulic scheme.....	81

Figure 3-3: Discharge and case pressure during nominal static point n°2 at 50°C.....	83
Figure 3-4: Discharge and case pressures PSD - Nominal conditions, 50°C, static point n°2.....	84
Figure 3-5: Case pressure behaviour depending on tank pressure, 50°C - static point n°2.....	85
Figure 3-6: Case pressure PSD depending on tank pressure, 50°C- static point n°2.....	85
Figure 3-7: Discharge pressure CPSD – 50°C, influence of system load.....	86
Figure 3-8: Case pressure CPSD – 50°C, influence of system load – $P_r = 0$ bar.....	86
Figure 3-9: Case pressure CPSD – 50°C, influence of system load – $P_r = 2.5$ bar.....	87
Figure 3-10: Discharge pressure PSD at several pump rotating speed – static point n°2.....	88
Figure 3-11: Discharge pressure CPSD at several pump rotating speed – static point n°2.....	88
Figure 3-12: Case pressure PSD at several pump rotating speed – 50°C, static point n°2.....	89
Figure 3-13: Case pressure CPSD at several rotating speed – 50°C, static point n°2.....	89
Figure 3-14: Pump pressure static characteristics at 50°C in several test conditions.....	90
Figure 3-15: Illustration of flow sensors top (measured).....	91
Figure 3-16: Impact of load variation on pump torque and speed.....	92
Figure 3-17: Average temperature at each port for every 50°C data set.	93
Figure 3-18: Temperature deviation for 50°C tests at each port - average the mean test values.....	93
Figure 3-19: Pump model hydraulic interfaces with the test bench.....	95
Figure 3-20: Test benches – a) Real hardware, b) Identified model, c) Bond-Graph.....	96
Figure 3-21: Test bench model parameters identification process.....	100
Figure 3-22: Simplification of the slipper/swashplate leakage model.....	103
Figure 3-23: Highlight of the complete axial piston hydraulic pump model.....	104
Figure 3-24: Effect of parameters on the virtual pump simulation results.....	109
Figure 3-25: Effect of rotating speed on model accuracy - depending on static points.....	111

List of tables

Table 1-1: Key figures of axial piston pumps on AH fleet (Paulmann & Mkadara, 2018)	12
Table 2-1: H225 axial piston pump steady state characteristics during ATP.....	16
Table 2-2: Examples of lumped and distributed parameters modelling approaches in literature	17
Table 2-3: Comparison of 3-D and 0-D models considering the pump main leakage paths.....	18
Table 2-4: List of requirements for the pump model.....	19
Table 2-5: Basics of Bond-Graph elements	26
Table 2-6: Generic main pump leakage lumped-parameter models.....	31
Table 2-7: Pressure compensator in lumped-parameter modelling literature.....	43
Table 2-8: Pump dynamic specification - from ATP (Airbus Helicopters, 2012, p. 137)	43
Table 2-9: Complete comparison of compensator models simulation against ATP specifications.....	51
Table 2-10: Total leakage from slipper/swashplate interface using the generic leakage model	56
Table 2-11: Comparison of literature on slipper modelling and physical phenomena considered	58
Table 2-12: Comparison of literature through numbers	58
Table 2-13: Comparison of total leakage at slipper/swashplate interface for 1 rev.	69
Table 2-14: Information on slipper attitude and leakage from literature	72
Table 3-1: Summary of testing conditions for data gathering	79
Table 3-2: Sensor data sheets summary	82
Table 3-3: Acquisition of sensor signals	83
Table 3-4: Test bench model identified fixed parameters.....	101
Table 3-5: Leakages considered in the complete pump model.....	104
Table 3-6: List of parameters to be fitted	105
Table 3-7: Normalization factors used in the optimization objective.....	106
Table 3-8: Optimization results in each experimental conditions	107
Table 3-9: Average and standard deviation of the optimized parameter sets.....	108
Table 3-10: Relative errors between measurements and simulation with averaged fitted parameters.....	108
Table 3-11: Simulation model errors – {Pr = 2.5 bar, ω = 4600rpm, T= 50 °C}	110
Table 4-1: Axial piston pump failure mechanisms and effects (Paulmann & Mkadara, 2018)	115
Table 4-2: Simulated pump degradation conditions	117
Table 4-3: Simulation results with increased piston clearance - average steady state values.....	117

Résumé de la thèse en français

L'objectif de la présente étude est de proposer et d'évaluer une solution à faible coût pour la surveillance des pompes à pistons axiaux sur hélicoptères. Le travail est concentré sur la possible utilisation de la pression au port de drain de la pompe dans un système de surveillance. Des questions, liées au contexte industriel de l'étude, ont été identifiées :

- Q1. Sur hélicoptère, un capteur externe de pression de drain peut-il être utilisé pour détecter la dégradation de la pompe avant une défaillance ?
- Q2. La dégradation de la pompe peut-elle être isolée de celle du système hydraulique lorsque l'on utilise un seul capteur de pression de drain supplémentaire ?

Le contexte industriel a soulevé la nécessité de développer un modèle à paramètres localisés de la pompe étudiée. Les questions scientifiques suivantes relatives à la modélisation de la pompe ont été identifiées :

- Q3. Quel est l'état actuel de la technique en matière de modélisation des pompes à pistons axiaux ?
- Q4. Quelles améliorations peuvent être apportées à la modélisation 1-D des pompes à pistons axiaux dans le cadre de la surveillance de l'état de santé de ces pompes, et qu'apportent-elles ?
- Q5. Le modèle de pompe, qui exécute un essai simulé dans des conditions de fonctionnement données, est-il capable de reproduire les mêmes données et motifs que des essais réels effectués dans les mêmes conditions de fonctionnement ?

Afin de répondre à ces questions, la thèse a été divisée en trois chapitres principaux (numérotés de 2 à 4).

Dans le chapitre 2, un modèle de pompe à pistons axiaux a été développé. Il est basé sur une pompe existante, et répond à des exigences industrielles. Dans un premier temps, un processus d'architecture a été présenté pour répondre aux exigences industrielles définies pour assurer la durabilité du modèle dans l'entreprise. Une revue de la littérature a été réalisée pour répondre à la question

3. Ensuite, deux façons d'améliorer l'état de l'art de la modélisation à paramètres localisés des pompes à pistons axiaux ont été détaillées, répondant ainsi à la question 4. Ces deux approches sont la conséquence du besoin en modèles précis, permettant de simuler des dégradations de la pompe. La première approche proposée se concentre sur le mécanisme de compensation de cylindrée de la pompe. Une approche basée sur les Bond-Graphs a été suggérée pour simuler des jeux (entre deux pièces) variables temporellement et un grippage de pièces. La seconde approche traite de l'interface patin / plateau inclinable. Un modèle de hauteur de jeu variable entre ces deux pièces a été proposé afin d'améliorer la représentativité des fuites simulées par les modèles de pompes à pistons axiaux à paramètres localisés. Le modèle, basé sur une représentation cinématique de la hauteur de jeu, permet de simuler sa variation pendant un cycle de pompage, en raison des forces hydrauliques et mécaniques appliquées sur les différentes parties de la pompe. Les limites du modèle cinématique ont été mises en évidence. Le long contact entre les patins et le plateau, observé pour les simulations réalisées pour un fort déplacement de la pompe, est l'une d'entre elles. Ce comportement simulé conduit à un débit de fuite irréaliste. Malgré les nombreuses solutions testées pour améliorer le modèle de patin/plateau, il n'a pas été possible de réduire ce comportement dans le temps imparti de la thèse. L'intégration de métamodèles a été proposée comme perspective au travail présenté, pour améliorer le modèle de pompe développé. Ces modèles pourraient être construits à partir de simulations de modèles à paramètres distribués (utilisant par exemple des logiciels CFD). Ils permettront de prendre en compte des phénomènes plus complexes (par exemple, l'inclinaison du patin par rapport au plateau ou les effets localisés de la température sur la viscosité du fluide), sans la charge de calcul des modèles détaillés sur lesquels ils sont basés.

Le chapitre 3 est dédié à apporter une réponse à la question Q5. Des expériences ont été réalisées afin de recueillir des données pour l'évaluation du modèle de pompe ainsi que pour étudier le comportement de la pression de drain en fonction des conditions de fonctionnement. L'auteur a spécifié le programme d'essai expérimental et en a analysé les résultats, qui ont été obtenus sur un banc d'essai déjà existant. Ce banc d'essai compte un réservoir pressurisé et une conduite de retour partiellement commune aux débits de drain et de décharge. L'analyse des résultats de mesure a montré que le comportement en fréquence du signal mesuré de la pression de drain dépend fortement de la pression du réservoir. Cependant, l'architecture du banc d'essai a empêché l'identification de l'influence de la vitesse de rotation sur la pression et le débit de drain de la pompe. Pour des recherches futures, un banc d'essai doit être conçu avec des lignes retour séparées pour les débits de décharge et de drain. Cela permettra d'étudier la pression et le débit de drain dans les domaines temporel et fréquentiel, sans autre influence que la pompe elle-même.

Le couplage des lignes de retour de décharge et de drain durant les expériences a augmenté le besoin d'un modèle de banc d'essai sur lequel évaluer le modèle de pompe. Un modèle paramétrique de banc d'essai a été développé. Sa structure est basée sur la physique, et ses paramètres ont été identifiés à partir des mesures expérimentales. Il a été estimé que le banc d'essai modélisé, à lui seul, génère une erreur sur le débit de drain d'environ 0,3 L/min en moyenne. Pour mettre cette valeur en perspective, cette erreur s'élève à 20 % de la fuite maximale de 1,5 L/min de la pompe autorisée en pratique. En outre, l'évolution de la température des paramètres du modèle identifiés a été jugée irréaliste. Ce modèle de banc d'essai a néanmoins été jugé suffisamment précis pour être utilisé pour évaluer le modèle de pompe à pistons axiaux développé (avec une hauteur de jeu patin/plateau fixe), dans des conditions nominales (température du fluide 50°C, vitesse de rotation 4600 tr/min, et pression du réservoir 0 bar rel.) Coupler le modèle de pompe avec celui du banc d'essai (après identification des paramètres du modèle de pompe) a permis de simuler avec précision la pression et le débit de refoulement ainsi que la pression drain dans des conditions nominales, avec une erreur relative inférieure à 20 %. Cependant, la précision du modèle est nettement moins bonne pour le débit drain : l'erreur relative est supérieure à 40 % dans toutes les simulations effectuées dans des conditions nominales. Deux approches distinctes peuvent être proposées pour améliorer la représentativité globale du modèle. La première se concentre sur le modèle du banc d'essai. Une meilleure collecte de données au cours des expériences et le changement du modèle de la ligne de drain (d'un orifice laminaire à un orifice avec une transition laminaire/turbulente) permettront d'améliorer considérablement la précision du modèle du banc d'essai. La deuxième approche est liée à l'inclusion de métamodèles dans le modèle de la pompe, comme nous l'avons déjà mentionné.

Le chapitre 4 s'est concentré sur la réponse aux questions industrielles Q1 et Q2. La littérature a répondu favorablement à la question Q1. Ensuite, une solution [contenu supprimé pour des raisons de confidentialité] a été proposée. Cet outil permet d'isoler la dégradation de la pompe de la dégradation du système hydraulique. Une attention particulière a été accordée à la faisabilité de cette approche en ce qui concerne sa robustesse face aux variations de pression du réservoir, de température du fluide et de vitesse de rotation de la pompe. Il a également été jugé d'une importance majeure de tenir compte du système de production du système hydraulique et des pompes, qui introduit de la variabilité dans le comportement de ces produits. Il a été suggéré de réaliser les mesures comparatives dans des conditions proches du zéro débit de refoulement, pour atténuer cette variabilité. En pratique, cela peut être réalisé, par exemple, en effectuant des mesures sur hélicoptère pendant un essai avant (ou après) le vol, lorsqu'aucune commande du pilote n'est appliquée. Il a également été suggéré de

caractériser la courbe de référence à partir de mesures prises sur des "ironbirds"⁴ d'Airbus Helicopters.

Afin d'augmenter le niveau de maturité de l'approche de surveillance des pompes proposée, plusieurs points restent à traiter :

- Ce doctorat a abordé l'intérêt et la faisabilité du suivi de la dégradation des pompes grâce à la solution proposée. Cependant, la détection elle-même de la dégradation de la pompe n'a pas été abordée. Cela nécessitera des recherches supplémentaires pour concevoir, mettre en œuvre et évaluer un algorithme de détection.
- Il est nécessaire de lancer une campagne expérimentale afin de démontrer la faisabilité de l'approche proposée, en faisant passer le niveau de maturité technologique (TRL) du niveau 3 au niveau 4.
- Pour mesurer la pression du corps de pompe, le capteur à ajouter devrait avoir une plage de mesure de 5 bar. Toutefois, il convient de prêter attention à la disponibilité et au coût d'un tel capteur de pression certifié pour le domaine aéronautique.
- Enfin et surtout, la mise en œuvre de l'approche proposée sur hélicoptère (par exemple, l'introduction d'une routine automatique de surveillance) reste un point clé qui nécessite un considérable travail transversal entre de nombreux départements de Airbus Helicopters.

⁴ Banc d'essais système reprenant l'entière de l'architecture et des composants d'un aéronef

Annexes

A-1 Test procedure for data gathering

A-2 Test bench photos

A-3 Test bench data (hoses and sensors location)

A-4 Test pump ATP results

A-5 Additional graphs from experiments

A-6 Published papers

A-1 Test procedure for data gathering

Note

From

Geneviève Mkadara
Airbus Helicopters
T: +33 442 858 190
E: genevieve.mkadara@airbus.com

To

PUMP SUPPLIER

Copy

Gregor Paulmann, Airbus Helicopters
Jean-Charles Maré, ICA / INSA Toulouse

15 July 2020

Test Procedure for the H225 pump for Condition Monitoring study**1. CONTEXT**

As we are trying to make a representative model of the EC225 for a HUMS approach, there is a need for us to validate this model against experiment results. As such it would be greatly appreciated if you could provide the data needed by carrying out the tests described below. Thus, we would be able to compare our results with experimental data in order to improve the model accuracy.

Please note that every test procedure mentioned is only proposed and could be optimized in accordance with the available testing equipment and the supplier's best practices.

2. GENERAL REQUIREMENTS

It is of primary importance for us to measure case drain pressure with a high bandwidth sensor and at least 10kHz sampling rate, as we trying to get an accurate image of the pressure pulses at drain, with 15 measurement point per period => $4600/60 \times 9 \times 15 = 10,350$ kHz.

If possible, all measurements (except temperature) should be done with high frequency response sensors at the same sampling rate (10 kHz). All data should be sampled in synchronism.

A high frequency pressure sensor, with measure range from 0 to 15bar max, is to be used at pump drain (see modified illustration taken from EC225 pump CMM), with direct access to drain line (i.e. without valve like sensor n°2).

For every test, Temperature, Pressure and Flow rate must be measured at every port (discharge, inlet and drain ports), as close as possible to the port (or with detailed info about the distance and diameter of the pipe from/to the port). Rated speed and shaft torque are also to be measured.

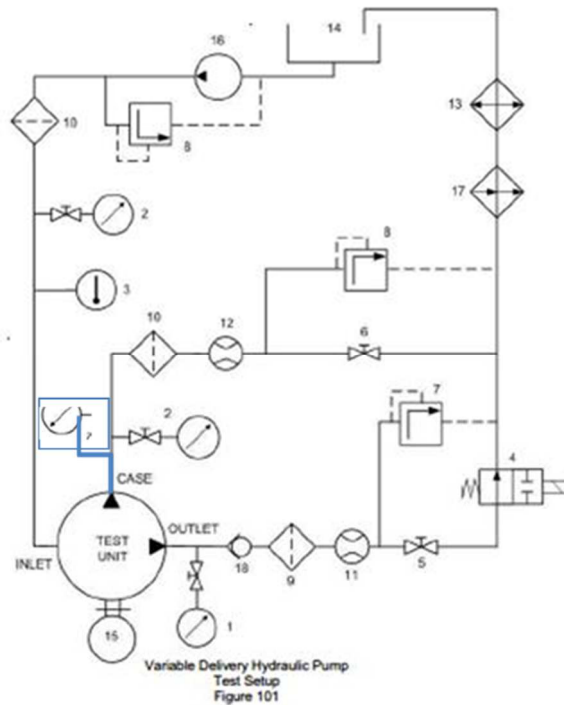


Figure 1: Modified hydraulic scheme from EC225 CMM

3. DATA TO BE SUPPLIED FOR CORRELATION WITH MODEL

3.1. *To be supplied by SUPPLIER*

3.1.1. For each sensor used

- Sampling rate, measurement range, drift, accuracy, bandwidth (including conditioner and phase lag).

3.1.2. For the hydraulic system

- Dynamics of the loading valve (constructor data sheet).
- Fluid type used on test bench. If possible, data from last fluid check for viscosity and air content.

3.2. *To be measured by Airbus Helicopter before tests*

3.2.1. For each sensor used

- For pipe from sensor to the pump: material, internal diameter, length, number of curves and angles, pipe type (rigid or flexible), characteristics of the fittings.

3.2.2. For the hydraulic system

- Full geometrical data about drain line from pump drain to reservoir (material, internal diameter, length, number of curves and angles, pipe type).
- Full geometrical data about hydraulic circuit down pump outlet to loading valve (material, internal diameter, length, number of curves and angles, pipe type).

4. STEADY STATE TESTS – A

4.1. *Test description*

The aim of these tests is to measure the steady state characteristics of the compensated pump, for several operating conditions. Five measurement points are defined for each operation condition, in the schematics and in the tables below. Point (3) (see following schematic) is to be searched for by action on the loading valve (or any other mean used during the test to change the load on the pump), so as to find the point of maximum pump power.

The operating conditions are the following:

- Temperature : 50°C or 100°C;
- Rotating speed : [920; 3450; 4600; 5500] rpm;
- Pump inlet pressure : 1 bar (absolute) or 3,5 bar (absolute);

The full test list and conditions are described in Annexe, parts 6.1 and 6.2.

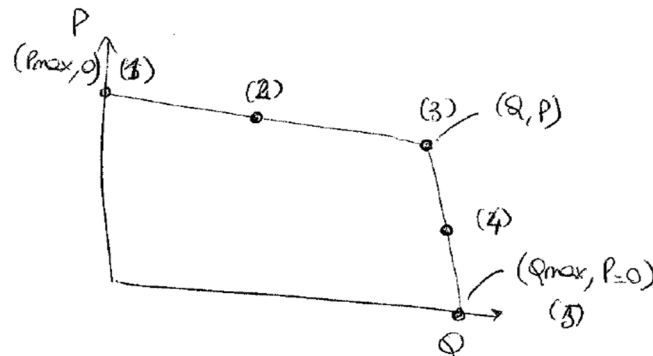


Figure 2: Schematics of the pump static characteristics points to be reproduced in tests

4.2. Test procedure

For each performance point, after stabilization of the imposed variables, record all variables for 2 seconds. A variable is considered "stabilized" when its variation is less than 1% of the full scale, on the variable's mean value.

5. DYNAMIC TESTS - B

5.1. Test description

The aim of this test is to obtain data on the dynamics of the pump. Two profiles for flow rate changes are used (step and ramp, see Table 1) to study the evolution of it. Also, in order to avoid the reaching the displacement end-stops, variations from 20 to 80% of pump displacement are asked. All tests should be made for both 50°C and 100°C at inlet port and are described in Annex, parts 6.3 and 6.4.

	CR-1	CR-2
Flow change rate (L/min/s)	27L/min in step response	27L/min in 1s

Table 1: Description of the two flow rate changes to be applied, CR-1 and CR-2

5.2. Test procedure

For each test, start recording all variables after stabilizing the imposed values. Wait for two seconds before modifying the flow rate. Keep recording until two seconds after stabilization of the pressure (see Figure 3). Please consider a variable "stabilized" when its variation is less than 1% of the full scale, on the variable's mean value.

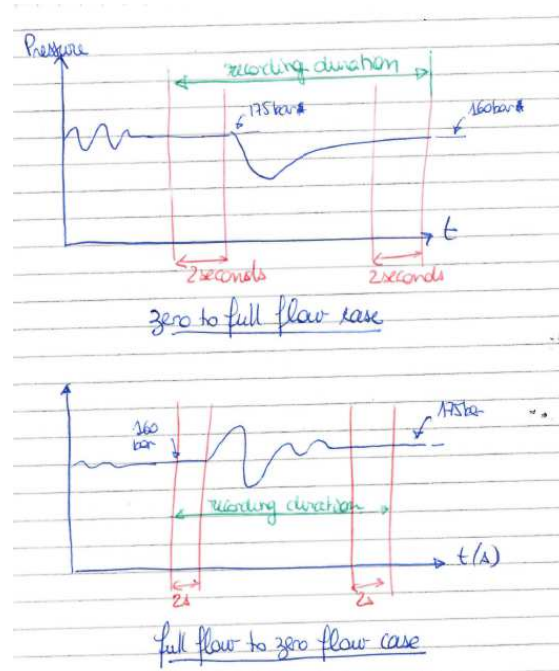


Figure 3: Schematics for recording duration during dynamic tests for both step and ramp load variation, increasing and decreasing.

6. ANNEXES

Legend

	Imposed AND to be measured
	To be measured

6.1. Steady state test (A) at 50°C

			NOMINAL					INLET PRESSURE VARIATION					SPEED VARIATION														
Test A2, n°			1	2	3	4	5	6	7	8	9	10	11	12	13	14	15	16	17	18	19	20	21	22	23	24	25
Variables to be measured	Fluid temperature (°C)	Inlet	50	50	50	50	50	50	50	50	50	50	50	50	50	50	50	50	50	50	50	50	50	50	50	50	
		Outlet																									
		Drain																									
	Pressure (bar Absolute)	Inlet	1	1	1	1	1	3,5	3,5	3,5	3,5	3,5	1	1	1	1	1	1	1	1	1	1	1	1	1	1	
		Outlet		167	*	50	1		167	*	50	1		167	*	50	1		167	*	50	1		167	*	50	1
		Drain																									
	Flow rate demand (L/min)	Inlet																									
		Outlet	0					0					0					0					0				
		Drain																									
	Rated speed (rpm)		4600	4600	4600	4600	4600	4600	4600	4600	4600	4600	3450	3450	3450	3450	3450	5500	5500	5500	5500	5500	920	920	920	920	920
	Shaft torque (N/m)																										

6.2. Steady state test (A) at 100°C

			NOMINAL					INLET PRESSURE VARIATION					SPEED VARIATION														
Test A3, n°			1	2	3	4	5	6	7	8	9	10	11	12	13	14	15	16	17	18	19	20	21	22	23	24	25
Variables to be measured	Fluid temperature (°C)	Inlet	100	100	100	100	100	100	100	100	100	100	100	100	100	100	100	100	100	100	100	100	100	100	100	100	100
		Outlet																									
		Drain																									
	Pressure (bar Absolute)	Inlet	1	1	1	1	1	3,5	3,5	3,5	3,5	3,5	1	1	1	1	1	1	1	1	1	1	1	1	1	1	1
		Outlet		167	*	50	1		167	*	50	1		167	*	50	1		167	*	50	1		167	*	50	1
		Drain																									
	Flow rate demand (L/min)	Inlet																									
		Outlet	0					0					0					0					0				
		Drain																									
	Rated speed (rpm)		4600	4600	4600	4600	4600	4600	4600	4600	4600	4600	3450	3450	3450	3450	3450	5500	5500	5500	5500	5500	920	920	920	920	920
	Shaft torque (N/m)																										

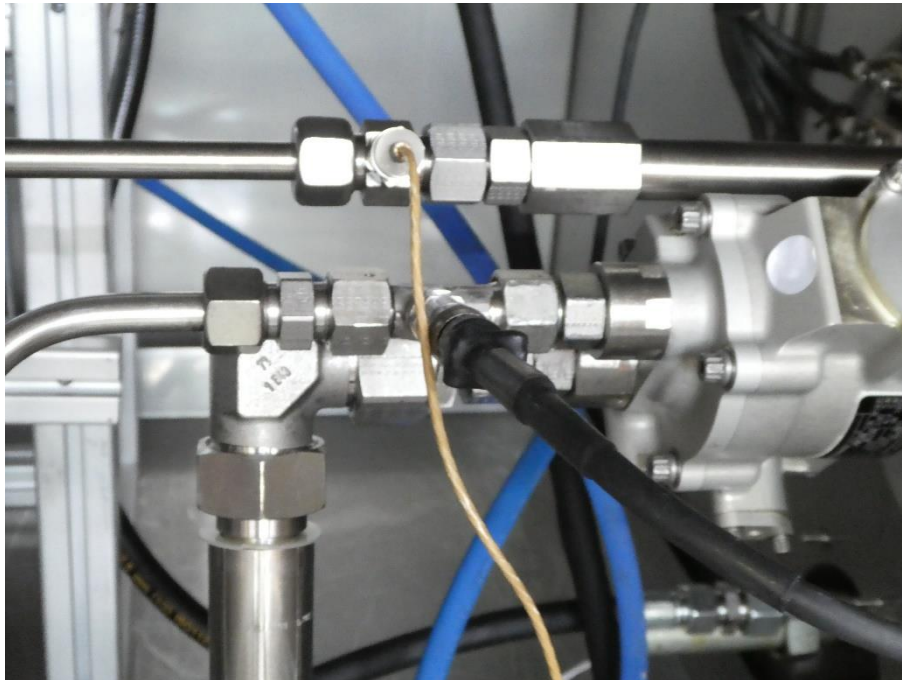
6.3. Dynamic tests (B) at 50°C

Test B2, n°			1	2	3	4	5	6	7	8
Variables to be measured	Fluid temperature (°C)	Inlet	50	50	50	50	50	50	50	50
		Outlet								
		Drain								
	Pressure (bar Absolute)	Inlet	1	1	1	1	1	1	1	1
		Outlet								
		Drain								
	Flow rate demand (L/min)	Inlet								
		Outlet	zero to full (CR-1)	full to zero (CR-1)	zero to full (CR-2)	full to zero (CR-2)	20% to 80% (CR-1)	20% to 80% (CR-1)	20% to 80% (CR-2)	20% to 80% (CR-2)
		Drain								
	Rated speed (rpm)		4600	4600	4600	4600	4600	4600	4600	4600
	Shaft torque (N/m)									

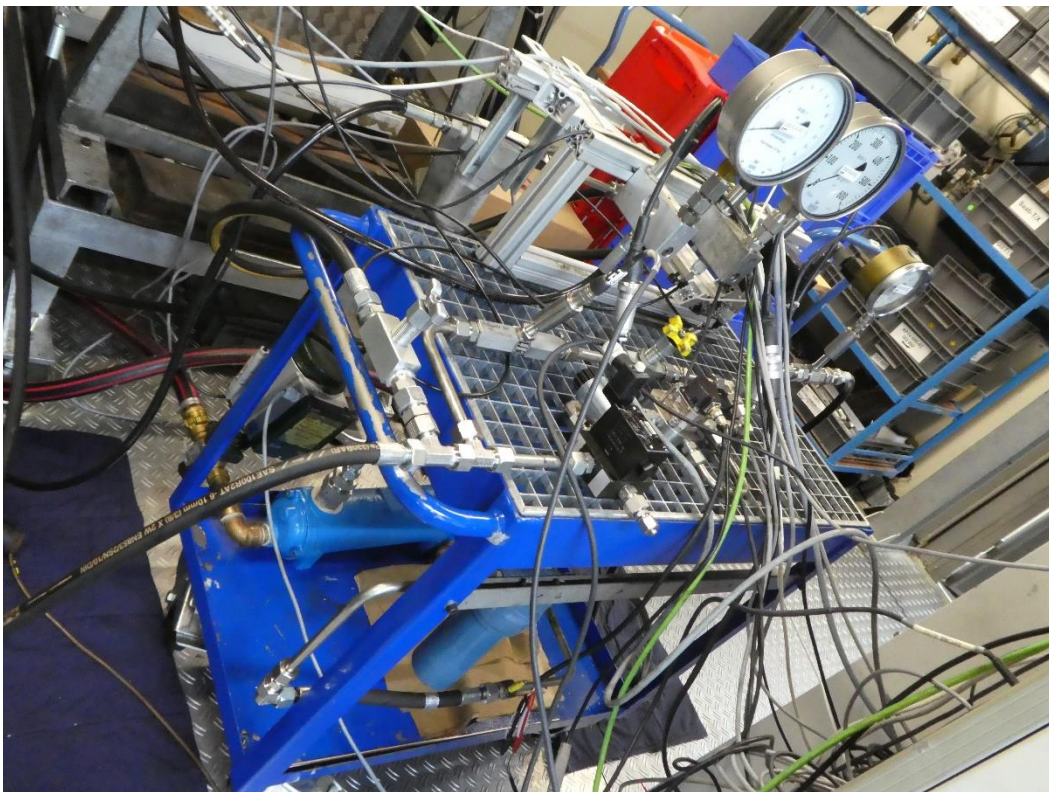
6.4. Dynamic tests (B) at 100°C

Test B3, n°			1	2	3	4	5	6	7	8
Variables to be measured	Fluid temperature (°C)	Inlet	100	100	100	100	100	100	100	100
		Outlet								
		Drain								
	Pressure (bar Absolute)	Inlet	1	1	1	1	1	1	1	1
		Outlet								
		Drain								
	Flow rate demand (L/min)	Inlet								
		Outlet	zero to full (CR-1)	full to zero (CR-1)	zero to full (CR-2)	full to zero (CR-2)	20% to 80% (CR-1)	20% to 80% (CR-1)	20% to 80% (CR-2)	20% to 80% (CR-2)
		Drain								
	Rated speed (rpm)		4600	4600	4600	4600	4600	4600	4600	4600
	Shaft torque (N/m)									

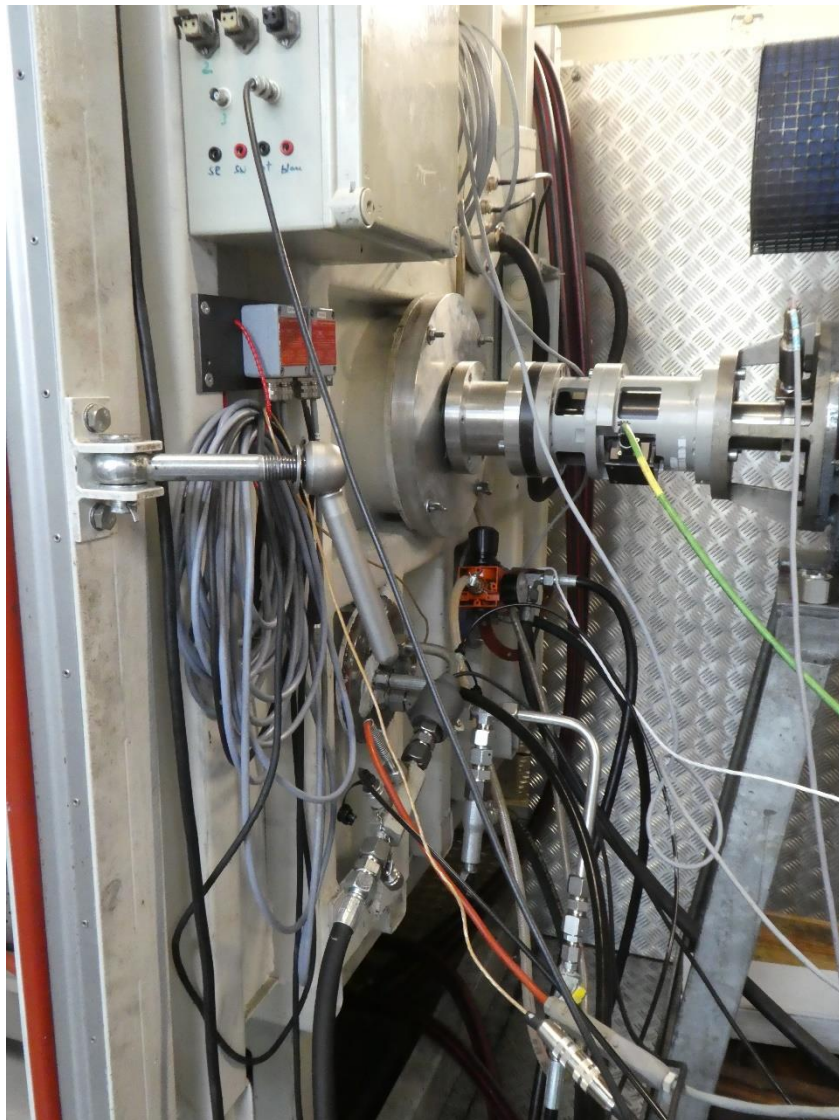
A-2 Test bench photos



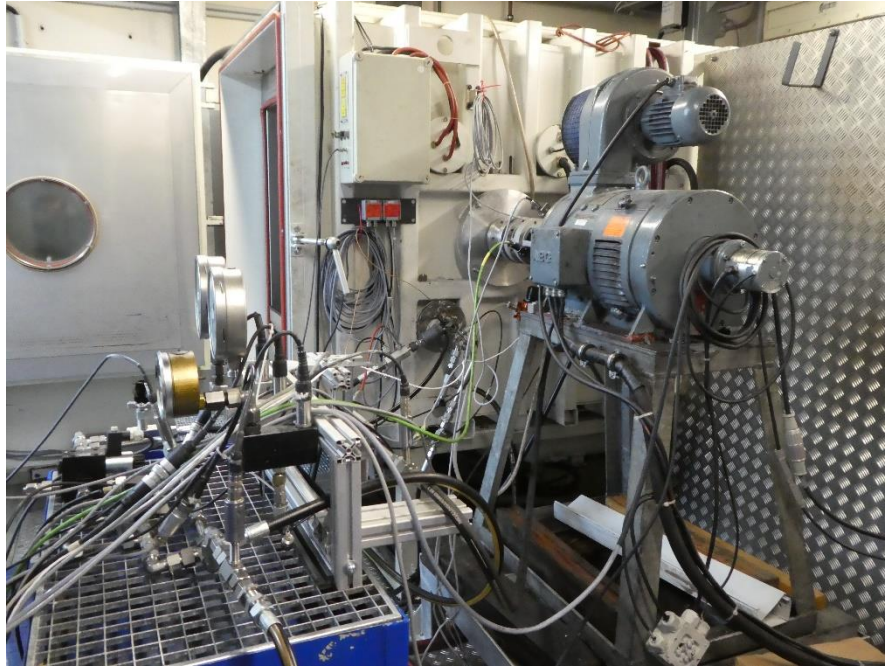
Contribution to the monitoring of hydraulic axial piston pumps for helicopters, with special focus on lumped parameter modelling
MKADARA G.



Contribution to the monitoring of hydraulic axial piston pumps for helicopters, with special focus on lumped parameter modelling
MKADARA G.



Contribution to the monitoring of hydraulic axial piston pumps for helicopters, with special focus on lumped parameter modelling
MKADARA G.



Contribution to the monitoring of hydraulic axial piston pumps for helicopters, with special focus on lumped parameter modelling
MKADARA G.

A-3 Test bench data (hoses and sensor locations)

SupplierTests_List of hydraulic lines

ICA-AH creation date : 20aug19 revision date:

G. MKADARA

Types

R

F

Rigid

Flexible

Nota : the numbers are given when going away from the pump port

XX'

On Mach valve side

In climatic chamber

Inlet			
Name	Type	Length (mm)	Inner diameter (mm)
I_1	F	1000	25
I_2	R	100	25
I_3	R	300	25

Case			
Name	Type	Length (mm)	Inner diameter (mm)
C_1	R	18	8
C_2	R	17	8
C_3	R	200	8
C_4	R	200	8
C_5	R	400	8
C_6	R	500	8
C_7	R	280	9
C_8	F	2000	6
C_9	R	200	9
C_10	F	2000	10

Case & Discharge			
Name	Type	Length (mm)	Inner diameter (mm)
CD_1	R	400	11
CD_2	F	2000	10
CD_3	R	200	11
CD_4	R	200	24

Outlet			
Name	Type	Length (mm)	Inner diameter (mm)
O_1	R	80	8
O_2	R	120	8
O_3	R	380	8
O_4	R	400	8
O_5	R	400	9
O_6	R	150	9
O_7	R	150	9
O_8	F	2000	10
O_9	R	100	9
O_10	R	150	9
O_11	R	200	9
O_12	R	200	9
O_13	R	100	9
O_10'	R	200	9
O_11'	R	150	9
O_12'	R	200	9
O_13'	R	200	9
O_14	R	200	9
O_15	R	100	9
O_16	F	2000	10
O_17	R	150	9
O_18	R	250	9
O_19	F	350	10
O_20	R	200	9
O_21	R	450	9
O_22	F	2000	10

Sensors locations

Pressure Intersection
Discharge O_1 / O_2
Case C_1 / C_2
Inlet TANK

Flow
Discharge O_13 / O_14
Case C_9 / C_10
Inlet N/A

Temperature
Discharge O_6 / O_7
Case C_3 / C_4
Inlet I_2 / I_3

Equipment locations

Mach valve O_12' / O_13'
Shut off valve O_10 / O_12
Pressure valve O_12 / O_13
Filter 1 O_16 / O_17
Cooler O_21 / O_22
Filter 2 C_8 / C_9

A-4 Test pump ATP results

FIGURE 5: ACCEPTANCE TEST REPORT
BILD 5: ABNAHMEPRÜFBERICHT

SHEET 2 OF 3

PART NUMBER: 46159 AMENDMENT:
MODEL NO.: AP2V-0120 S.O.:
SERIAL NO.: DT 907 TAG NO.:
TEST STAND: 12

4.5

CALIBRATION (Kalibrierung)

Schmidt 04.07.18

at By-Pass Flow
(0,5 ± 0,2 l/min)

Actual

Required

Rated Speed	4605	rpm	(4500 to 4700 rpm)
Discharge Pressure	174.4	bar	(173,0 to 177,0 bar)
Inlet Pressure	0.1	bar	(0,0 to 0,2 bar)
Case Drain Pressure	0.8	bar	(0,8 to 1,0 bar)
Inlet Temperature	63	°C	(55,0 to 65,0 °C)
Case Drain Flow	1.39	l/min	(0,3 to 1,5 l/min)
Torque	2.4	Nm	record

At Full Flow

Actual

Required

Rated Speed	4605	rpm	(4500 to 4700 rpm)
Discharge Pressure	160.8	bar	(160,0 bar minimum)
Inlet Pressure	0.1	bar	(0,0 to 0,2 bar)
Case Drain Pressure	0.4	bar	(0,0 to 1,0 bar)
Inlet Temperature	63	°C	(55,0 to 65,0 °C)
Delivery	24.67	l/min	(27,0 - 28,0 l/min)
Case Drain Flow	0.83	l/min	(1,5 l/min maximum)
Torque	15.8	Nm	

(in accordance with Figure 3)

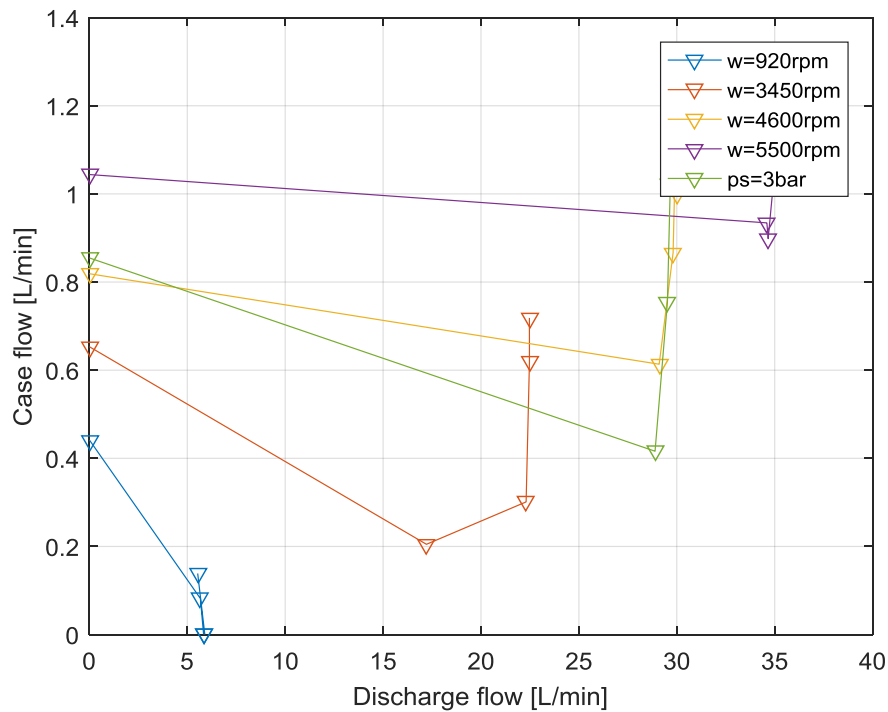
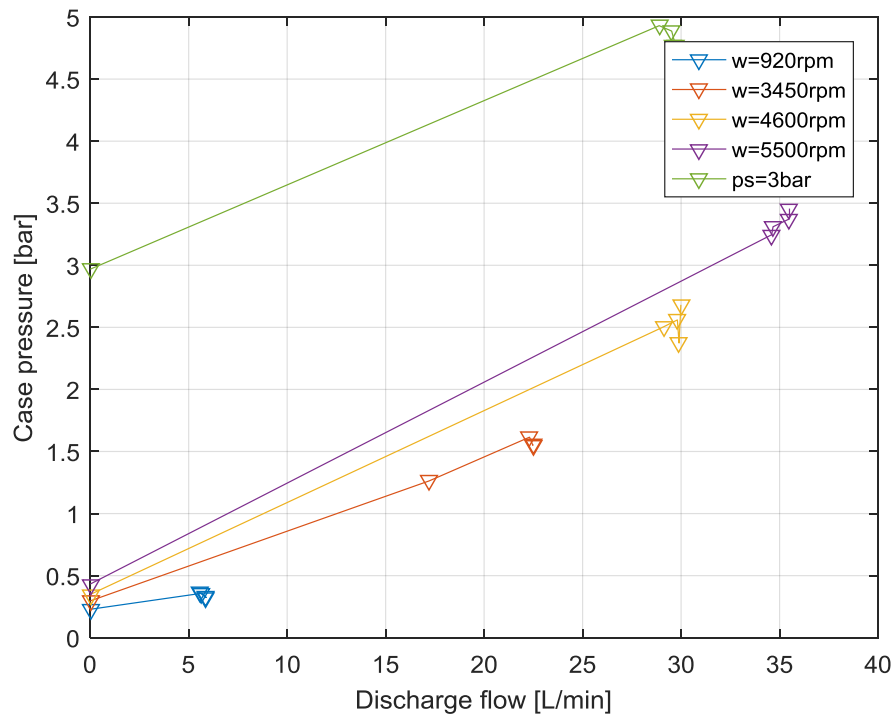
Use or disclosure of data contained on this sheet is subject to the restrictions on the title page of this document.

Contribution to the monitoring of hydraulic axial piston pumps for helicopters, with special focus on lumped parameter modelling

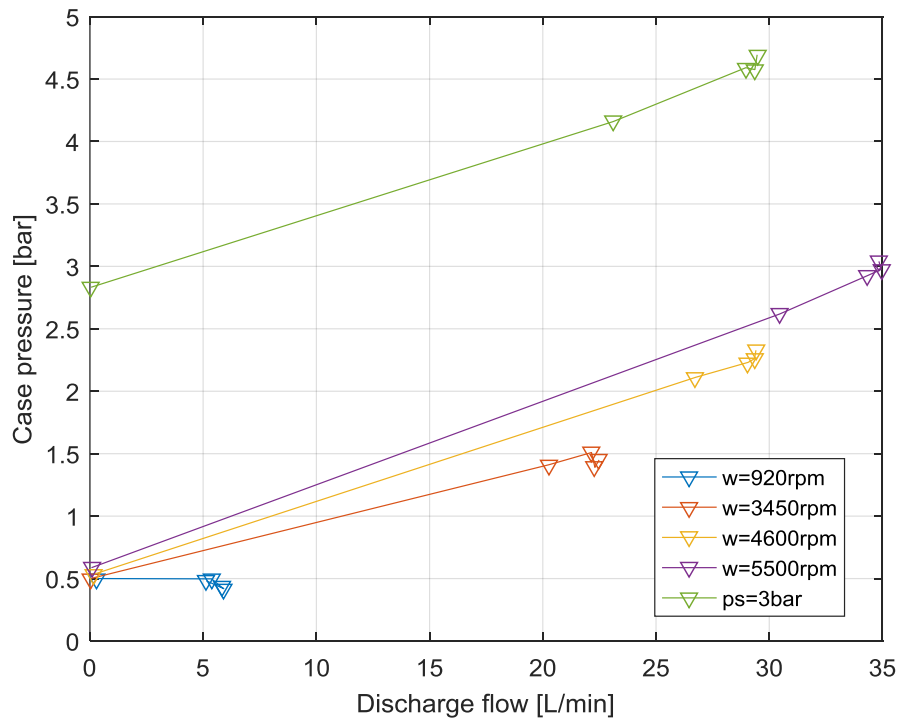
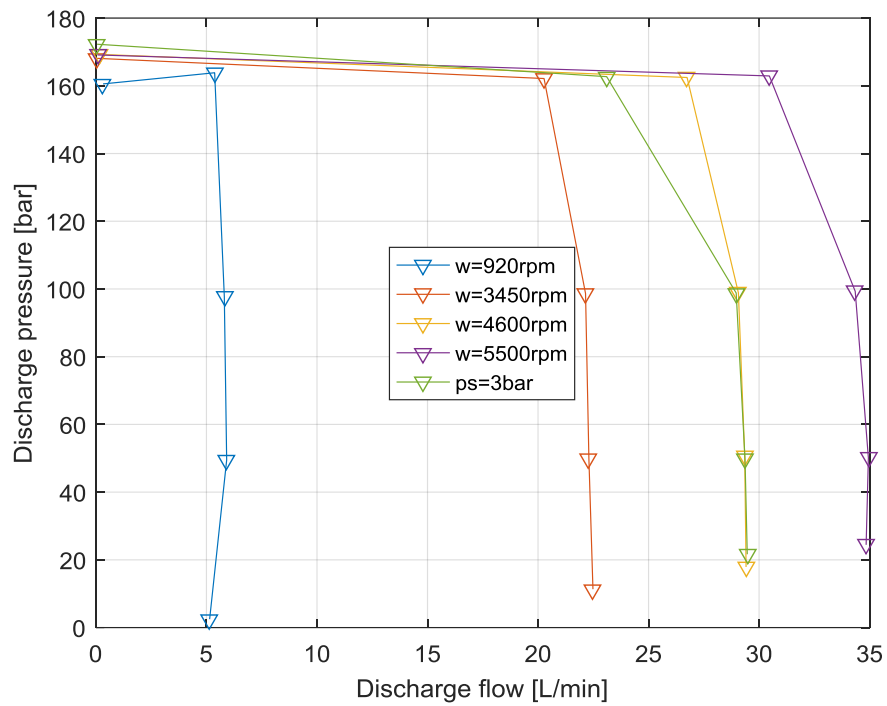
MKADARA G.

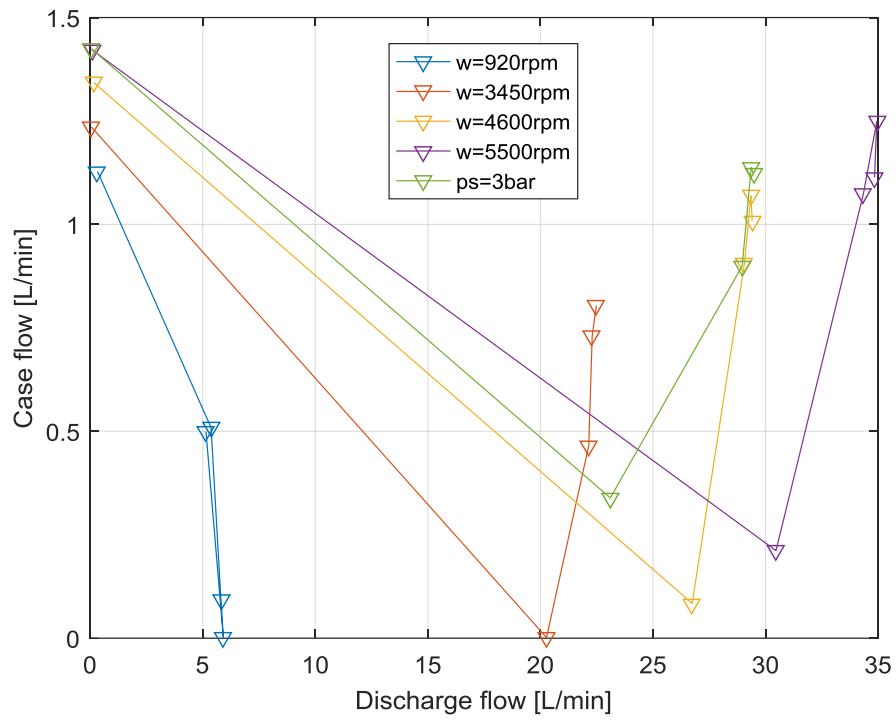
A-5 Additional graphs from experiments

a) Measurements at 50°C



b) Measurements at 100°C





A-6 Published papers

- 1 Paulmann, G. & Mkadara, G., 2017. *Condition Monitoring of hydraulic pumps - lessons learnt*. Milan, Italy, European Rotocraft Forum, September 12-15, 2017.
- 2 Paulmann, G. & Mkadara, G., 2018. *Condition Monitoring of hydraulic pumps - lessons learnt*. Aachen, Germany, Proceedings of the 11th International Fluid Power Conference, March 19-21.
- 3 Mkadara, G. & Maré, J.-C., 2020. *Development of a lumped parameter model of an aerospace pump for condition monitoring purposes*. Dresden, Germany, Proceedings of the 12th International Fluid Power Conference, October 12-14.

Abstracts are provided on the next page.

Condition monitoring of hydraulic pumps – lessons learnt

Gregor Paulmann and Geneviève Mkadara***

Airbus Helicopters Deutschland GmbH, Hydraulics and Flight Controls, Industriestraße 4,
86609 Donauwörth, Germany*

Institut Clément Ader / INSA Toulouse, Groupe MS2M, 3 rue Caroline Aigle, F-31400
Toulouse, France**

E-Mail: gregor.paulmann@airbus.com*

An overview to the performed analysis and lessons-learnt from flight control & hydraulic designers' perspective on a condition monitoring (CM) concept for helicopters (H/C) hydraulic pump is given. A selection of already performed studies on condition monitoring applications for hydraulic pumps is discussed and the main obstacles in the CM implementation process for H/C hydraulic pumps are drawn from it as lessons-learnt. It is considered unavoidable to enter the CM concept by a data collecting and processing phase. Thanks to the CM hybrid algorithm continuous maturity improvement by data feeding, the obtained in-service data will be then directly used to identify the failure in real-time. In parallel, the data trend evolution analysis should allow to decide if it can be used also as a predictive element into the CM system for the dedicated failure mode.

Keywords: Helicopters, axial piston pumps, condition monitoring, lessons learnt.

Development of a lumped parameter model of an aerospace pump for Condition Monitoring purposes

Geneviève Mkadara, Pr. Jean-Charles Maré*

Institut Clément Ader / INSA Toulouse, Groupe MS2M, 3 rue Caroline Aigle, F-31400
Toulouse, France

* Corresponding author E-mail address: mkadara@insa-toulouse.fr

This paper presents the development of a helicopter axial piston pump model with condition monitoring in mind. Industrial constraints and needs ask for modelling with a lumped-parameter approach and require model architecture to be addressed with care. The aim of the proposed model is to assess the merits of pump leakage monitoring through measurement of case pressure. Once reviewed the state of the art in pump modelling, the slipper/swashplate interface is taken as an example to propose and implement in Simcenter AMESim a variable gap height model. The simulation results show that commonly used lumped-parameter models overestimate leakage. It also points out that average leakage at slipper may reverse at high pump displacement.

Keywords: Axial piston pump, Helicopters, Modelling, Model architecting

*Contribution to the monitoring of hydraulic axial piston pumps for helicopters, with special
focus on lumped parameter modelling*

MKADARA G.

